Fisheries and Oceans Canada | Pêches et Océans Canada
Ecosystems and Oceans Science | Sciences des écosystèmes et des océans

Canadian Science Advisory Secretariat (CSAS)

Research Document 2023/048

Quebec Region

Summer Abundance Estimates for St. Lawrence Estuary Beluga (*Delphinapterus leucas*) from 52 Visual Line Transect Surveys and 11 Photographic Surveys Conducted from 1990 to 2022

Anne P. St-Pierre[1], Véronique Lesage[1], Arnaud Mosnier[1], M. Tim. Tinker[2], Jean-François Gosselin[1]

[1] Maurice Lamontagne Institute
Fisheries and Oceans Canada
850 route de la Mer
Mont-Joli, Québec, G5H 3Z4

[2] Nhydra Ecological Consulting
St. Margaret's Bay, NS B3Z 2G6

March 2024

Canada

Foreword

This series documents the scientific basis for the evaluation of aquatic resources and ecosystems in Canada. As such, it addresses the issues of the day in the time frames required and the documents it contains are not intended as definitive statements on the subjects addressed but rather as progress reports on ongoing investigations.

Published by:

Fisheries and Oceans Canada
Canadian Science Advisory Secretariat
200 Kent Street
Ottawa ON K1A 0E6

http://www.dfo-mpo.gc.ca/csas-sccs/
csas-sccs@dfo-mpo.gc.ca

ISSN 1919-5044
ISBN 978-0-660- 69068-1 Cat. No. Fs70-5/2023-048E-PDF

Correct citation for this publication:

St-Pierre, A.P., Lesage, V., Mosnier, A., Tinker, M.T., Gosselin, J.-F. 2024. Summer Abundance Estimates for St. Lawrence Estuary Beluga (*Delphinapterus leucas*) from 52 Visual Line Transect Surveys and 11 Photographic Surveys Conducted from 1990 to 2022. DFO Can. Sci. Advis. Sec. Res. Doc. 2023/048. v + 82 p.

Aussi disponible en français :

*St-Pierre, A.P., Lesage, V., Mosnier, A., Tinker, M.T., Gosselin, J.-F. 2024. Estimations de l'abondance estivale du béluga (*Delphinapterus leucas*) dans l'estuaire du Saint-Laurent basées sur 52 relevés visuels et 11 relevés photographiques réalisés de 1990 à 2022. Secr. can. des avis sci. du MPO. Doc. de rech. 2023/048. v + 86 p.*

TABLE OF CONTENTS

ABSTRACT

The St. Lawrence Estuary (SLE) beluga population has been surveyed repeatedly via photographic and visual aerial surveys to evaluate its abundance and trends following similar survey designs since 1988. Published abundance indices from both types of surveys up to 2014 were corrected for availability bias only, using a fixed correction factor. The present study presents results from recently-conducted photographic strip-transect (four surveys, in 2019), and visual line-transect surveys (16 surveys, in 2015, 2016, 2018, 2019, 2020, 2021, and 2022) of the SLE beluga population, as well as a re-analysis of past surveys conducted since 1990 using newly-estimated survey-specific correction factors for both availability (photographic and visual) and perception biases (visual surveys only). The latest photographic survey in 2019 resulted in a total average abundance estimate of 2,119 whales (SE = 267). The latest visual survey in 2022 resulted in a total abundance estimate of 1,257 whales (SE = 400). The 2022 visual survey has the lowest abundance estimate of all visual surveys conducted since 2001. Mean abundance estimates from visual surveys were consistently higher than for photographic surveys once fully corrected for both availability and perception biases. In past survey analyses, no perception bias correction factors were applied due to lack of data, but their use in the present study yielded fully corrected abundance estimates which are 1.5 to 2 times greater than the abundance indices corrected only for availability. While past analyses were adequate to produce abundance indices for this population, the current study represents a major step forward not only for an improved precision and accuracy of abundance estimates for the SLE beluga population but also for understanding the caveats associated with different methodological and analytical approaches to aerial surveys.

INTRODUCTION

Beluga, *Delphinapterus leucas*, are social and gregarious marine mammals which typically segregate spatially by sex and age class during summer, and occur in large concentrations in coastal estuaries, particularly in the Arctic (Finley et al. 1982, Michaud 2005, Richard 1991). Several beluga populations are found in Canadian waters, and are distinguished based on their summer distributions, genetics, and movements inferred from satellite telemetry (Reeves and Mitchell 1989, Richard 2010, Brennin et al. 1997, Brown Gladden et al. 1997, De March and Postma 2003, Postma et al. 2012). One of those populations occurs in the St. Lawrence Estuary (SLE), at the southernmost limit of the species' distribution. The SLE population occupies the area from Ile-aux-Coudres to Rimouski/Forestville, and in the Saguenay River during summer, but shifts its distribution towards the eastern part of the SLE and the northwestern Gulf of St. Lawrence in winter (Boivin 1990, Michaud 1993, Pippard and Malcolm 1978, Vladykov 1944). The current distribution range of the population represents about 65% of the historical extent (COSEWIC 2014).

The SLE beluga population has been surveyed repeatedly since 1975 to evaluate its abundance and trends (Kingsley 1998). While the population was thought to be stable at around 1000 individuals (Hammill et al. 2007), an assessment conducted following unusually high young of the year mortality events indicated that the population had likely been declining at an estimated rate of approximately 1% per year since the early 2000's, and numbered around 900 individuals in 2012 (DFO 2014). Based on these results, the Committee on the Status of Endangered Wildlife in Canada (COSEWIC) re-evaluated the status of SLE beluga in 2014 and designated the population as 'Endangered' (COSEWIC 2014).

To improve monitoring of the SLE beluga population, the 1995 SLE beluga recovery plan recommended that a standard method, systematic strip-transect photographic aerial surveys, be adopted to estimate its abundance (Bailey and Zinger 1995). Eight surveys following that standard protocol were carried out between 1988 and 2009 (Kingsley and Hammill 1991, Kingsley 1993, Kingsley 1996, Gosselin et al. 2001, Kingsley 1999, Gosselin et al. 2007, Gosselin et al. 2014). Considerable variability was observed in the resulting survey indices. This variability is thought to result from the challenges of surveying a small population with a non-random or aggregated distribution, with individuals that spend most of their time below the surface (Gosselin et al. 2007, Gosselin et al. 2014, Kingsley and Gauthier 2002).

A possible solution to this problem is to capture the variability associated with the aggregated distribution using repeated surveys. Line transect surveys are more efficient than strip transect surveys to estimate abundance of scarcely distributed animals over a large geographic area (Buckland et al. 2001). Visual line transect surveys are also generally less costly than large format photographic surveys, making them more practical for repeated surveys. Multiple aerial visual line-transect surveys have been completed in the SLE from 2001 to 2014 (Gosselin et al. 2014, Gosselin et al. 2017), and used to evaluate the variability in abundance indices associated with clumping for this population. For instance, 14 visual surveys conducted within 21 days in 2005 resulted in 4-fold changes in abundance indices within the period (Gosselin et al. 2007).

Estimates of marine mammal abundance obtained using aerial photographic or visual surveys can be affected by two main sources of bias: 1) observers not detecting whales because the animals are diving below visible depth (availability bias) and 2) observers not detecting animals that are at or near the surface within the observer's field of view (perception bias; McLaren 1961, Melville et al. 2008, Fleming and Tracey 2008, Laake et al. 1997, Marsh and Sinclair 1989). In theory, both types of biases have different values for photographic and visual surveys.

Photographic surveys take instantaneous images of the water's surface. In contrast, during visual surveys observers have a longer time period to monitor any given point at the surface within visible range, providing more time for submerged animals to come to the surface while within visible range. This difference would imply a greater correction factor for availability for photographic than for visual surveys. On the other hand, during photographic surveys, photo readers can take the time they need to carefully examine the recorded images, while observers during visual aerial surveys only have a given number of seconds to examine the water surface passing in front of them. This would imply a lower correction factor for perception bias for photographic than for visual surveys. For the SLE beluga photographic surveys, multiple readers examine the imagery and review each other's counts, thus reader interpretation is compared and a consensus count is determined (e.g., Gosselin et al. 2014).This method alleviates the need for a perception correction factor for photographic surveys. In the case of visual surveys observers operate independently, therefore, perception bias corrections need to be considered for abundance estimates to represent total population size.

The analysis of past aerial surveys (both photographic and visual) applied a correction factor for availability bias specifically developed for photographic aerial surveys of SLE beluga, with the probability of a whale being detectable at the surface of 0.478, or equivalent to the inverse correction factor of 2.09 also used in publications (Kingsley and Gauthier 2002, Gosselin et al. 2014, Gosselin et al. 2017). This correction factor was obtained by continuously counting the number of beluga visible at the surface from a helicopter hovering over a group and, in the case of photographic surveys, it was adjusted (i.e., 0.443 or equivalent to a crude correction factor of 2.26) to account for the typical overlap between consecutive photographs (30%) and the time interval between frames (16 s). When estimating abundance using visual survey data, using an availability correction developed for photographic surveys likely underestimated the availability of an animal during visual surveys, and thus biased abundance estimates upwards compared to photographic surveys. In a recent study, Lesage et al. 2023) developed an availability bias correction factor specific to SLE beluga using dive profiles and patterns obtained from 27 SLE beluga equipped with archival tags. This new correction factor takes into account the effects of environmental and behavioural factors on the availability for detection. In addition, Lesage et al. (2023) suggest correction factors based on different survey methods; one instantaneous correction factor suitable for photographic surveys, as well as a correction suitable for visual surveys which accounts for flight characteristics that impact the period of time a surfaced beluga could be sighted. These new, habitat-specific correction methods are likely to improve the accuracy of abundance estimates for the SLE beluga population.

To date, no correction for perception bias has been applied to SLE beluga visual abundance indices due to lack of data. During surveys conducted between 2001 and 2014, the number and position of the observers onboard the aircraft did not allow for the calculation of a perception bias correction factor based on mark-recapture distance sampling. Hence, abundance estimates published to date were only partially corrected (i.e., only for availability). During recent beluga surveys in James Bay and Eastern Hudson Bay using similar survey methods as those used in the SLE, the probability of detecting beluga at the surface during visual line-transect surveys was estimated between 0.392 and 0.601 (St-Pierre et al. In press). Hence, correcting survey estimates for perception bias may have a large impact on abundance estimates.

The present study presents results from photographic strip-transect and visual line-transect surveys of the SLE beluga population conducted since 2015, as well as a re-analysis of previous surveys (1990-2014) using the newly-estimated correction factors for both availability (photographic and visual) and perception biases (visual surveys only).

METHODS

STUDY AREA

The study area within the St. Lawrence Estuary was divided into two strata (Figure 1), and also included the Saguenay River from Tadoussac to St-Fulgence. The upstream stratum (hereafter "Main stratum") covered the major summer concentration of beluga in the SLE, which is centered at the confluence with the Saguenay River (Mosnier et al. 2010). Downstream of the Saguenay River this stratum is characterized by the 300 m deep Laurentian Channel in the northern half that rises to 40 m at the confluence of the Saguenay River, and a shelf less than 40 m deep with a few islands in the southern half. Upstream of the Saguenay River, this stratum is characterized by a channel with depths varying from 40 m to 140 m in the northern half, and a narrow channel reaching 40 m with wide 10 m banks along the coast and several islands in the southern half. The Main stratum is also characterized by a water turbidity and temperature gradient, with more turbid and warmer waters at the upstream end than at the downstream end. The effects of tidal currents are most noticeable at the confluence of the Saguenay River and the Estuary, and around islands and reefs, creating local variations in apparent Beaufort sea states affecting the detection of beluga. The downstream stratum of the St. Lawrence Estuary (hereafter "Downstream stratum") is used by beluga mainly outside of summer and is characterized by a wider extent of the Laurentian Channel, from Rimouski/Forestville to Pointe-des-Monts. The Saguenay River, in the area surveyed from Tadoussac to Saint-Fulgence, is a deep and relatively narrow (< 2 km) fjord reaching depths of 270 m and bordered by steep cliffs up to 300 m tall, creating wind channels and local variations in apparent Beaufort sea state and detection conditions.

PHOTOGRAPHIC SURVEYS

Photographic survey design

In surveys prior to 2019, two aircraft (e.g., Piper Navajo, Rockwell Aero commander, Piper Aztec, Cessna 414) flew a total of 49—57 transects spaced two nautical miles (3.7 km) apart, which crossed the Estuary on headings of 320° and 140° true. The two aircraft flew in opposite directions from a mid-starting point in the Main stratum to ensure complete coverage of the beluga main summer habitat without refueling. The two aircraft were equipped with 9 inch x 9 inch mapping cameras (cameras and measured film widths: e.g., Zeiss A15/23 229 mm x 229 mm; Zeiss Top 15, 230 mm x 230 mm; Wild RC 20, 229 cm x 229 cm; Wild-Leitz RC10 229 mm x 229 mm) loaded with colour positive film (e.g., Kodak 2448; Kodak 2427-0061-014, Agfa, Aviphot Chrome 200 PE1), and fitted with calibrated lenses (152.720 mm to 153.091 mm), filters (e.g., Clair A/V 124354, A2 + 36%; Clair 420 nm 2X), and a forward motion compensation system. Time between successive frames varied from 15 to 20 s depending on the survey, resulting in a forward photo overlap of 17 to 33% (Table 1). Target altitude was 1219 m (4000 ft) to ensure an approximate 50% coverage of the study area in all years except in 1990, when the study area was divided into three strata, with two of them having a lower coverage (see Kingsley and Hammill 1991 for details).

In 2019, photographic surveys were conducted using a single aircraft instead of two, and differed from previous surveys in the technology used and coverage. The discontinuation of colour positive films forced a change in technology toward digital imagery in 2019. That year, the photographic and visual surveys were flown simultaneously from the same aircraft (a de Havilland DHC-6-300 Twin Otter) with a line spacing of four NM instead of two NM as in previous photographic surveys resulting in about half the usual number of transects being flown (28—29 transects; Figure 1). However, the study area was flown four times instead of just once

as in previous photographic surveys. Images were acquired using two cameras (Nikon D800) with a 35 mm lens (Zeiss Distagon T 2/35) mounted in the belly of the Twin Otter, with the longest side perpendicular to the transect lines, each facing down at an angle of 25° from vertical, resulting in a slight overlap of the images under the plane. The Nikon Camera Control Pro 2.26 software on laptop computers (one per camera) was used to remotely operate the cameras and adjust the settings (shutter speed, aperture, and capture interval). Photographs were georeferenced for each camera via a cable adaptor to a GPS (Garmin GPSmap 78s). Capture interval was set to 3 s for a targeted photograph overlap of 39%. The Twin Otter was flown at the same target altitude (305 m or 1000 ft) and speed (185 km/h or 100 knots) as previous visual surveys to limit behavioural reactions of beluga to the passing aircraft. Note that this altitude was four times lower than for past photographic surveys. Strip width was ~800 m (i.e., ~400 m on each side of the plane), or approximately 44% of that produced using the large format film camera (~1826 m; Gosselin et al. 2014).

Only the Main stratum was photographed, i.e., the survey area that was consistently covered by previous photographic surveys (Figure 1). The Downstream stratum was surveyed visually only using a Partenavia P68C (see Visual Survey section).

Saguenay River counts

As in past photographic surveys, the Saguenay River was surveyed visually (using the Twin Otter in 2019) and was timed to minimize the delay between photographic and visual surveys of adjacent areas. Observers on each side of the plane recorded the number and position of beluga on both an upstream and a downstream pass between Tadoussac and Saint-Fulgence (Figure 1). Duplicate sightings were identified based on the sighting location recorded on the two passes, and a maximum displacement speed for a beluga of 10 knots. The maximum cluster size recorded between the two passes was retained for duplicate sightings. Animals that were only seen on one of the passes were added to the total number of animals observed.

Saguenay counts were considered total counts: the narrow search area, low water turbidity compared to most of the Estuary, longer detection time for visual as compared to photographic surveys, and double opportunity to count individuals during the upstream and downstream flights increased beluga availability in this sector. This total count was added to the abundance estimates calculated for the adjacent areas for each survey.

Photographic interpretation

All digital photographs were examined for beluga by two independent readers and each individual beluga was georeferenced in QGIS. Animals which were ≤ 0.5 the length of other beluga in the group were logged as calves. This category included both newborn and one-year old calves, as they could not be reliably distinguished from one another in the photographs. All photographs flagged as containing beluga were examined by a third reader, providing a third independent total and calf count for each photo. The total count for each photograph was obtained through consensus. For a small number of photographs (11%) where a consensus could not be reached among the three readers, and for all photographs in which calves were detected, a final calf and total count was made by a fourth and highly experienced reader and observer (J.-F. Gosselin, DFO). The proportion of calves (i.e., number of calves divided by total number of animals detected) was obtained for each survey day.

An R script was developed to geo-reference each image and calculate the footprint and overlap between photographs. Since the photographs were taken at an angle (i.e., low oblique photos), their resulting footprint was trapezoidal in shape (Grenzdörffer et al. 2008). The achieved footprint of each photograph was 109,010 m^2 (i.e., 400 m width by 195 m directly under the

airplane and 318 m at the outer edge of the strip). The achieved forward overlap was calculated for each frame by subtracting the overlapping area with the next one, while also accounting for lateral overlap (Appendix 1). Beluga located within the overlap portion of a frame were compared with those observed on the overlapping frames to ensure that there were no duplicates or new individuals. Transect width was calculated by doubling the mean distance between the vertical and outer edge of left and right images.

The effective survey coverage was estimated by summing the footprint area of each photograph and subtracting the overlap; the expansion factor was obtained by dividing the survey stratum area by the effective survey coverage.

Photographic data analyses

In surveys using colour film (1990—2009), the georeferenced unit was a sighting, i.e., all beluga within approximately 1—2 body length from each other forming a group. In 2019, each beluga was geo-referenced independently on digital images, requiring each sighting to be reconstructed and geolocated using the same definition (i.e., a sighting included all beluga located within eight m of each other).

Before moving to digital imagery, the proportion of each frame hidden by sun glare was estimated manually using overlaid acetate with a grid of 100 cells. In 2019, however, an automated method was developed by exploiting primary colors of light (RGB; i.e., red, green, and blue, with 0,0,0 and 256,256,256 representing black and white, respectively). After multiple tests, pixels where the red, blue and green layers all exceeded 200 were considered representative of glare “colour” (i.e., “burned” or overexposed area; see Appendix 2). The glare proportion was obtained by dividing the number of “glare” pixels by the total number of pixels in an image.

Availability bias correction

In past photographic survey analyses, a correction factor of 2.09 (SE=0.16) was applied to surface abundance indices to account for availability bias, i.e., animals have an availability, or probability of detection at the surface of the water of 0.478 (SE = 0.0625) given that some are under the surface (e.g., Gosselin et al. 2014). Given the heterogeneity of the SLE beluga habitat and the potential effect of behaviour on availability, a new approach to assess availability bias was developed using individual beluga diving data acquired using archival tags (see Lesage et al. 2023). Photographic surveys from 1990-2009 were reanalyzed using this approach, along with the new 2019 surveys. Each sighting was assigned a turbidity zone and seafloor depth value, and was geolocated as being either inside or outside of defined Areas of High Density (AHD, see Lesage et al. 2023). A sighting-specific availability bias estimate (*P)* was then simulated 5,000 times for each sighting using the best model identified by Lesage et al. 2023 (i.e., one that accounts for local turbidity, and incorporates as covariates information on the zone used, seafloor depth at the location of the beluga, and its location relative to AHDs). The 5,000 estimates of *P* were produced by resampling the model parameters with replacement (i.e., seafloor depth, Zone, AHD and a random effect accounting for tagged individuals). These availability bias values were then adjusted for the forward photo overlap and capture interval specific to each survey (Appendix 3) following Kingsley and Gauthier (2002):

$$\underline{P} = \frac{(1-2V)P+VP_D}{1-V} \qquad \text{[Eq. 1]}$$

where, $\underline{P}$ is the availability corrected for photo overlap (*V)*, and P_D is the probability of a beluga being imaged in at least one of two photographs taken 3, 6, 16, 19, 20, or 22 s apart depending on the survey, as estimated using tag data (Lesage et al. 2023).

Cluster size corrected for availability biases $\underline{E}$ was obtained using the 5,000 estimated $\underline{P}$ values as follows:

$$\underline{E} = E \cdot \frac{1}{\underline{P}} \quad \text{[Eq. 2]}$$

Calculation of abundance estimates via bootstrapping

For each of the 5,000 iterations, counts were summed per transect and corrected for glare. Since glare conditions were affected by time of day (sun height), wind and cloud cover, the glare correction was applied on a per transect basis.

The total count for each iteration was then scaled to the un-surveyed area using the expansion factor for the specific stratum to obtain an index of surface abundance for the Estuary (Table 1). The mean abundance was obtained from the 5,000 estimates. To account for the variance associated to the availability bias correction, the variance associated to the mean bootstrap estimate (σ_B^2) was calculated by the following formula :

$$\sigma_B^2 = var(V) + mean(\sigma_V^2) \quad \text{[Eq. 3]}$$

where *V* is a vector of the 5,000 abundance indices estimated by the bootstrap procedure, each of which has an associated variance estimate (σ_V^2). In photographic surveys, the variance σ_V^2 was estimated using the serial differences between transects including the finite population correction (Cochran 1977, Kingsley and Smith 1981) and estimated as:

$$\sigma_V^2 = \frac{f(f-1)k}{2(k-1)} \sum_{j=1}^{k-1} (n_j - n_{j+1})^2 \quad \text{[Eq. 4]}$$

where *f* represents the expansion factor for a specific survey, *k* represents the number of transects, *j* is a given transect and *n* is the total beluga count per transect. Finally, the total count obtained from the Saguenay River was added to the mean abundance.

When more than one survey was conducted during a year (e.g., 2019), a mean abundance estimate was obtained by weighting each survey estimate by its respective effort (i.e., total length of transect surveyed) and dividing by the total survey effort for that year. Variance was estimated using the delta method (i.e., the variance of a weighted mean of independent variables) as the sum of the products of the variances and the squared weights (where the weights summed to 1 for a given year).

VISUAL SURVEYS

Visual survey design

All visual surveys from 2001 to 2022 followed a systematic design with random placement of parallel lines oriented perpendicular (130° true) to the main axis of the estuary and a spacing between lines of 7.4 km (4 NM) in both the Main and Downstream strata (Figure 1). The Downstream stratum was only surveyed in 2007, 2009, 2018, 2019, 2021, and 2022. In each year, the strata were surveyed between one and 14 times. The Saguenay River was covered by two passes, from Tadoussac to Saint-Fulgence and back. The length of the transect lines (used to estimate density) and the area of each stratum (used to estimate abundance) were measured in either a GIS (ArcView 3.2, ESRI) or in R 4.2.2 (R Development Core Team 2018) with the package “sp” (Bivand et al. 2013), in both cases using the Lambert Azimuthal Equal Area (Canada) projection, with -68.77°W as the central meridian and reference latitude of 48.22°N. The Main stratum, measuring 4,531 to 5,787 km^2 depending on the year, was covered by 26 to 29 lines. The Downstream stratum, measuring 6,243 to 6,840 km^2 depending on the year, was covered by 7 to 16 lines, depending on line placement (Table 2, Figure 1).

Details regarding the aircraft used and flight characteristics of each survey year are presented in Table 2. In short, the aircraft used varied among surveys, between Cessna-337 Skymasters (2001- 2009, 2015, 2016, 2020, 2021, and 2022), Partenavia P68C Observers (2014, 2018, 2021 and 2022), and a DeHavilland DH-6-300 Twin Otter (2019). All aircraft were equipped with bubble windows in the observer seats except for the co-pilot seat in the Partenavia, which had a large window instead. The visual surveys were flown at a target speed of 185 km/h (100 knots) except for 2001 where 241 km/h (130 knots) was used. Surveys were flown at a target altitude of 305 m (1,000 ft), except in 2001 and in 2005 when a series of surveys were also conducted at an altitude of 457 m (1500 ft), as well as in 2007, 2016, and 2020 when surveys were flown at 198 m (650 ft), 183 m (600 ft), and 243 m (800 ft) respectively, as part of multi-species surveys. A single aircraft was used for surveys in 2001, 2003, 2005, 2009, 2014, 2018, 2019 and 2020, while two planes flying simultaneously over different lines were used in 2015, 2016, 2021, and 2022. In 2007 and 2008, two planes were used to fly the same lines with the second plane following the first plane a few minutes later to compare counts to assess the probability of detection on the track line, *g(0)* (Gosselin et al. 2014). Before 2005, position and altitude were recorded every two or 10 s from a GPS (D-GPS in 2005) output into a laptop computer with mapping software (Garmin GPS76, GPS Map 60c; D-GPS antenna from Prairies Geomatics; Fugawi versions 3.0 and 4.0) except for 2001, when GPS tracking was not used. Between 2005 and 2022, position and altitude were recorded every two seconds on a GPS (Garmin GPSMap 78s, Garmin GPSMap 64s, and/or BadElf Pro+).

The observers received line-transect sampling training on the ground prior to the surveys. All observers had aerial survey experience or field experience with marine mammals prior to their first survey. From 2001 to 2005, the observers used seats with bubble windows which were located in the back of the aircraft. Starting in 2007, the right-hand observer moved to the front seat (i.e., co-pilot seat), except in the Partenavia P68 aircraft in 2022, when the main observer on the right side was seated in the right rear seat. When more than two observers were onboard, the additional observer was considered as a secondary observer and their data were only used to calculate a perception bias correction factor (see section “Perception correction” below). All observers within an aircraft were isolated from each other visually and aurally.

Observers recorded beluga sightings as groups, defined as a group of individuals within 2-3 body lengths of each other. Observers measured the inclination angle to the centre of each group using clinometers (Suunto) and recorded the time when animals passed abeam of the aircraft. The relative bearing was recorded using an angle meter when inclination was measured for distant animals that were not abeam. The perpendicular distance of the animals from the plane was obtained from the inclination angle and the altitude using the formula by Lerczak and Hobbs (1998). Observers were instructed to give priority to the estimation of group size and time of observation, followed by inclination angle and then other variables, including animal behaviour and any changes in behaviour assumed to be a reaction to the approaching plane, if time permitted. The time recorded by each observer for beluga sightings and conditions was synchronized with the GPS. The position of each observation was then estimated using time and interpolation from consecutive GPS outputs.

Weather and observation conditions were recorded at the beginning of each transect, at regular intervals along the lines, and whenever changes in sighting conditions occurred. The conditions noted included sea state (Beaufort scale), subjective visibility (5 levels: excellent, good, medium, low, null), cloud cover (percent), angle of searching area affected by sun reflection (i.e., glare), along with sun reflection intensity (4 levels: 1- intense when animals were certainly missed in the center of reflection angle; 2- medium when animals were likely missed in the center of reflection angle, 3- low when animals were likely detected in center of reflection angle and 4- none when there was no reflection), and water colour (4 levels based on sediments in

suspension: 1-dark: clear with no sediment in suspension, 2- green, 3- light green and 4- beige: high concentration of sediments). All the information was recorded on digital voice recorders by each observer. Surveys were only initiated when sea conditions were Beaufort 3 or less, and when cloud cover was above the target altitude.

Saguenay River counts

As was done for the photographic surveys, the Saguenay River was covered by two passes (from Tadoussac to Saint-Fulgence and back) during almost all surveys of the Main stratum, using the same aircraft. As outlined above (see Photographic survey – Saguenay River counts section), the number and position of the observed beluga groups were recorded, and duplicate sightings between the first and second pass were identified. The total count was obtained as described above.

Counts in the Saguenay were not corrected for availability nor perception biases because of the narrow searching area, the curves in the plane trajectory which allowed observers to spend more time searching any given location, and the replicate passes (upstream and downstream). As was done for the photographic surveys, the total count of beluga seen in the Saguenay River (or average of total counts in years when the river was surveyed multiple times) was added to the average fully-corrected abundance estimate of the SLE strata.

Data preparation and analyses

Analysis of the visual survey can be separated into five steps, described in more details below: 1) data preparation by identification of outliers and truncation distances; 2) selection of the key function and covariates of the detection function; 3) application of the availability bias correction factor to each observation; 4) bootstrapping of the abundance estimates; and 5) application of the perception bias correction factor. These five steps were applied to each of the 14 survey years (2001 to 2022, Table 2), followed by the addition of the average count of beluga observed in the Saguenay River to the fully corrected abundance of the Main stratum, when applicable.

Analyses were completed using the perpendicular distances of observed beluga groups, without binning. For all analyses, the minimal statistical unit was an “observation” or “sighting”, which refers to a group of animals detected by an observer where group size is one individual or more. The survey flights were generally conducted with the same crew within a given year, and the weather-related criteria to fly the survey remained the same from the first to the last day each year. Therefore, a single analysis per survey year was used to estimate abundance in all strata, except in 2005 where the surveys flown at two different target altitudes were analyzed separately. Beluga abundance for each survey was estimated using a distance sampling approach and the package “mrds” (Laake et al. 2013) in R 4.2.2 (R Development Core Team, 2018).

The overall distribution of perpendicular distances was examined to determine if right truncation was necessary to discard outliers far from the track line because large gaps sometimes appeared among observations made at the greatest perpendicular distances. Five potential right truncation distances were tested: 1) no truncation; 2) removal of the observations with distances greater than that of an obvious gap in the observed perpendicular distances; 3) removal of 10% of the furthest observations from the track line; 4) removal of outliers based on a boxplot analysis; and 5) removal of observations with distances greater than the perpendicular distance at which the detection function from a hazard rate model reached a probability of detection of 0.15 (Buckland et al. 2001). For each survey year, the right truncation distance which improved the fit of the detection function near the track line, while maintaining good overall fit by maximizing the *p* value of the Cramér-von Mises test, was applied (Buckland et al. 2001).

Generally, line transect surveys assume maximum probability of detection on the track line but, because there may a blind area underneath the plane depending on the type of aircraft and size of bubble windows used, this assumption is not always met. This can be corrected for by applying a left truncation to the data (Thomas et al. 2009) to discard observations with perpendicular distances shorter than that at which the maximum probability of detection is estimated. Although this was done for previous analyses of visual survey data from the SLE, no left truncations were applied in the present study. Instead, to fit the reduced number of detections near the track line, a gamma key function was tested during detection function selection (Laake et al. 2013; see below). This approach is more objective than applying a left truncation to the data and allows the complete use of the raw data.

Choice of detection function

For each survey year, model selection and inclusion of covariates followed the stepwise procedure detailed in Marques and Buckland (2003). In short, half-normal, hazard-rate, and gamma key function models, with and without adjustment terms, were fitted to the right truncated distribution of the ungrouped perpendicular sighting distances, and the model with the lowest AIC was selected as the key function. Using the selected key function, we examined if AIC could be reduced further (ΔAIC >2) by the addition of one of the following covariates: group size, observer identity (2 to 7 each survey year), sea state (Beaufort: 0 to 4), glare intensity (4 levels: Intense, medium, low, none), cloud cover (%), water colour (4 levels: dark, green, light green, and beige) and visibility (5 levels: excellent, good, medium, reduced, none). The four variables for sea state, glare intensity, cloud percentage and visibility are not independent and, therefore, were never combined in the same model. In 2001 and 2003, glare intensity, cloud percentage, water colour and visibility were not collected systematically, and were therefore not used in model selection. In 2005, water colour and visibility were not systematically collected and were not used in the analyses. If AIC was significantly reduced by the addition of a covariate (ΔAIC >2), the model with the covariate was retained if it also satisfied the following additional conditions: 1) if the addition of the covariate only affected the scale and not the form of the detection function (e.g., covariate was not included if its addition created a new spike compared to the key function or previous step's model); and 2) if < 5% of the estimated probabilities of detection of sightings were < 0.2 and none were < 0.1 (Buckland et al. 2001). The addition of a second covariate into the model was tested and retained only if it improved the AIC by > 2 while still respecting the above conditions.

In some cases, observations lacked a perpendicular distance measurement. This usually occurred when high beluga densities were encountered over a short period of time, during which observers did not have sufficient time to record detailed information about all groups and were instructed to prioritize recording group size. These observations were not used for the selection of the detection function. However, observations without a recorded perpendicular distance measurement were assumed to be within truncation distances, as the effective searching width was expected to be narrower at higher densities. We assumed that the observations without perpendicular distance followed the same distribution as the observations with distance measurements. To include these observations without distances in the estimates of density and abundance, we assigned a randomly-selected perpendicular distance from the distribution of perpendicular distances observed within the same survey to each observation with a missing distance during bootstrapping (see below).

Availability bias correction

An availability bias occurs when observers cannot detect whales because the animals are diving below depths at which they can be seen. Hence, the number of animals recorded by the

observers is an underestimate. In this study, the group size of each observation, was corrected to account for this bias using the approach described in Lesage et al. (2023).

In short, the availability depends on beluga surface intervals and dive durations, and the amount of time a point at the surface of the water at a perpendicular distance *x* from the track-line remains within observer's view. The availability correction factor is calculated as (equation 4 in Laake et al. 1997):

$$a(x) = \frac{s}{s+d} + \frac{d\left[1-e^{-w(x)/d}\right]}{s+d} \quad \text{[Eq.5]}$$

Where *s* is the surface interval, and *d* is the dive duration. The value of *w(x)* is the time period that a point at the surface of the ocean at a perpendicular distance *x* from the track line remains in the field of view of the observers, given a conical field of view on each side of the aircraft, limited horizontally forward by an angle Φ_1 and backward by an angle Φ_2, given plane speed *v* and perpendicular distance *x* of the sighting (Forcada et al. 2004, Gómez de Segura et al. 2006), such that:

$$w(x) = \frac{x}{v}\left[cot\left(\emptyset_1\right) + cot\left(\emptyset_2\right)\right] \quad \text{[Eq. 6]}$$

The obstructed field-of-view forward and backward varied with the type of aircraft and were 30° forward and 20° backward for the Partenavia and Cessna 337, and 5° each in the case of the Twin Otter.

The values of *s* and *d* were modelled as a function of the surface and dive durations obtained from tag data, and environmental covariates (Lesage et al. 2023). For visual surveys, the availability bias accounted for the variation in turbidity within the beluga summer habitat, and was estimated using a null model for *s* (i.e., no environmental covariates) and a model including seafloor depth, turbidity zone, and location relative to areas of high densities for *d*. The few sightings with missing perpendicular distances were allocated a geolocation using preferably double-platform observation data; if unavailable or uncertain, they were given the default value of 0 m (i.e., directly underneath the aircraft) (see Lesage et al. 2023). To quantify the variance of the availability bias corrections, 5,000 availability bias estimates and corrected group sizes were produced for each sighting in each survey using a bootstrap procedure. These 5,000 estimates per sighting were then used in the bootstrap procedure applied to the abundance calculation (see below).

Calculation of abundance estimates via bootstrapping

In distance sampling analyses, the estimated indices of density ($\widehat{D_i}$) and abundance ($\widehat{N_i}$) of beluga at the surface during each systematic survey of each stratum, *i*, are estimated using the following equations (equation 3.67 in Buckland et al. 2001).

$$\widehat{D_i} = \frac{n_i \cdot \hat{E}_i(s)}{2L_i \cdot \widehat{ESHW}} \quad \text{[Eq. 7]}$$

$$\widehat{N_i} = \widehat{D_i} \cdot A_i \quad \text{[Eq. 8]}$$

where n_i is the number of groups detected, $\hat{E}_i(s)$ is the expected cluster size, L_i is the sum of lengths of all transects, and A_i is the area of the stratum *i*. The estimated effective strip half-width ($\widehat{ESHW}$) is estimated from the selected detection function (see above, "Choice of detection function"). In theory, the associated variance of density and abundance of animals at the surface during the systematic survey is estimated by the following formula:

$$\widehat{var}\left(\widehat{D_i}\right) = \widehat{D_i}^2 \cdot \left[\frac{\widehat{var}[(n/L)_i]}{(n/L)_i^2} + \frac{\widehat{var}(\widehat{ESHW})}{(\widehat{ESHW})^2} + \frac{\widehat{var}[\hat{E}_i(s)]}{[\hat{E}_i(s)]^2}\right] \quad \text{[Eq. 9]}$$

$$\widehat{var}\left(\widehat{N}_i\right) = A_i^2 \cdot \widehat{var}(\widehat{D}_i) \quad \text{[Eq. 10]}$$

In our case, the corrected group size obtained by applying the availability bias correction factor has an inherent variance associated with it, which needs to be incorporated into the variance of the abundance estimates. To that effect, a bootstrap procedure was used to calculate abundance estimates for each stratum in each survey year. In each of 5,000 bootstrap iterations, the algorithm used the following three steps. First, each observation recorded without a perpendicular distance was assigned a distance randomly from the distribution of observed distances within the same survey year. Second, for each observation, one value of availability bias was extracted randomly from the set of 5,000 values (extracted from models of surface and dive duration, see Lesage et al. 2023) and used to calculate a corrected group size. Lastly, the detection function previously selected for a given survey (key function and associated covariates, if any) was applied to the newly created dataset of observations with corrected group size. Estimates of abundance, density, encounter rate, expected group size, probability of detection ($\hat{P}$), and *ESWH* were obtained per stratum from the detection function applied to the newly created dataset for each iteration, with associated variances for each estimate.

Abundance indices per survey and stratum were calculated (separately for each survey pass for years when a given stratum was surveyed multiple times) as the mean of the abundances obtained via the bootstrap procedure. To account for the variance associated to the availability bias correction, the variance associated to the mean bootstrap estimate (σ_B^2) was calculated by the following formula :

$$\sigma_B^2 = var(V) + mean(\sigma_V^2) \quad \text{[Eq. 11]}$$

where *V* is a vector of the 5,000 abundance indices estimated by the bootstrap procedure, each of which has an associated variance estimate (σ_V^2) calculated by the software using equation 9. For density, encounter rate, expected group size, probability of detection ($\hat{P}$), and *ESWH,* the mean of the bootstrap estimate per survey and stratum is presented, with associated bootstrap 95% confidence intervals derived using the percentile method.

For each survey year, the abundance index for a given stratum was obtained by taking the average of the abundance indices from all passes of that stratum. The associated combined variance was calculated via the delta method. The total abundance index and its variance for a given survey year was calculated as the sum of the average abundance indices from the Main and Downstream strata.

Perception bias correction

Surveys in 2015, 2016, 2019, 2021, and 2022 were conducted using a double-platform configuration to estimate perception biases, with a secondary observer positioned on the right side of the plane in addition to the two primary observers always positioned on the left and right of the aircraft. The two right-sided observers were seated a few meters apart and isolated from each other visually by an opaque curtain and aurally by headset intercom while searching the same area. Hence, these observers were considered as two independent platforms and their observations were used to estimate perception bias correction factors via mark-recapture distance sampling (MRDS) analyses (Laake and Borchers 2004). All observations made by observers on the right side of the plane while both observers were actively searching for animals (i.e., “on effort”) were used for this analysis. In 2015, 2021 and 2022, only one of the two aircraft flying simultaneously had a double-platform configuration. Observations made by the observer on the left side of the aircraft were not used for MRDS analyses. All MRDS analyses were performed in R 4.2.2 (R Development Core Team 2018) with the package “mrds” (Laake et al. 2013).

Prior to conducting MRDS analyses, duplicate sightings, i.e., groups of animals detected by both the primary and secondary observers, were identified through coincidence in location based on: 1) the difference in time of recording, and 2) the difference in clinometer measurement. Species identity was also used as a criterion in duplicate identification, meaning that both sightings needed to have the same species recorded to be considered duplicates. However, only beluga sightings were used for the MRDS model and estimation of the perception bias. In the primary literature, time thresholds used in surveys of cetacean species generally vary from 3 to 10 s, while clinometer thresholds generally range from 5 to 15° (e.g., Pike and Doniol-Valcroze 2015, Pike et al. 2008, Panigada et al. 2017, Lambert et al. 2019). Based on the previous surveys using the same protocol and aircraft (St-Pierre et al. In press) and expert opinion, thresholds of 10 s and 10° were selected for identifying duplicates for all survey years. It was considered that these thresholds were the most likely to capture true duplicate sightings while minimizing the number of false duplicates. For observations with missing clinometer values, only the time threshold was considered.

Because MRDS analyses require that perpendicular distance and covariate values be identical for a given duplicate sighting, we attributed an average value (for numeric covariates, i.e., perpendicular distance, cluster size, cloud cover, and Beaufort, although the latter was converted as a categorical factor after averaging) to these variables for the observations identified as duplicates if the two observers had recorded different values. The average perpendicular distance was used for distance analyses. For categorical covariates (i.e., glare intensity and visibility), duplicates for which the two observers had recorded different values were assigned the value with the greatest negative effect on one's ability to observe animals (e.g., if one observer recorded visibility as good and the other recorded visibility as low, the latter value was assigned for this duplicate sighting).

MRDS analyses consist of two functions: 1) a multiple covariate distance sampling (MCDS) detection function for detections pooled across the two right-side observers, and 2) a MRDS detection function to estimate the probability of detection on the track line (Buckland et al. 2001, Buckland et al. 2009). Both functions used the same right truncation distances as those identified during the analysis of the single-platform dataset of their respective survey (see "Choice of the detection function" section). For the MCDS function, AIC was used to select between half-normal, hazard-rate, and gamma key functions, and to examine if the addition of covariates (group size, Beaufort state, glare intensity, cloud cover, and visibility) yielded a better fit following the procedure outlined in Marques and Buckland (2003). The key function and covariates yielding the lowest AIC in the MCDS detection function were used in the MRDS models. The latter were built with and without covariates and compared using AIC. A point independence configuration was applied in the MRDS models because detection probabilities may be correlated between observers even though the primary and secondary observers acted independently and were isolated from each other. For example, detection probabilities could be correlated to factors like group size if both observers are more likely to detect larger groups than smaller groups as distance increases. This configuration assumes that platforms are symmetrical and that sightings are independent only on the track line, which is more robust then a configuration assuming independent detection at all perpendicular distances (Buckland et al. 2009, Burt et al. 2014). By definition, perpendicular distance is included as a covariate in all point-independence MRDS models (Buckland et al. 2009). The best fitting MRDS model was selected and used to estimate the perception bias *p(0)* for each observer position. Estimates of *p(0)* for the primary observer were then used to correct the abundance estimates calculated using data from the primary observers, assuming that *p(0)* was the same for primary observers on the right and left side of the aircraft, using the following formula:

$$corrected\ abundance = abundance \cdot \frac{1}{p(0)} \qquad \text{[Eq. 12]}$$

Perception bias was calculated separately for the 2015, 2016, 2019, 2021, and 2022 surveys to yield a survey-specific value of *p(0)*. Because surveys prior to 2015 and in 2018 were flown as single platforms, no survey-specific perception bias estimates could be calculated for these surveys. Instead, these surveys were corrected using an average *p(0)* based on surveys where double-platform data were available.

COMPARISONS WITH PREVIOUS METHODOLOGY

Photographic surveys

For comparison purposes, the 2019 photographic surveys were also analyzed using the previously accepted methodology (see Gosselin et al. 2014 for details). Briefly, cluster sizes detected on photographs (uncorrected for availability bias) were summed over all transects, then multiplied by an expansion factor estimated as the transect spacing divided by the strip width to obtain a surface index per stratum. This surface index was first corrected for availability bias assuming a 16 s photo capture interval and 30% photo overlap, i.e., 0.478 or equivalent to a 2.09 (SE = 0.16) correction factor (as per Kingsley and Gauthier 2002), to which was then added the Saguenay River counts to get a population abundance index.

In previous assessments the variance was estimated differently from the current study whereby the serial differences in counts between adjacent transects, including the finite population correction was used (Cochran 1977, Kingsley and Smith 1981). In that approach, squared differences in counts between adjacent transects were summed, while accounting for surveyed area and number of transects flown.

Visual surveys

In previous analyses of the visual survey data collected between 2001 and 2014, the detection function for each survey year was based on a hazard-rate or half-normal key function applied to left-truncated data to account for the blind spot under the aircraft. The variance of the surface abundance estimates was calculated based on information from Buckland et al. (2001), as detailed in Gosselin et al. (2014, 2017). This surface index was then corrected for availability biases using a probability of detection at the surface of 0.478 from Kingsley and Gauthier (2002) with the associated variance calculated as the combined variance from the surface index and the correction factor. The Saguenay River counts were then added to the abundance index, but no perception bias correction was applied.

RESULTS

PHOTOGRAPHIC SURVEYS

Survey completion

The four replicates of the 2019 photographic survey were carried out on four consecutive days, on 13—16 August 2019, between 11h42 UTC and 20h41 UTC (7h42 and 16h41 local time) when sun elevation was > 30° in the morning, within the prescribed 30° at the end of surveys on 15 and 16 August, but below this level on 13 and 14 August (18° and 22°, respectively). The hourly wind speed recorded at Rivière-du-Loup, in the centre of the survey area, on these dates between 7h00 and 17h00 was consistently ≤ 8 km/h (Environment Canada, climate data online).

The survey was completed as planned on the 15 and 16 August. On 13 August, although all transects were flown, problems with the cameras resulted in variable capture intervals and image overlap, and parts of some transects being photographed using a single camera

(Appendix 4). On 14 August, four transects downstream of the Saguenay River were flown almost entirely with a single camera active, or were only partly covered. As a result, the achieved capture interval and overlap between adjacent frames (unflown areas not included) was on average 6 s and 29% on 13 August, and 3 s and 37—39% on 14—16 August. While 10,062 and 9,846 photos were taken on the 15 and 16 August, only 6,700 and 8,836 were taken on 13 and 14 August. Overall, between 9.8—11.1% of the Estuary was photographed, resulting in expansion factors of 9.72, 10.19, 9.03 and 9.09 for the 13, 14, 15 and 16 August 2019, respectively.

The Saguenay survey was flown on each survey day, within 2—3 min from the passage of the plane in front of the entrance of the fjord on each survey day. The number of beluga seen in the Saguenay was 18, 46, 23, and 84 for the 13, 14, 15, and 16 August 2019, respectively.

Photographic reading

All 35,443 frames were examined by two readers, of which 199 frames contained one or more beluga. Reader 1 and 2 counted a similar number of beluga (340 versus 343, respectively), although differences in interpretation actually occurred for 31 frames. After interpretation by the third reader and subsequent discussions, duplicates were removed and 272 images were accepted as beluga. Counts on the 13 August were approximately half those obtained during the following three surveys (36 versus 76—82 individuals) (Figure 2; Appendix 5). No beluga were counted on the first 3—7 downstream lines nor the last 2—7 upstream lines on neither of the survey days (Appendix 5). Glare varied throughout the day with a mean glare correction of 2.6—3.7% on 13—15 August, and 8.0% on 16 August (Appendix 5).

Abundance estimates from photographic surveys

The 5,000 estimates of cluster size, corrected for location-specific availability biases, photo overlap, and glare produced an estimate of 1,022—2,801 beluga present at the surface during these surveys, once the corresponding expansion factor was applied to bootstrap counts per transects (Table 1). The addition of individuals seen in the Saguenay to these estimates resulted in a mean total estimate of 2,119 beluga in 2019 (SE = 267; Table 1).

Proportion of calves

The proportion of small individuals, which includes newborn calves as well as yearlings still accompanied by a female, was consistent among three of the four surveys at around 6.4—8.3%, and was higher on 14 August at 14.6%, for an average of 9.0% in 2019 (Table 1). The proportion of calves among the photographed animals appears to have declined over time, with calves comprising 15.1% to 17.8% of the photographed animals during the 1990—1997 surveys, and 3.2% to 9% since 2000 (Table 1).

VISUAL SURVEYS

Survey completion

From 2001 to 2022, 52 visual line transect surveys of the Main stratum between Rimouski/Forestville and Île-aux-Coudres were completed between the end of July and early September (Table 2). Starting in 2007, 14 surveys of the Downstream stratum between Pointe-des-Monts and Rimouski were completed over 8 survey years between the end of July and early September (Table 2). Surveys of a single stratum were completed within a day in all survey years except in 2016, when the Downstream stratum was covered in two days, and in 2022 when both strata were covered on two days within a 2-week period due to inclement

weather. The spacing between lines for visual surveys was always 7.4 km (4 NM) in the Main stratum, but the area covered increased over the years to consider the possible expansion of beluga summer range. Therefore, 24 lines were flown in 2001, the area of the Main stratum was extended in 2003 leading to 26-27 lines flown from 2003 to 2008, and extended again in 2009 leading to 28-29 lines flown from 2009 to 2022 (Table 2, see also Gosselin et al. 2007; 2014; 2017). Small variations in total transect length are also present among years, due to the random placement of the systematic transect lines. The line spacing in the Downstream stratum was 18.5 km (10 NM) in 2007 and 2016, but 7.4 km (4 NM) in all other survey years. Survey results from 2001 to 2014 have already been presented (Lawson and Gosselin 2009, Gosselin et al. 2007, Gosselin et al. 2014, Gosselin et al. 2017), but they have been reanalyzed here, using the new approach for availability bias correction and gamma key functions where appropriate.

Beluga sightings

In the Main stratum, an average of 90 groups (219 individuals) were observed for equivalent effort (i.e., weighted by total effort for each survey), with a wide range of 23-153 groups (39-393 individuals) observed during the 52 surveys (Table 2, Figure 3, Appendix 6). Groups with distance measurement not recorded occurred on 27 of the 52 surveys, ranging from 1-48 groups (1-143 individuals in total; Table 2). These groups with missing distances represent between 0.4 and 47% of the individuals observed in a given survey.

In the Downstream stratum, an average of 4 groups (22 individuals) were observed for equivalent effort, with a range of 0-24 groups (0-140 individuals) during the 14 surveys (Table 2, Figure 3, Appendix 6). Groups with missing distance measurements occurred in only one of the surveys (3 groups or 4 individuals, 5% of the individuals observed; Table 2). Of the 14 Downstream surveys conducted, beluga were observed in only eight of the surveys.

Detection curve

The distributions of the perpendicular distances for each year (and at each altitude in 2005) showed variability in distances and number of outliers among years. The right truncation distance applied varied among years, with the shortest distance used being 1350 m in 2020, and no truncation used in 2001, 2007, 2009, and 2016. An average of 3.2% (range 0 to 9.9%) of the sightings were discarded by right truncation, leaving 44 to 709 each year for estimating the detection function (Table 3; Appendix 7).

In most survey years, the gamma key function provided the best fit of the detection function to the data (Table 3). Only in two survey years (2019 and 2022) did a hazard-rate key yield a better fit than the gamma key function, based on comparison of AIC. The addition of covariates to the detection function improved model fit in all but three survey years (2003, 2008, and 2022; Table 3). The covariates selected varied among years, with Beaufort (five survey years), observer (seven survey years), water colour (one survey year), glare intensity (three survey years), cluster size (one survey year), and cloud cover (one survey year) being selected. The selected models yielded effective strip half-width (ESHW) values ranging from 705 m in 2001 to 1433 m in 2005 (at an altitude of 457 m; Table 3).

Expected group size

Raw group size was tested as a covariate in the detection functions, and was selected as an informative covariate on one occasion. Based on bootstrap results, the expected average group size corrected for availability bias and calculated for each stratum and survey pass, varied from 3.07 to 15.24 in the Main stratum over the 52 surveys (average of 5.62), highlighting how variable clumping can be among surveys (Table 4). In the Downstream stratum, expected group

size varied from 1.50 to 61.79 in the 9 out of 14 surveys in which beluga were observed (average of 13.05; Table 4). The group sizes observed by the primary observers varied among years, and are presented in Appendix 8.

Encounter rate

Total survey effort (km of transects flown) in the Main stratum between Rimouski and Ile-aux-Coudres varied among surveys depending on the placement of the transect lines within the survey area, averaging 757 km except in 2007 and 2008 when effort was doubled (i.e., two airplanes flying over the same transect within minutes of each other). The area of the Main stratum was increased after the 2001 survey, and again after the 2008 survey, by adding transect lines to better cover the distribution of high summer density areas of SLE beluga. However, in all surveys, the observed beluga distribution remained within the central portion of the surveyed area, with fewer sightings on lines at the extremities of the stratum. The mean encounter rate per survey, as estimated by the bootstrap procedure, ranged from 0.130-1.217 animals per km of transect in the Main stratum, with a mean of 0.578 over the entire time series (Table 4).

The total survey effort in the Downstream stratum also varied among surveys, depending on the placement of transect lines and the number of transects completed within the survey area, ranging from 311-854 km flown. The mean encounter rate per survey in this stratum ranged from 0.002-0.455 animals per km of transect, with a mean of 0.101 over the entire time series (Table 4).

Perception bias estimate

A double-platform configuration, used to estimate perception bias, was only available in five survey years within this time series (2015, 2016, 2019, 2021, and 2022). As indicated previously, duplicate sightings between the primary and secondary observers on the right side of the planes were based on coincidence in location, using time and clinometer thresholds of 10 s and 10°. Only observations taken while both observers were on effort were considered for this analysis. In each survey year used for perception bias analysis, less than 3% of the duplicate matches were considered ambiguous (e.g., an observation by the primary observer having a possible match with multiple secondary observations, where the choice of pairs had an impact on the number of duplicate pairs assigned) and needed to be assigned manually.

From the 2015 data, 73 unique beluga sightings were recorded by the observers on the right side of the plane. Of these, 29 sightings were identified as duplicates between the primary and secondary observers. Using the same right truncation distances as the detection function for the 2015 survey (see above and Table 5), the MRDS analysis identified a model with a Gamma key function (without adjustment) and no covariates as the best fitting model. This model yielded a perception bias estimate or primary *p(0)* of 0.593 (CV = 19.9%, Table 5). This primary *p(0)* was used to correct the 2015 abundance indices.

From the 2016 data, 120 unique beluga sightings were available for estimating *p(0)*. Of these, 14 sightings were duplicates. Using the same truncation distances as the detection function for the 2016 survey (see above and Table 5), a MRDS model with a Gamma key function (polynomial adjustment) and glare intensity and cloud cover as covariates was identified as the best fitting model, yielding a primary *p(0)* of 0.142 (CV = 47.3%, Table 5). This perception bias estimate is unrealistically low, likely as a result of the inexperience of the secondary observers that year, who were on their first day of surveying. Therefore, the primary *p(0)* calculated from the 2016 data was discarded. The average *p(0)* (see below) was applied in 2016, as for years in which double-platform data were lacking.

The 2019 double-platform data from the Twin Otter yielded 277 unique beluga sightings, of which 89 sightings were duplicates. Using the same truncation distances as the detection function for the 2019 survey (see above and Table 5), a MRDS model with a hazard-rate key function (without adjustment) and cloud cover, visibility and water colour covariates was identified as the best fitting model. This model yielded a primary *p(0)* of 0.514 (CV = 12.8%, Table 5). This primary *p(0)* was used to correct the 2019 abundance indices.

In 2021, only 3 unique beluga sightings were recorded by the observers on the right side of the plane, of which 2 were duplicates. Due to the low number of observations, an MRDS model could not be applied (Table 5). Therefore no perception bias estimate was calculated from the 2021 data.

In 2022, 15 unique beluga sightings were recorded by the observers on the right side of the plane, of which 7 were duplicate sightings. Using the same truncation distances as the curve for the 2022 survey (see above and Table 5), a MRDS model with a half-normal key function (without adjustment) and no covariates was identified as the best fitting model. This model resulted in a primary *p(0)* of 0.748 (CV = 23.2%, Table 5), which was used to correct the 2022 abundance indices.

Only the primary *p(0)* from the 2015 data and the 2022 data were used to estimate an average perception bias estimate, for application to surveys without a double-platform configuration, and for 2016 when the double-platform data were discarded. The average primary *p(0)* for these two survey years was 0.670 (CV = 27.5%, Table 5). The primary *p(0)* calculated from the 2019 data was not included in this average because of the use of a Twin Otter aircraft that year, a platform which offers a different field of view compared to the smaller aircrafts used in all other years (Cessna 337 and Partenavia).

Saguenay River counts

The Saguenay River count, considered to be a total count, can represent up to 15% of the abundance estimate (after correction for both availability and perception biases), but accounted for only 1.9% of the fully corrected abundance estimate on average. The number of beluga in the Saguenay River can change from day to day, as was seen in August 2005 (Table 6) and ranged from zero (on several occasions) to a high of 163 animals in 2022.

Abundance estimates from visual surveys

In the Main stratum, abundance indices per survey corrected for availability bias only ranged from 358 animals (2009, pass 4) to 3,504 animals (2018, pass 2; Table 6). In the Downstream stratum, the same partially corrected abundance indices ranged from zero (multiple surveys) to a maximum of 1,827 animals (2018, pass 2; Table 6). Correcting these indices for perception bias increased these values by 55% on average, leading to fully corrected abundance estimates of 556 to 5,717 animals in the Main stratum (including the Saguenay River counts), and of 0 to 2,727 animals in the Downstream stratum (Table 6). The highest abundance estimate in the Downstream stratum was observed in 2018 during the second pass as a result of the observation of two very large groups (raw group sizes of 75 and 60 animals; ~215 and ~169 after correction for availability, respectively) which were detected on the same transect line. These groups were unusually large, being 18-23 times greater than the average raw group size across all other surveys of the Downstream stratum, and 3.8-4.7 times larger than the third largest group seen in that stratum (16 individuals, in 2021).

Summing mean abundance estimates from the two strata yielded final and fully corrected estimates for the population, ranging from 1,257 animals in 2022 (CV: 31.8%, 95% CI: 684-2,311), to 4,981 animals in 2018 (CV: 23.9%, 95% CI: 3,138-7,907; Table 6).

COMPARISON OF PHOTOGRAPHIC AND VISUAL SURVEYS

Mean abundance estimates from visual surveys were consistently higher than for photographic surveys once fully corrected for both availability and perception biases (Figure 4). The variance associated with visual surveys also generally exceeded that of photographic surveys, except in years with multiple repeats of the visual survey.

Photographic and visual surveys were only conducted simultaneously, from the same aircraft, in 2019. This provided an opportunity to compare results from both survey methods more directly, but also constrained the coverage of the photographic survey given the need to accommodate the visual survey design by flying at a low altitude and maintaining a 4 NM distance between transects of 4 NM. For both survey types, the first pass of the 2019 surveys (August 13th) yielded the lowest abundance estimates and the second pass (August 14th) yielded the highest. The fully corrected 2019 abundance estimate for all survey passes combined was slightly higher for the photographic survey (2,119, CV: 12,6%, 95% CI: 1,657-2,710) than for the visual survey (1,957, CV: 16.7% 95% CI: 1,414-2,709).

COMPARISON WITH PREVIOUS METHODOLOGY

For the photographic surveys, abundance estimates obtained using the previously accepted approach, where a 2.09 availability correction factor (corresponding to a 0.478 availability bias estimate) was applied *a posteriori* on surface indices, were consistently lower than estimates obtained using our new method (Figure 4). The 0.478 availability estimate was calculated for a photo overlap of 30% and capture interval of 16 s, a condition that has not been consistent among surveys (Appendix 3). In 2019 for instance, overlap (36–39%) and capture interval (3–6 s) strongly deviated from these values. The availability study using tag data indicated a 6.0–9.7% decrease in the probability of photographing a beluga in at least one of two consecutive frames when the capture interval decreased from 16 s (0.371) to 3–6 s (Lesage et al. 2023). Adjusting the 2.09 availability correction for this and for the higher photo overlap in 2019, resulted in a 6–9.7% decrease in availability, or correction factors of 2.21—2.26 depending on the survey. Even after adjustments for these more realistic survey conditions, abundance estimates using the previously accepted approach remained lower than those obtained using the new method (Figure 4, see estimates for 2019).

For the visual surveys, comparing the surface abundances from 2001 to 2014 calculated using the left-truncation method with hazard-rate or half-normal key functions with those obtained using a Gamma key function without left truncation, we observed a better fit of the detection function to the data but varying effects on the surface abundance indices. For example, using the new analysis resulted in a 2-67% increase in surface abundance indices (average of 24% compared to the traditional approach) in 27 surveys, but a 2-46% decrease (average 18%) in 10 other surveys (data not shown). The new method for estimating the availability bias applied here (developed by Lesage et al. 2023) led to an increase in abundance indices of 15% on average compared to using the fixed availability correction factor of 0.478 (Kingsley and Gauthier 2002, Lawson and Gosselin 2009, Gosselin et al. 2007, Gosselin et al. 2014, Gosselin et al. 2017) (Table 7), except in 2005 and 2019, where the new method led to a decrease in availability of ~4% and 32%, respectively. In past survey analyses, no perception bias correction were applied, but their use in the present study yielded fully corrected abundance estimates which were 1.5 to 2 times greater than abundance indices corrected only for availability (Table 7).

DISCUSSION

Since 1990, a considerable time series of photographic (11 surveys in 8 survey years) and visual surveys (52 surveys in 14 survey years) has been built for estimating SLE beluga

abundance and population trends. The survey effort for both the photographic and visual surveys (covering approximately 50% and 12% of the survey area, respectively) is considered exemplarily high for surveys of marine mammal populations. While past analyses were adequate to produce abundance indices for the SLE beluga population, the current study represents a major step forward, not only in improved precision and accuracy of abundance estimates, but also for understanding the caveats associated with applying different methodological and analytical approaches to aerial survey data.

One of the methodological changes applied to the visual survey analysis was the use of a Gamma key function in model selection for the detection function. Previous studies of beluga and other cetacean species have generally applied either a hazard-rate or half-normal key function, as was standard for such analyses given the available tools (Buckland et al. 2001, Thomas et al. 2009). Recently, the Gamma key function has been made available within the R packages dedicated to distance-sampling analysis (Laake et al. 2013). This key function has the advantage of better fitting data for which the maximum detection probability is not on the trackline – as is the case for aerial surveys using aircraft which have a blind spot under the plane. The use of a Gamma key function eliminates the need for left-truncation, which is generally required to meet the assumption that maximum detection probability occurs on the trackline (Buckland et al. 2001). Thus, compared to the half-normal of hazard-rate, the Gamma key function yields a more objective fitting of the data, while retaining all observations made close to the plane in the analysis.

The availability correction factors applied in the present study differed from past analyses in that they were developed specifically for the study area by accounting for heterogeneity in environmental and behavioural factors affecting the detection of beluga at (or near) the water's surface (Lesage et al. 2023). These new correction factors were applied to each individual observation based on its position and, in the case of visual surveys, the characteristics of the aircraft (affecting observer's field of view) and perpendicular distance of the sighting from the aircraft. The correction factors were also specific to survey conditions during photographic and visual surveys, i.e., reflecting the instantaneous versus prolonged detection time available for these two types of surveys, respectively. The new correction factor for photographic surveys was generally higher than the previous instantaneous correction which was derived from observing the appearance and disappearance of groups of beluga from a hovering helicopter (Kingsley and Gauthier 2002). In the Kingsley and Gauthier (2002) study, two factors may have led to an overestimation of availability and, thus, a lower correction factor: 1) the assumption that surface behaviour was synchronous within a group, as the authors used the maximum number of beluga simultaneously visible at any one time as a metric for group size and availability (i.e., to estimate the proportion of individuals visible); 2) the likely underestimation of beluga use of the zone upstream of the Saguenay River, where availability is less compared to other zones due to turbidity and diving behaviour (Lesage et al. 2023).

The new correction factors for visual surveys flown with the Cessna 337 or Partenavia P68 Observer aircraft were coincidently similar to the 2.09 instantaneous correction factor that was applied to visual surveys, but initially developed for photographic surveys. Correction factors were much lower for the Twin Otter as a result of the larger field of view this platform provided to observers (170 deg) compared to the Cessna or Partenavia (130 deg; Lesage et al. 2023). These results emphasize the major impact that the observers' field of view and distance of sightings from the aircraft have on abundance estimates. Yet, aerial surveys for other beluga populations or other cetaceans, rarely account for these factors, and only apply *a posteriori* instantaneous correction factors directly to abundance estimates (e.g., Hammond et al. 2013, Watt et al. 2021, Gosselin et al. 2013, Gosselin et al. 2014, Gosselin et al. 2017, Marcoux et al.

2016, Heide-Jørgensen and Acquarone 2002, Marcoux et al.[1]). These availability bias correction factors are suitable for instantaneous photographic surveys in homogeneous environments, but may not be representative of true availability during visual surveys because they do not account for the variability in the amount of time that a given point at the water's surface remains in the observer's field of view depending on its distance from the trackline. For instance, points at 300, 600 and 1000 m remain in the field of view of an observer for about 20, 40, and 67 s in a Cessna 337 or a Partenavia P68 Observer, and for about 133, 311, and 444 s for a Twin Otter, values much higher than the 0-1 s estimated time-in-view using an instantaneous correction factor. As a result, studies using such instantaneous correction factors likely overestimated abundance unless the true time-in-view was extremely short.

In previous assessments, the variances associated with the correction factor and the abundance indices were simply combined. However, because we directly applied the availability bias correction to each observation to correct cluster size prior to calculating the surface index estimate, there was a need to consider a different approach to variance estimation. Here, a variance term that combined the variance from availability estimation with that from the surface index estimation was obtained by first generating 5,000 possible values of availability for each observed beluga group detected, calculating an abundance index associated with each of these availability corrections, and finally calculating the mean variance of the individual abundance indices combined to the variance of the 5,000 indices. In preliminary analyses, a bootstrap procedure was tested to account for these variances, but this approach was later discarded because in many bootstrap replicates from the visual surveys in particular, we noted that iterations that disproportionately resampled transects with very high concentrations of animals, or conversely, transects without observations, produced extreme abundance estimates and led to highly unbalanced distributions of abundance values. The method currently applied is more robust as it eliminated the need for resampling. Yet, alternative methods including Bayesian approaches should be explored, as they may improve precision and accuracy of abundance estimates, especially for visual surveys.

A major change in the analysis of the visual survey data is the use of a perception bias correction factor. A double-platform configuration during the visual surveys was applied in five survey years, with sufficient reliable data to calculate perception bias correction factors in three of those years (i.e., 2015, 2019, and 2022). The SLE abundance estimates published to date were only partially corrected (i.e., for availability only) and were thus underestimates. As expected, the correction of the abundance estimates from visual surveys for both availability and perception biases has resulted in higher estimates. It is important to note that the perception bias estimates calculated here are not comparable with those published elsewhere from surveys with a double-platform configuration on both sides of the aircraft, as is often used in beluga surveys in the Canadian Arctic (Marcoux et al. 2016, Watt et al. 2021). In the surveys of the SLE beluga population, the double-platform configuration was possible only on the right side of the plane, given the aircraft used in all years but 2019. Therefore, the perception biases calculated (primary *p(0)*) are applicable only to the primary observers on each side of the plane whose observations are used to calculate surface abundance estimates. In contrast, surveys conducted with a double-platform configuration on both sides of the aircraft generally calculate the surface abundance based on the total number of unique observations of both observers, *i.e.,* those seen only by the primary observer, those seen only by the secondary observer, and

[1] Marcoux, M., Mayette, A., Ferguson, M., Hornby, C. et Loseto, L. L. In preparation. Beluga whales (*Delphinapterus leucas*) abundance estimate from the 2019 aerial surveys of the Eastern Beaufort Sea population.

those seen by both observers. Because the surface estimate is already based on observations from two observers, the perception bias estimate for the combined observers (combined *p(0)*) will always be higher, *i.e.*, it will not increase the abundance as much, compared to the bias estimate applicable to primary observers only (primary *p(0)*). However, it is important to note that the values of combined *p(0)* calculated in the present study were between 0.748 and 0.936, which is comparable to those obtained in beluga surveys using double-observer platforms on both sides of the plane (e.g., 0.95 reported by Watt et al. (2021) in Cumberland Sound, 0.920 reported by Heide-Jørgensen et al. (2013) in the North Water Polynya, and between 0.979 and 0.985 reported by Hobbs et al. (2000) in Cook Inlet). The primary *p(0)* estimates calculated in the present study are also similar with those calculated for the James Bay and Belcher Islands-Eastern Hudson Bay beluga populations in the 2015 and 2021 visual surveys (primary *p(0)* = 0.392 and 0.601, respectively), which used the same small aircraft and protocol as the SLE surveys.

The differences among years in perception bias estimates for the SLE beluga surveys can be linked to a few possible causes. First, differences in experience between the observer in the primary and secondary seat can impact perception bias. In 2015 for instance, the least experienced observer was the secondary observer, which yielded a lower perception bias estimate, i.e., higher correction, compared to that of the 2022 surveys, when the experience levels of the two right-side observers were more similar. In cases where the observers have varying degrees of experience, rotating the observer positions during the surveys would help ensure that both the abundance indices and the perception bias correction factor are representative of the observers overall. When the least experienced observer is consistently seated in the secondary position, this could lead to overestimated corrected abundances, as the abundance indices are calculated from the most experienced (primary) observer, but corrected for the perception biases of the least experienced one. Secondly, differences in platforms can also affect perception bias due to differences in field of view. For example, the field of view both horizontally (from front to back) and vertically (close to the plane to far away) is greater in the Twin Otter than in the smaller planes used in the SLE beluga surveys. Because of the difference in field of view, observer searching patterns may differ between platforms thus influencing perception bias estimates. Finally, differences in environmental conditions or beluga distribution and clumping could also cause variations in perception bias estimates. For instance, a sudden occurrence of multiple groups over a short distance may reduce the capacity of observers to log them all or log them accurately (with respect to position and cluster size), compared to groups that are more dispersed over transects, and may complicate the identification of duplicate sightings. Further surveys using the double-platform configuration will be needed to better investigate the causes of variability in perception bias correction factors. Until this information can be obtained, we can only assume that both the 2015 and 2022 perception bias correction factors are equally representative of surveys using the same protocol and aircraft types, and apply the average *p(0)* from these two surveys to surveys where a double-platform configuration was not used.

When the Saguenay River was surveyed, the total count of animals observed within the river was added to the abundance estimates of the Main stratum, after correction of the latter for availability and perception biases. However, the number of animals observed in the Saguenay River was not corrected for these biases. Given the shape of the trackline as the plane is following the river path and variations in altitude due to physical obstacles (power lines) along the river, observers onboard are able to detect animals ahead of the plane more easily and may also record animals twice as the plane travels up and down river. Thus, beluga sightings made by the different observers are not fully independent and may overlap. In addition, differences in water turbidity in the Saguenay, and potential differences in beluga behaviour in this area compared to the Main and Downstream strata, indicate that other correction factors would need

to be developed specifically for the Saguenay River if these numbers were to be corrected. In the absence of such correction, animals observed in the Saguenay River to date have been considered as a total count and added to the abundance estimate of the Main stratum. However, these are likely an underestimate of the true number of beluga in the river at a given time.

When conducting aerial surveys of small populations with a clumped distribution, as is the case for SLE beluga, two sources of uncertainty are generally encountered: 1) an uneven distribution of group size among sightings which influences the expected mean group size and, thus, the density estimates, and 2) an uneven distribution of clusters among lines which impacts the encounter rate (Gosselin et al. 2007). An example of this is found in the 2018 visual surveys, where the average group size recorded was higher than in other surveys. If this observation of larger groups was an artifact of the observer's data gathering approach in areas of higher beluga densities (i.e., if groups that should have been recorded as separate were clumped together and associated with a shared, approximate inclinometer measurement), this would result in a shorter perpendicular distance than the average of perpendicular distances of several groups using the inclinometer measurement in degree in the center of each group. This could lead to narrower estimated ESHWs and to higher abundance estimates. However, it is not possible to determine if the larger group sizes recorded in 2018 are a result of observer behaviour or if the true group sizes were different in that year. In survey years with greater clumping and, thus, more heterogeneity in the number of groups observed per transect line, more extreme values are expected regardless of the variance estimation method.

The highly clumped distribution of this small beluga population represents a considerable challenge for abundance estimation (Gosselin et al. 2007). High coverage of the study area and multiple replicate surveys can help address this inherent characteristic of the SLE beluga population. Photographic and visual surveys both have pros and cons in this context. Past photographic surveys with large film format offered ~50% coverage of the study area, but the film costs and extensive time necessary for photo reading prevented replication of the survey more than once per year. Switching to small format digital images in 2019 sped up the reading process, but limitations of the camera resolution and lenses (35 mm) reduced flying altitude to a maximum of 1000 ft and consequently, the transect footprints covered by the photographs became smaller. However, there is currently no digital cameras that could provide a strip width as wide as the one provided by the large format photographs (1.8 km) while maintaining the resolution to adequately detect adult beluga and calves, based on tests that we conducted with large format digital cameras used for harp seals surveys (Vexcel UltraCam). Surveys conducted with these large format digital cameras have the same hourly flying cost of large format film cameras, but would be more expensive as more flying lines would be required to achieve a 50% coverage given the resolution limitation. Obviously, digital photography development may overcome this problem in coming years. While total coverage of the survey area decreased as a result of these limitations, the overall lower cost of small format digital imagery compared to large format film allowed an increase in the number of replicate surveys. Photographic surveys also have the advantage of retaining a permanent visual record, providing estimates for the proportion of newborn calves and yearlings, and allowing repeated counts by different readers, thus, eliminating the need to correct for perception bias. Visual surveys result in coverages that are relatively comparable to small-format digital imagery (10-15%), but require correction for perception bias and do not allow for calves to be reliably identified and counted. However, visual surveys are overall cheaper to fly and, thus, can be repeated many more times than photographic surveys for the same price, given the absence of costs for photo reading. Using a Cessna 337 or Partenavia P68 Observer is currently approximately five times cheaper than flying a survey with a Twin Otter. However, platforms differ in field of view and seating capacity

for double-platform experiments which has a direct bearing on the estimation of availability and perception bias (Lesage et al. 2023, this study).

In 2019, digital photographic surveys were conducted simultaneously with visual surveys flown in a double-platform configuration using a Twin Otter, along transects spaced 4 NM apart to accommodate the greater detection distance of visual surveys and avoid double-counting of beluga on adjacent transects. Despite the lower coverage achieved, the replication of the survey (four times) reduced the uncertainty around abundance estimates for both photographic and visual surveys. The Twin Otter offered a wider field of view, considerably reducing the availability correction required compared to a smaller aircraft. It also allows double-platform experiments on both sides of the aircraft (although this was not applied in 2019) – compared to just one side for Cessna and Partenavia aircraft. Ways to increase coverage, either through camera technology, flight altitude or transect spacing is desirable. In the case of visual surveys, the current transect spacing (every 4 NM), does not allow for an increase in the number of transect as this would lead to potential double counting for distant sightings. Nevertheless, an increased coverage can be achieved through repeat surveys within a short time period. While multiple surveys highlight the high variability in beluga detection and distribution over time, even over a few days only (e.g., Gosselin et al. 2007) our results clearly demonstrate that the replication of surveys within a year can increase the precision of abundance estimates for both photographic and visual surveys. Hence, the replication of surveys should be implemented in the future regardless of the type of survey conducted. However, the variability in abundance estimates observed within and among years is also a reminder that care should be taken at interpreting survey abundance estimates at face value, i.e., outside the framework of a population dynamics model. In this time series, some variations among years are not biologically plausible and should be further investigated. A population model can take into account numerous sources of information (e.g., age-structure data, survival and mortality rates, pregnancy and carcass data) in addition to the abundance estimates from aerial surveys to constrain population trends and dynamics within a plausible biological range while explicitly accounting for uncertainty (Tinker et al. In press).

ACKNOWLEDGEMENTS

We thank the numerous marine mammal observers and photo readers who participated in the surveys throughout the years: Pierre Carter, Virginie Chadenet, Thomas Doniol-Valcroze, Richard Labbé, Yves Morin, Pierre Rivard, Jean-François Ouellet, Alain Carpentier, Angelia Vanderlaan, Samuel Turgeon, Joanie van de Walle, Valérie Harvey, Caroline Sauvé, Claudie Lacroix-Lepage, Isabeau Pratte, Antoine Dispas, Camille Mancion, Pascale Caissy, Talia Koll-Egyed, Serge Aucoin, Kerrith McKay, Victoria Graveline-Renaud, Myriam-Esther Hadland, Miranda Unger, Sophie Bédard, Josiane Riopel, Kathy Bajzak, Amélie Robillard, Paul Roy, Michael Kozicki, Wybrand Hoek, Anne Evely, Garry Sleno, Isabelle Gauthier, Serge Gosselin, Lucie Lavigueur, Coralie Tournois, and Sandrine Guittard. Airplanes used to survey beluga were provided by Hauts-Monts Inc. in 2001, 2003, and 2005, by SASAIR in 2007, 2008, 2009, 2015, 2016, 2021, and 2022, and by Air Montmagny in 2014, 2018, 2021 and 2022. Airplanes used in the photographic surveys were provided by Hauts-Monts (1990—2009), and by PAL Airlines in 2019. We are thankful to all the pilots who worked with us throughout the years. These surveys were funded by the Regional Fund and Interdepartmental Recovery Fund for Species at Risk, by large survey Fund from the Ecosystems Science Regional Initiative and by the Centre of Expertise on Marine Mammals (CEMAM).

REFERENCES CITED

Bailey, R. and Zinger, N. 1995. St. Lawrence beluga recovery plan. World Wildlife Fund.

Bivand, R. S., Pebesma, E. J., Gómez-Rubio, V. and Pebesma, E. J. 2013. Applied spatial data analysis with R. Springer, New York.

Boivin, Y. 1990. Survols aeriens pour l'estimation de la distribution saisonniere et des deplacements des belugas. Institut national d'écotoxicologie du Saint-Laurent.

Brennin, R., Murray, B. W., White, B. N., Clayton, J. W., Friesen, M. K. and Maiers, L. D. 1997. Population genetic structure of beluga whales (*Delphinapterus leucas*): mitochondrial DNA sequence variation within and among North American populations. Can. J. Zool. 75**,** 795-802.

Brown Gladden, J., Ferguson, M. and Clayton, J. 1997. Matriarchal genetic population structure of North American beluga whales *Delphinapterus leucas* (Cetacea: Monodontidae). Mol. Ecol. 6**,** 1033-1046.

Buckland, S. T., Anderson, D. R., Burnham, K. P., Laake, J. L., Borchers, D. L. and Thomas, L. 2001. Introduction to distance sampling: estimating abundance of biological populations. Oxford University Press, New York.

Buckland, S. T., Russell, R. E., Dickson, B. G., Saab, V. A., Gorman, D. N. and Block, W. M. 2009. Analyzing designed experiments in distance sampling. J. Agric. Biol. Environ. Stat. 14, 432-442.

Burt, M. L., Borchers, D. L., Jenkins, K. J. and Marques, T. A. 2014. Using mark–recapture distance sampling methods on line transect surveys. *M*ethods Ecol. Evol. 5, 1180-1191.

Cochran, W. G. 1977. Sampling techniques. 3rd Edition, John Wiley & Sons, New York.

COSEWIC. 2014. COSEWIC assessment and status report on the beluga whale *Delphinapterus leucas*, St. Lawrence Estuary population, in Canada. Committee on the Status of Endangered Wildlife in Canada Ottawa.

De March, B. and Postma, L. 2003. Molecular genetic stock discrimination of belugas (*Delphinapterus leucas*) hunted in eastern Hudson Bay, northern Quebec, Hudson Strait, and Sanikiluaq (Belcher Islands), Canada, and comparisons to adjacent populations. Arctic**,** 111-124.

DFO. 2014. Status of beluga (*Delphinapterus leucas*) in the St. Lawrence River estuary. DFO Can. Sci. Advis. Sec. Sci. Advis. Rep. 2013/076.

Finley, K., Miller, G., Allard, M., Davis, R. and Evans, C. 1982. The belugas (*Delphinapterus leucas*) of northern Quebec: distribution, abundance, stock identity, catch history and management. Can. Tech. Rep. Fish. Aquat. Sci. 1123**,** v + 57.

Fleming, P. J. and Tracey, J. P. 2008. Some human, aircraft and animal factors affecting aerial surveys: how to enumerate animals from the air. Wildl. Res. 35, 258-267.

Forcada, J., Gazo, M., Aguilar, A., Gonzalvo, J. and Fernández-Contreras, M. 2004. Bottlenose dolphin abundance in the NW Mediterranean: addressing heterogeneity in distribution. Mar. Ecol. Prog. Ser. 275, 275-287.

Gómez de Segura, A., Tomás, J., Pedraza, S. N., Crespo, E. A. and Raga, J. A. 2006. Abundance and distribution of the endangered loggerhead turtle in Spanish Mediterranean waters and the conservation implications. Anim. Conserv. 9, 199-206.

Gosselin, J.-F., Lesage, V. and Robillard, A. 2001. Population index estimate for the beluga of the St. Lawrence Estuary in 2000. DFO Can. Sci. Advis. Sec. Res. Doc. 2001/049. 21 p.

Gosselin, J.-F., Hammill, M. O. and Lesage, V. 2007. Comparison of photographic and visual abundance indices of belugas in the St. Lawrence Estuary in 2003 and 2005. DFO Can. Sci. Advis. Sec. Res. Doc. 2007/025. ii + 27 p.

Gosselin, J.-F., Doniol-Valcroze, T. and Hammill, M.O. 2013. Abundance estimate of beluga in eastern Hudson Bay and James Bay, summer 2011. DFO Can. Sci. Advis. Sec. Res. Doc. 2013/016. vii + 20 p.

Gosselin, J.-F., Hammill, M. O., and Mosnier, A. 2014. Summer abundance indices of St. Lawrence Estuary beluga (*Delphinapterus leucas*) from a photographic survey in 2009 and 28 line transect surveys from 2001 to 2009. DFO Can. Sci. Advis. Sec. Res. Doc. 2014/021. iv + 51 p.

Gosselin, J.-F., Hammill, M.O., Mosnier, A. and Lesage, V. 2017. Abundance index of St. Lawrence Estuary beluga, *Delphinapterus leucas*, from aerial visual surveys flown in August 2014 and an update on reported deaths. DFO Can. Sci. Advis. Sec. Res. Doc. 2017/019. v + 28 p.

Grenzdörffer, G. J., Guretzki, M. and Friedlander, I. 2008. Photogrammetric image acquisition and image analysis of oblique imagery. The Photogrammetric Record, 23, 372-386.

Hammill, M. O., Measures, L. N., Gosselin, J.-F., and Lesage, V. 2007. Lack of recovery in St. Lawrence Estuary beluga. DFO Can. Sci. Advis. Sec. Res. Doc. 2007/026.

Hammond, P. S., Macleod, K., Berggren, P., Borchers, D. L., Burt, L., Cañadas, A., Desportes, G., Donovan, G. P., Gilles, A. and Gillespie, D. 2013. Cetacean abundance and distribution in European Atlantic shelf waters to inform conservation and management. Biol. Conserv. 164, 107-122.

Heide-Jørgensen, M. P. and Acquarone, M. .2002. Size and trends of the bowhead whale, beluga and narwhal stocks wintering off West Greenland. NAMMCO Sci. Publ. 4, 191-210.

Heide-Jørgensen, M. P., Burt, L. M., Hansen, R. G., Nielsen, N. H., Rasmussen, M., Fossette, S. and Stern, H. 2013. The significance of the North Water polynya to Arctic top predators. Ambio, 42, 596-610.

Hobbs, R. C., Rugh, D. J. and DeMaster, D. P. 2000. Abundance of belugas, Delphinapterus leucas, in Cook Inlet, Alaska, 1994–2000. Mar. Fish. Rev. , 62(3), 37-45.

Kingsley, M. C. 1993. *Census, trend and status of the St. Lawrence beluga population in 1992.* Can. Tech. Rep. Fish. Aquat. Sci. 1938.

Kingsley, M. C. 1996. Population index estimate for the belugas of the St Lawrence in 1995. Can. Tech. Rep. Fish. Aquat. Sci. 2117.

Kingsley, M. C. 1998. Population index estimates for the St. Lawrence belugas, 1973–1995. Mar. Mamm. Sci. 14, 508-529.

Kingsley, M. 1999. Population indices and estimates for the belugas of the St. Lawrence estuary. Can. Tech. Rep. Fish. Aquat. Sci. 2226.

Kingsley, M. C. and Gauthier, I. 2002. Visibility of St Lawrence belugas to aerial photography, estimated by direct observation. NAMMCO Sci. Publ. 4, 259-270.

Kingsley, M. and Hammill, M. O. 1991. Photographic census surveys of the St. Lawrence beluga population, 1988 and 1990. Can. Tech. Rep. Fish. Aquat. Sci. 1776.

Kingsley, M.C.S., and Smith, G.E.J. 1981. Analysis of data arising from systematic transect surveys, p.40-48. In F.L. Miller and A. Gunn (eds), Proc. Symp. Census and Inventory Methods for Populations and Habitats, Banff, April 1980. Contribution # 217, Forest, Wildlife and Range Experiment Station, U. of Idaho, Moscow, Idaho.

Laake, J. L. and Borchers, D. L. 2004. Methods for incomplete detection at distance zero. *Advanced Distance Sampling* (eds S. T. Buckland, D. R. Anderson, K. P. Burnham, J. L. Laake, D. L. Borchers & L. Thomas), pp. 108–189. Oxford University Press: Oxford.

Laake, J. L., Calambokidis, J., Osmek, S. D. and Rugh, D. J. 1997. Probability of detecting harbor porpoise from aerial surveys: estimating g (0). J. Wildl. Manag. 63-75.

Laake, J., Borchers, D., Thomas, L., Miller, D. and Bishop, J. 2013. mrds: Mark-Recapture Distance Sampling (mrds). R package version 2.1. 5.

Lambert, C., Authier, M., Doremus, G., Gilles, A., Hammond, P., Laran, S., Ricart, A., Ridoux, V., Scheidat, M. and Spitz, J. 2019. The effect of a multi-target protocol on cetacean detection and abundance estimation in aerial surveys. R. Soc. Open Sci. 6, 190296.

Lawson. J.W., and Gosselin, J.-F. 2009. Distribution and preliminary abundance estimates for cetaceans seen during Canada's marine megafauna survey - A component of the 2007 TNASS. DFO Can. Sci. Advis. Sec. Res. Doc. 2009/031. vi + 28 p.

Lerczak, J. A. and Hobbs, R. C. 1998. Calculating sighting distances from angular readings during shipboard, aerial, and shore-based marine mammal surveys. Mar. Mamm. Sci. 14, 590-598.

Lesage, V., Wing, S., Zuur, A.F., Gosselin, J.-F., Mosnier, A., St-Pierre, A.P., Michaud, R., and Berteaux, D. 2024. Environmental Factors and Behaviour of St. Lawrence Estuary Beluga Generate Heterogeneity in Availability Bias for Photographic and Visual Aerial Surveys. DFO Can. Sci. Advis. Sec. Res. Doc. 2023/046. iv + 40 p.

Marcoux, M., Young, B.G., Asselin, N.C., Watt, C A., Dunn, J.B., and Ferguson, S.H. 2016. Estimate of Cumberland Sound beluga (*Delphinapterus leucas*) population size from the 2014 visual and photographic aerial survey. DFO Can. Sci. Advis. Sec. Res. Doc. 2016/037. iv + 19 p. (Erratum: October 2016)

Marques, F. F. and Buckland, S. T. 2003. Incorporating covariates into standard line transect analyses. Biometrics, 59, 924-935.

Marsh, H. and Sinclair, D. F. 1989. Correcting for visibility bias in strip transect aerial surveys of aquatic fauna. J. Wildl. Manag. 1017-1024.

McLaren, I. A. 1961. Methods of determining the numbers and availability of ringed seals in the eastern Canadian Arctic. Arctic, 14, 162-175.

Melville, G. J., Tracey, J. P., Fleming, P. J. and Lukins, B. S. 2008. Aerial surveys of multiple species: critical assumptions and sources of bias in distance and mark–recapture estimators. Wildl. Res. 35, 310-348.

Michaud, R. .1993. Distribution estivale du béluga du Saint-Laurent: synthèse 1986 à 1992. Rapp. tech. can. sci. halieut. aquat. 1906.

Michaud, R. 2005. Sociality and ecology of the odontocetes. *Sexual segregation in vertebrates*, 303-326.

Mosnier, A., Lesage, V., Gosselin, J.-F., Lemieux Lefebvre, S., Hammill, M. O. and Doniol-Valcroze, T. 2010. Information relevant to the documentation of habitat use by St. Lawrence beluga (*Delphinapterus leucas*), and quantification of habitat quality. DFO Can. Sci. Advis. Sec. Res. Doc., 2009/098: iv + 35 p.

Panigada, S., Lauriano, G., Donovan, G., Pierantonio, N., Cañadas, A., Vázquez, J. A. and Burt, L. 2017. Estimating cetacean density and abundance in the Central and Western Mediterranean Sea through aerial surveys: implications for management. Deep Sea Res. Part II: Top. Stud. Oceanogr. 141, 41-58.

Pike, D. and Doniol-Valcroze, T. 2015. Identification of duplicate sightings from the 2013 double-platform High Arctic Cetacean Survey. DFO Can. Sci. Advis. Sec. Res. Doc. 2015/034. v + 22 p.

Pike, D. G., Gunnlaugsson, T., and Víkingsson, G. 2008. T-NASS Icelandic aerial survey: Survey report and a preliminary abundance estimate for minke whales. SC/60/PFI12 for the IWC Scientific Committee.

Pippard, L. and Malcolm, H. 1978. White Whales (*Delphinapterus Leucas*)-Observations on Their Distribution, Population and Critical Habitats in the St. Lawrence and Saguenay Rivers. Parks Canada.

Postma, L.D., Petersen, S.D., Turgeon, J., Hammill, M.O., Lesage, V., and Doniol-Valcroze, T. 2012. Beluga whales in James Bay: a separate entity from eastern Hudson Bay belugas? DFO Can. Sci. Advis. Sec. Res. Doc. 2012/074. iii + 23 p.

R Development Core Team 2018. R: A language and environment for statistical computing. R Foundation for Statistical Computing, Vienna, Austria.

Reeves, R. R. and Mitchell, E. 1989. Status of white whales, *Delphinapterus leucas,* in Ungava Bay and eastern Hudson Bay. Can. Field-Nat. 103, 220-239.

Richard, P. R. 1991. Status of the belugas, *Delphinapterus leucas*, of southeast Baffin Island, Northwest Territories. Can. Field-Nat. 105, 206-214.

Richard, P. R. 2010. Stock definition of belugas and narwhals in Nunavut. DFO Can. Sci. Advis. Sec. Res. Doc. 2010/022. iv + 14 p.

St-Pierre, A.P., Gosselin, J.-F., Mosnier, A., Sauvé, C. and Hammill, M.O. In press. Abundance estimates for beluga (*Delphinapterus leucas*) in James Bay and the Belcher Islands-eastern Hudson Bay area in summer 2021. DFO Can. Sci. Advis. Sec. Res. Doc. 2023/040. iv + 38 p.

Thomas, L., Laake, J., Rexstad, E., Strindberg, S., Marques, F., Buckland, S., Borchers, D., Anderson, D., Burnham, K. and Burt, M. 2009. Distance 6.0. Release 2. Research Unit for Wildlife Population Assessment, University of St. Andrews, St. Andrews, UK. distancesampling. org.

Tinker, M.T., Mosnier, A., St-Pierre, A.P., Gosselin, J-F., Lair, S., Michaud, R. and Lesage, V. In press. An Integrated Population Model for St. Lawrence Estuary Belugas (*Delphinapterus leucas*). DFO Can. Sci. Advis. Sec. Res. Doc. 2023/047. iv + 64 p.

Vladykov, V. D. 1944. Etudes sur les mammifères aquatiques. III. Chasse, biologie et valeur économique du marsouin blanc ou béluga (*Delphinapterus leucas*) du fleuve et du golfe Saint-Laurent. (ed Q. Département des Pêcheries, QC).

Watt, C.A., Marcoux, M., Hammill, M.O., Montsion, L., Hornby, C., Charry, B., Dunn, J.B., Ghazal, M., Hobbs, R., Lee, D.S., Mosnier, A., and Matthews, C.J.D. 2021. Abundance and total allowable landed catch estimates from the 2017 aerial survey of the Cumberland Sound beluga (*Delphinapterus leucas*) population. DFO Can. Sci. Advis. Sec. Res. Doc. 2021/050. iv + 33 p.

TABLES

Table 1. Photographic survey abundance indices corrected for availability biases by multiplying the surface Estuary estimate by 2.09 ('older method'; SE = 0.16; Kingsley and Gauthier 2002), or by a factor accounting for location-specific condition ('current study'; Lesage et al. 2023). Corrected estimates include the Saguenay counts. Indices using the 'older method' were taken from the literature for 1990—2009 (Kingsley and Hammill 1991, Kingsley 1993, 1996, 1999; Gosselin et al. 2001; 2007; 2014), and were estimated as part of the current study for the 2019 surveys. The Saguenay was not covered in 1990 and the number are based on the average percentage of 4.95% observed in the Saguenay during 8 complete aerial surveys from 1988 to 1992 (Michaud 1993).

Year	Date	Expansion factor	Surface abundance index in Estuary (older method)[1]	Surface abundance index in Estuary (this study)[2]	Saguenay count	Corrected estimate (SE) (older method)[3]	Corrected estimate (SE) (this study)[3]	Corrected estimate CV (%) (this study)	Percentage of newborn calves and yearlings (calf count / total count)
1990	12/09/90	2.03, 2,6 and 8.09	527	1,488	28	1,129 (567)	1,516 (492)	32.5	16.8 (25/149)
1992	12/09/92	2	454	1,429	3	952 (149)	1,432 (208)	14.5	16.3 (37/227)
1995	25/08/95	2	568	1,582	52	1,239 (217)	1,634 (241)	14.8	15.1 (43/284)
1997	26/08/97	2.03	575	1,665	20	1,222 (190)	1,685 (231)	13.7	17.8 (51/287)
2000	28/08/00	2.03	453	1,320	6	953 (134)	1,326 (163)	12.3	7.8 (17/219)
2003	02/09/03	2.02	630	1,757	2	1,319 (263)	1,759 (302)	17.1	3.2 (10/311)
2009	28/08/09	1.98	319	949	10	676 (105)	959 (119)	12.4	8.4 (13/154)
2019	13/08/19	9.72	351	1,022	15	749 (115)	1,037 (171)	16.5	8.3 (3/36)
	14/08/19	10.19	825	2,801	49	1,774 (380)	2,850 (715)	25.1	14.6 (12/82)
	15/08/19	9.03	686	2,127	15	1,449 (236)	2,142 (399)	18.6	6.6 (5/76)
	16/08/19	9.09	709	2,372	85	1,567 (304)	2,457 (672)	27.4	6.4 (5/78)
2019	**Mean**	-	-	-	-	-	**2,119 (267)**	**12.6**	-

[1] Before applying correction factor for availability bias (2.09; SE=0.16) or adding Saguenay count
[2] Already incorporating availability bias correction, but without Saguenay count
[3] Fully corrected estimates
[4] Incorporated correction factor for availability bias, with Saguenay count

Table 2. Description of the survey design, effort, and number of groups and individual beluga detected during 52 line transect surveys of the St. Lawrence Estuary (SLE) and 14 surveys of the marine Estuary (EST) from late July to early September, from 2001 to 2022.

Year	Date	Strata	Stratum area (km2)	Target altitude (m)	Aircraft type	Number of transects	Total track length (km)	Number of groups (individuals)	Groups without distance (individuals)
2001	2001-08-12	Main (pass 1)	4,531	457	Cessna 337	24	639	88 (177)	0 (0)
2003	2003-08-20	Main (pass 1)	5,377	305	Cessna 337	27	718	99 (39)	3 (11)
	2003-08-25	Main (pass 2)	5,377	305	Cessna 337	26	686	43 (132)	3 (10)
	2003-08-26	Main (pass 3)	5,377	305	Cessna 337	27	718	51 (143)	0 (0)
	2003-09-02	Main (pass 4)	5,377	305	Cessna 337	26	686	80 (183)	1 (1)
	2003-09-06	Main (pass 5)	5,377	305	Cessna 337	27	718	77 (195)	4 (15)
2005	2005-08-12	Main (pass 1)	5,377	305	Cessna 337	27	734	105 (245)	0 (0)
	2005-08-15	Main (pass 2)	5,377	305	Cessna 337	27	718	129 (282)	1 (5)
	2005-08-25	Main (pass 3)	5,377	305	Cessna 337	27	734	77 (228)	0 (0)
	2005-08-26	Main (pass 4)	5,377	305	Cessna 337	27	718	75 (225)	0 (0)
	2005-09-04	Main (pass 5)	5,377	305	Cessna 337	27	734	70 (98)	0 (0)
	2005-09-06	Main (pass 6)	5,377	305	Cessna 337	27	718	81 (118)	0 (0)
	2005-09-09	Main (pass 7)	5,377	305	Cessna 337	27	734	98 (175)	0 (0)
	2005-08-14	Main (pass 1)	5,377	457	Cessna 337	27	734	90 (199)	1 (10)
	2005-08-18	Main (pass 2)	5,377	457	Cessna 337	27	718	57 (160)	0 (0)
	2005-08-19	Main (pass 3)	5,377	457	Cessna 337	27	734	120 (261)	0 (0)
	2005-08-27	Main (pass 4)	5,377	457	Cessna 337	27	718	98 (249)	1 (2)
	2005-09-05	Main (pass 5)	5,377	457	Cessna 337	27	734	125 (260)	0 (0)
	2005-09-08	Main (pass 6)	5,377	457	Cessna 337	27	718	104 (175)	0 (0)
	2005-09-10	Main (pass 7)	5,377	457	Cessna 337	27	734	65 (104)	3 (14)
2007	2007-07-21	Main (pass 1)	5,231	198	Cessna 337	27	1438 (2x734)	184 (426)	0 (0)
	2007-07-22	Downstream (pass 1)	6,840	198	Cessna 337	7	365	17 (27)	0 (0)
2008	2008-07-17	Main (pass 1)	5,377	305	Cessna 337	27	1,437 (2x734)	140 (352)	10 (40)
2009	2009-08-20	Main (pass 1)	5,787	305	Cessna 337	28	788	66 (130)	0 (0)
	2009-08-23	Main (pass 2)	5,787	305	Cessna 337	28	801	55 (165)	6 (10)
	2009-08-24	Main (pass 3)	5,787	305	Cessna 337	28	804	93 (250)	5 (65)
	2009-09-01	Main (pass 4)	5,787	305	Cessna 337	28	785	23 (45)	0 (0)
	2009-09-04	Main (pass 5)	5,787	305	Cessna 337	28	794	65 (144)	9 (15)
	2009-09-05	Main (pass 6)	5,787	305	Cessna 337	28	784	76 (175)	0 (0)

Year	Date	Strata	Stratum area (km2)	Target altitude (m)	Aircraft type	Number of transects	Total track length (km)	Number of groups (individuals)	Groups without distance (individuals)
	2009-08-25	Downstream (pass 1)	6,265	305	Cessna 337	16	783	1 (1)	0 (0)
	2009-08-28	Downstream (pass 2)	6,265	305	Cessna 337	16	849	0 (0)	0 (0)
2014	2014-08-19	Main (pass 1)	5,770	305	Partenavia	29	802	107 (241)	0 (0)
	2014-08-20	Main (pass 2)	5,770	305	Partenavia	28	779	153 (389)	0 (0)
	2014-08-21	Main (pass 3)	5,770	305	Partenavia	29	775	53 (145)	1 (4)
	2014-08-24	Main (pass 4)	5,770	305	Partenavia	29	801	73 (162)	1 (3)
	2014-08-29	Main (pass 5)	5,770	305	Partenavia	28	769	144 (321)	48 (107)
	2014-09-03	Main (pass 6)	5,770	305	Partenavia	29	800	66 (158)	6 (27)
	2014-09-08	Main (pass 7)	5,770	305	Partenavia	28	769	123 (299)	25 (70)
	2014-09-10	Main (pass 8)	5,770	305	Partenavia	29	801	118 (302)	41 (143)
	2014-08-27	Downstream (pass 1)	6,245	305	Partenavia	16	830	0 (0)	0 (0)
	2014-09-09	Downstream (pass 2)	6,245	305	Partenavia	16	851	0 (0)	0 (0)
2015	2015-07-16	Main (pass 1)	5,787	305	Cessna 337	28	767	125 (393)	13 (37)
	2015-07-16	Main (pass 2)	5,787	305	Cessna 337	29	808	133 (248)	0 (0)
2016	2016-08-02	Main (pass 1)	5,774	183	Cessna 337	28	758	96 (228)	0 (0)
	2016-08-02	Main (pass 2)	5,774	183	Cessna 337	29	791	105 (248)	3 (11)
	2016-08-04 & 2016-08-12	Downstream (pass 1)	6,243	183	Cessna 337	7	311	0 (0)	0 (0)
2018	2018-08-16	Main (pass 1)	5,770	305	Partenavia	28	778	43 (251)	1 (1)
	2018-08-20	Main (pass 2)	5,770	305	Partenavia	28	760	69 (318)	0 (0)
	2018-08-30	Main (pass 3)	5,770	305	Partenavia	28	769	63 (207)	0 (0)
	2018-09-04	Main (pass 4)	5,770	305	Partenavia	29	800	56 (263)	0 (0)
	2018-09-06	Main (pass 5)	5,770	305	Partenavia	28	772	50 (272)	1 (30)
	2018-08-17	Downstream (pass 1)	6,245	305	Partenavia	12	637	0 (0)	0 (0)
	2018-08-21	Downstream (pass 2)	6,245	305	Partenavia	16	848	6 (140)	0 (0)
	2018-08-31	Downstream (pass 3)	6,245	305	Partenavia	15	804	2 (3)	0 (0)
	2018-09-05	Downstream (pass 4)	6,245	305	Partenavia	15	805	3 (39)	0 (0)
2019	2019-08-13	Main (pass 1)	5,770	305	Twin Otter	28	777	61 (167)	3 (10)
	2019-08-14	Main (pass 2)	5,770	305	Twin Otter	28	776	86 (246)	0 (0)
	2019-08-15	Main (pass 3)	5,770	305	Twin Otter	29	801	88 (236)	5 (16)
	2019-08-16	Main (pass 4)	5,770	305	Twin Otter	29	802	69 (194)	3 (6)
	2019-08-15	Downstream (pass 1)	6,246	305	Partenavia	16	839	0 (0)	0 (0)

Year	Date	Strata	Stratum area (km2)	Target altitude (m)	Aircraft type	Number of transects	Total track length (km)	Number of groups (individuals)	Groups without distance (individuals)
	2019-08-21	Downstream (pass 2)	6,245	305	Partenavia	16	811	1 (6)	0 (0)
2020	2020-07-22	Main (pass1)	5,770	243	Cessna 337	28	767	98 (206)	0 (0)
2021	2021-07-03	Main (pass 1)	5,787	305	Cessna 337 & Partenavia	28	767	99 (146)	7 (9)
	2021-07-03	Downstream (pass 1)	6,265	305	Cessna 337 & Partenavia	16	854	24 (79)	3 (4)
2022	2022-08-20 & 2022-09-04	Main (pass 1)	5,770	305	Cessna 337 & Partenavia	28	764	42 (70)	0 (0)
	2022-08-25 & 2022-09-04	Downstream (pass 1)	6,265	305	Cessna 337 & Partenavia	16	851	3 (17)	0 (0)

Table 3. Summary per survey year of the number of groups observed (all survey pass and strata combined) with and without distance measurements, as well as the detection function parameters and associated covariates. The covariates included in the detection model were selected following the stepwise procedure of Marques and Buckland (2003), applied to each survey year separately.

Year	Number of groups (individuals)	Groups without distance (individuals)	Right truncation distance (m)	Groups remaining after truncation	Key function (adjustment term)	Covariates	Effective strip half width (m)	Probability of detection P
2001	88 (177)	0 (0)	None	88	Gamma (NA)	Beaufort	705	0.329
2003	350 (962)	11 (37)	1,970	326	Gamma (Poly.)	NA	805	0.409
2005 (305m)	635 (1,371)	1 (5)	2,165	597	Gamma (Poly.)	Observer	1,027	0.474
2005 (457m)	659 (1,408)	5 (26)	3,300	653	Gamma (Poly.)	Beaufort + Observer	1,433	0.434
2007	201 (453)	0 (0)	None	201	Gamma (Poly.)	Observer + Watercolor	1,127	0.324
2008	140 (352)	10 (40)	1,750	126	Gamma (NA)	NA	1,074	0.614
2009	379 (910)	20 (90)	None	359	Gamma (Poly.)	Glare intensity + Cluster size	1,001	0.340
2014	837 (2,017)	122 (354)	2,580	709	Gamma (Poly.)	Observer + Glare intensity	1,221	0.337
2015	258 (641)	13 (37)	2,700	236	Gamma (NA)	Observer + Beaufort	1,217	0.451
2016	201 (476)	3 (11)	None	198	Gamma (Poly.)	Observer	834	0.308
2018	292 (1,493)	2 (31)	1,661	261	Gamma (NA)	Glare intensity	773	0.465
2019	305 (849)	11 (32)	1,910	279	Hazard rate (NA)	Observer + Cloud cover	1,066	0.558
2020	98 (206)	0 (0)	1,350	94	Gamma (NA)	Beaufort	951	0.704
2021	123 (225)	10 (13)	2,155	101	Gamma (NA)	Beaufort	1,090	0.506
2022	45 (87)	0 (0)	1600	44	Hazard rate (NA)	NA	920	0.575

Table 4. Mean individual density, encounter rate, expected group size, detection probability, and effective strip half-width (ESHW) for all survey passes, based on results from the bootstrapping procedure (see Methods). Numbers in parentheses represent lower and upper 95% confidence intervals for each value.

Year (altitude)	Year (altitude) and stratum	Mean density of individuals		Mean encounter rate		Mean expected group size		Mean probability of detection (*P*)		Mean ESHW	
2001	Main (pass 1)	0.45	(0.41-0.49)	0.63	(0.57-0.69)	4.58	(4.18-5.04)	0.33	(0.33-0.33)	705	(705-705)
2003	Main (pass 1)	0.30	(0.27-0.33)	0.48	(0.44-0.53)	6.83	(6.24-7.51)	0.41	(0.40-0.42)	805	(790-822)
	Main (pass 2)	0.40	(0.37-0.44)	0.65	(0.60-0.71)	5.72	(5.24-6.26)	0.41	(0.40-0.42)	805	(790-822)
	Main (pass 3)	0.39	(0.36-0.43)	0.63	(0.58-0.68)	5.87	(5.39-6.39)	0.41	(0.40-0.42)	805	(790-822)
	Main (pass 4)	0.56	(0.51-0.61)	0.90	(0.82-0.98)	6.85	(6.31-7.48)	0.41	(0.40-0.42)	805	(790-822)
	Main (pass 5)	0.28	(0.25-0.30)	0.45	(0.41-0.49)	7.89	(7.25-8.61)	0.41	(0.40-0.42)	805	(790-822)
2005 (305 m)	Main (pass 1)	0.29	(0.27-0.31)	0.58	(0.54-0.63)	4.39	(4.07-4.73)	0.47	(0.47-0.48)	1027	(1025-1030)
	Main (pass 2)	0.40	(0.37-0.44)	0.83	(0.75-0.91)	4.89	(4.45-5.39)	0.47	(0.47-0.48)	1027	(1025-1030)
	Main (pass 3)	0.29	(0.27-0.32)	0.58	(0.54-0.63)	6.16	(5.67-6.70)	0.47	(0.47-0.48)	1027	(1025-1030)
	Main (pass 4)	0.28	(0.26-0.31)	0.57	(0.52-0.62)	5.52	(5.07-6.04)	0.47	(0.47-0.48)	1027	(1025-1030)
	Main (pass 5)	0.16	(0.14-0.17)	0.31	(0.28-0.35)	3.40	(3.08-3.76)	0.47	(0.47-0.48)	1027	(1025-1030)
	Main (pass 6)	0.15	(0.14-0.17)	0.31	(0.28-0.34)	3.08	(2.81-3.37)	0.47	(0.47-0.48)	1027	(1025-1030)
	Main (pass 7)	0.25	(0.23-0.28)	0.51	(0.46-0.56)	4.30	(3.90-4.76)	0.47	(0.47-0.48)	1027	(1025-1030)
2005 (457 m)	Main (pass 1)	0.21	(0.19-0.23)	0.57	(0.52-0.63)	4.89	(4.45-5.39)	0.43	(0.43-0.44)	1433	(1425-1445)
	Main (pass 2)	0.14	(0.12-0.15)	0.42	(0.38-0.46)	5.29	(4.81-5.86)	0.43	(0.43-0.44)	1433	(1425-1445)
	Main (pass 3)	0.27	(0.25-0.30)	0.75	(0.68-0.83)	4.76	(4.30-5.28)	0.43	(0.43-0.44)	1433	(1425-1445)
	Main (pass 4)	0.20	(0.19-0.22)	0.58	(0.55-0.62)	4.31	(4.06-4.57)	0.43	(0.43-0.44)	1433	(1425-1445)
	Main (pass 5)	0.26	(0.23-0.28)	0.70	(0.64-0.76)	4.23	(3.88-4.62)	0.43	(0.43-0.44)	1433	(1425-1445)
	Main (pass 6)	0.18	(0.16-0.20)	0.51	(0.46-0.56)	3.56	(3.25-3.91)	0.43	(0.43-0.44)	1433	(1425-1445)
	Main (pass 7)	0.11	(0.10-0.13)	0.32	(0.29-0.36)	3.73	(3.34-4.19)	0.43	(0.43-0.44)	1433	(1425-1445)
2007	Main (pass 1)	0.27	(0.24-0.29)	0.62	(0.58-0.67)	4.80	(4.42-5.19)	0.33	(0.32-0.34)	1155	(1127-1180)
	Downstream (pass 1)	0.05	(0.04-0.06)	0.13	(0.11-0.15)	2.57	(2.15-3.19)	0.33	(0.32-0.34)	1155	(1127-1180)
2008	Main (pass 1)	0.23	(0.21-0.26)	0.50	(0.47-0.54)	5.32	(4.95-5.74)	0.61	(0.59-0.64)	1074	(1038-1118)
2009	Main (pass 1)	0.16	(0.14-0.17)	0.36	(0.33-0.40)	3.99	(3.67-4.37)	0.34	(0.34-0.35)	1010	(992-1036)
	Main (pass 2)	0.19	(0.17-0.21)	0.44	(0.41-0.48)	5.83	(5.36-6.36)	0.34	(0.34-0.35)	1010	(992-1036)
	Main (pass 3)	0.33	(0.30-0.37)	0.71	(0.67-0.76)	5.09	(4.69-5.63)	0.34	(0.34-0.35)	1010	(992-1036)
	Main (pass 4)	0.06	(0.06-0.07)	0.13	(0.12-0.14)	4.21	(3.81-4.68)	0.34	(0.34-0.35)	1010	(992-1036)
	Main (pass 5)	0.19	(0.17-0.21)	0.39	(0.36-0.43)	4.59	(4.18-5.05)	0.34	(0.34-0.35)	1010	(992-1036)
	Main (pass 6)	0.24	(0.22-0.27)	0.53	(0.49-0.58)	4.91	(4.50-5.39)	0.34	(0.34-0.35)	1010	(992-1036)
	Downstream (pass 1)	0.001	(0.001-0.001)	0.002	(0.001-0.003)	1.50	(1.17-1.99)	0.34	(0.34-0.35)	1010	(992-1036)

Year (altitude)	Year (altitude) and stratum	Mean density of individuals		Mean encounter rate		Mean expected group size		Mean probability of detection (*P*)		Mean ESHW	
	Downstream (pass 2)	NA	-	NA	-	NA	-	NA	-	NA	-
2014	Main (pass 1)	0.30	(0.27-0.33)	0.67	(0.61-0.73)	5.17	(4.73-5.64)	0.34	(0.33-0.36)	1233	(1192-1293)
	Main (pass 2)	0.41	(0.37-0.45)	0.99	(0.9-1.09)	5.11	(4.68-5.61)	0.34	(0.33-0.36)	1233	(1192-1293)
	Main (pass 3)	0.18	(0.17-0.20)	0.43	(0.39-0.48)	6.12	(5.56-6.74)	0.34	(0.33-0.36)	1233	(1192-1293)
	Main (pass 4)	0.21	(0.18-0.24)	0.44	(0.40-0.49)	4.92	(4.41-5.51)	0.34	(0.33-0.36)	1233	(1192-1293)
	Main (pass 5)	0.36	(0.33-0.39)	0.86	(0.80-0.93)	4.71	(4.38-5.09)	0.34	(0.33-0.36)	1233	(1192-1293)
	Main (pass 6)	0.13	(0.12-0.14)	0.34	(0.32-0.38)	4.20	(3.87-4.60)	0.34	(0.33-0.36)	1233	(1192-1293)
	Main (pass 7)	0.32	(0.28-0.35)	0.85	(0.78-0.94)	5.35	(4.88-5.89)	0.34	(0.33-0.36)	1233	(1192-1293)
	Main (pass 8)	0.34	(0.31-0.38)	0.93	(0.86-1.00)	6.14	(5.71-6.62)	0.34	(0.33-0.36)	1233	(1192-1293)
	Downstream (pass 1)	NA	-	NA	-	NA	-	NA	-	NA	-
	Downstream (pass 2)	NA	-	NA	-	NA	-	NA	-	NA	-
2015	Main (pass 1)	0.58	(0.53-0.65)	1.22	(1.11-1.34)	7.54	(6.86-8.31)	0.45	(0.44-0.47)	1222	(1191-1258)
	Main (pass 2)	0.19	(0.17-0.20)	0.55	(0.51-0.6)	3.60	(3.34-3.90)	0.45	(0.44-0.47)	1222	(1191-1258)
2016	Main (pass 1)	0.34	(0.31-0.38)	0.66	(0.59-0.73)	5.46	(4.91-6.08)	0.31	(0.30-0.31)	836	(826-854)
	Main (pass 2)	0.50	(0.45-0.55)	0.77	(0.70-0.83)	5.34	(4.89-5.84)	0.31	(0.30-0.31)	836	(826-854)
	Downstream (pass 1)	NA	-	NA	-	NA	-	NA	-	NA	-
2018	Main (pass 1)	0.52	(0.46-0.58)	0.78	(0.7-0.88)	15.10	(13.46-17.00)	0.47	(0.46-0.47)	773	(769-781)
	Main (pass 2)	0.61	(0.54-0.68)	0.90	(0.8-1.01)	10.43	(9.33-11.69)	0.47	(0.46-0.47)	773	(769-781)
	Main (pass 3)	0.39	(0.35-0.43)	0.61	(0.55-0.67)	7.90	(7.15-8.74)	0.47	(0.46-0.47)	773	(769-781)
	Main (pass 4)	0.37	(0.33-0.42)	0.59	(0.53-0.67)	11.05	(9.88-12.46)	0.47	(0.46-0.47)	773	(769-781)
	Main (pass 5)	0.57	(0.50-0.64)	0.83	(0.72-0.93)	15.24	(13.42-17.02)	0.47	(0.46-0.47)	773	(769-781)
	Downstream (pass 1)	NA	-	NA	-	NA	-	NA	-	NA	-
	Downstream (pass 2)	0.29	(0.16-0.55)	0.45	(0.25-0.86)	61.79	(33.58-116.48)	0.47	(0.46-0.47)	773	(769-781)
	Downstream (pass 3)	0.003	(0.002-0.004)	0.004	(0.003-0.005)	3.16	(2.25-4.39)	0.47	(0.46-0.47)	773	(769-781)
	Downstream (pass 4)	0.01	(0.01-0.02)	0.02	(0.01-0.04)	8.38	(5.08-15.18)	0.47	(0.46-0.47)	773	(769-781)
2019	Main (pass 1)	0.13	(0.13-0.14)	0.29	(0.27-0.31)	4.12	(3.88-4.40)	0.56	(0.55-0.57)	1067	(1051-1085)
	Main (pass 2)	0.20	(0.19-0.21)	0.41	(0.39-0.43)	3.88	(3.69-4.11)	0.56	(0.55-0.57)	1067	(1051-1085)
	Main (pass 3)	0.16	(0.15-0.17)	0.39	(0.37-0.41)	3.74	(3.55-3.94)	0.56	(0.55-0.57)	1067	(1051-1085)
	Main (pass 4)	0.19	(0.17-0.20)	0.33	(0.31-0.35)	4.05	(3.83-4.30)	0.56	(0.55-0.57)	1067	(1051-1085)
	Downstream (pass 1)	NA	-	NA	-	NA	-	NA	-	NA	-
	Downstream (pass 2)	0.002	(0.002-0.003)	0.008	(0.007-0.008)	6.18	(6.01-6.66)	0.56	(0.55-0.57)	1067	(1051-1085)
2020	Main (pass 1)	0.31	(0.29-0.34)	0.59	(0.54-0.64)	4.85	(4.44-5.31)	0.70	(0.70-0.70)	951	(951-951)
2021	Main (pass 1)	0.20	(0.18-0.22)	0.43	(0.38-0.48)	3.44	(3.09-3.85)	0.51	(0.49-0.54)	1099	(1051-1166)

Year (altitude)	Year (altitude) and stratum	Mean density of individuals		Mean encounter rate		Mean expected group size		Mean probability of detection (*P*)		Mean ESHW	
2022	Downstream (pass 1)	0.06	(0.04-0.07)	0.15	(0.12-0.19)	8.31	(6.57-10.65)	0.51	(0.49-0.54)	1099	(1051-1166)
	Main (pass 1)	0.12	(0.11-0.13)	0.21	(0.19-0.23)	3.93	(3.61-4.28)	0.57	(0.57-0.57)	920	(920-920)
	Downstream (pass 1)	0.02	(0.02-0.03)	0.04	(0.03-0.06)	12.51	(8.89-17.77)	0.57	(0.57-0.57)	920	(920-920)

Table 5. Results from the mark-recapture distance-sampling analysis, applied to double-platform data. Only the beluga observations sighted while both right-side observers were on effort (i.e., actively observing) and outside the Saguenay River were considered. Note that the total number of datapoints used by the MRDS model is twice the amount of unique sightings.

Year	Number of sightings				MCDS		MRDS covariates			*p(0)* (CV)	
	Unique	By primary	By secondary	By both	Key function (adjustment)	Covariates	Covariates	# of parameters	*df residuals*	Primary	Combined
2015	73	56	46	29	Gamma (NA)	NA	NA	2	144	0.593 (0.199)	0.834 (0.106)
2016	120	107	27	14	Gamma (Poly)	Glare intensity	Cloud cover	8	237	0.142 (0.473)	0.257 (0.444)
2019	277	154	212	89	Hazard rate (NA)	Cloud cover	Visibility + Watercolor	10	547	0.514 (0.128)	0.748 (0.090)
2021	3	0	1	2	NA	NA	NA	NA	NA	NA	NA
2022	15	12	10	7	Half-normal (NA)	NA	NA	3	28	0.748 (0.232)	0.936 (0.093)

Table 6. Abundance indices obtained from the bootstrap procedure after removal of outliers which fell outside predetermined limits (see Methods section). Abundances per stratum represent the mean of all survey passes for a given stratum, while the annual abundance is the sum of strata mean (when more than one stratum is surveyed in a given year).

Year and strata		Stratum (pass)	Bootstrap abundance corrected for availability only		Saguenay counts	Abundance corrected for availability and perception & Saguenay counts		
			Median	CI		Value	CV	CI
2001	Per survey pass	Main (1)	2029	(1852-2233)	15	3042	0.404	(1419-6519)
	Per stratum (combined surveys)	Main	-	-	-	3042	0.404	(1419-6519)
	Annual (all strata combined)					**3042**	**0.404**	**(1419-6519)**
2003	Per survey pass	Main (1)	1618	(1476-1780)	2	2416	0.433	(1071-5446)
		Main (2)	2171	(1985-2380)	0	3239	0.415	(1482-7080)
		Main (3)	2097	(1920-2288)	0	3129	0.378	(1527-6408)
		Main (4)	3000	(2740-3277)	7	4484	0.405	(2089-9623)
		Main (5)	1499	(1371-1640)	25	2262	0.446	(982-5211)
	Per stratum (combined passes)	Main	-	-	-	3106	0.189	(2151-4484)
	Annual (all strata combined)					**3106**	**0.189**	**(2151-4484)**
2005 (305m)	Per survey pass	Main (1)	1550	(1438-1674)	55	2367	0.350	(1217-4605)
		Main (2)	2168	(1968-2390)	59	3294	0.352	(1687-6433)
		Main (3)	1573	(1448-1710)	24	2371	0.412	(1092-5148)
		Main (4)	1507	(1385-1646)	35	2283	0.380	(1112-4690)
		Main (5)	842	(762-931)	28	1285	0.427	(576-2867)
		Main (6)	824	(753-903)	39	1268	0.370	(628-2559)
		Main (7)	1351	(1223-1493)	18	2034	0.389	(975-4241)
	Per stratum (combined passes)	Main	-	-	-	2129	0.146	(1602-2828)
	Annual (all strata combined)					**2129**	**0.146**	**(1602-2828)**
2005 (457m)	Per survey pass	Main (1)	1144	(1043-1263)	52	1760	0.433	(781-3966)
		Main (2)	727	(659-805)	0	1085	0.490	(437-2694)
		Main (3)	1462	(1320-1620)	12	2193	0.449	(947-5077)
		Main (4)	1094	(1032-1162)	73	1705	0.473	(706-4117)
		Main (5)	1373	(1262-1499)	94	2143	0.427	(961-4778)
		Main (6)	965	(882-1061)	40	1480	0.462	(625-3506)
		Main (7)	613	(549-689)	19	934	0.479	(384-2275)

	Year and strata	Stratum (pass)	Bootstrap abundance corrected for availability only		Saguenay counts	Abundance corrected for availability and perception & Saguenay counts		
			Median	CI		Value	CV	CI
	Per stratum (combined passes)	Main	-	-	-	1614	0.174	(1151-2263)
	Annual (all strata combined)					**1614**	**0.174**	**(1151-2263)**
	Average for 2005 (both altitudes combined)					***1872***	***0.112***	***(1505-2328)***
2007	Per survey pass	Main (1)	1398	(1274-1530)	29	2115	0.387	(1018-4396)
		Downstream (1)	337	(282-420)	NA	504	0.532	(189-1340)
	Per stratum (combined passes)	Main	-	-	-	2115	0.387	(1018-4396)
		Downstream	-	-	-	504	0.532	(189-1340)
	Annual (all strata combined)					**2619**	**0.329**	**(1398-4905)**
2008	Per survey pass	Main (1)	1259	(1155-1374)	11	1890	0.400	(889-4019)
	Per stratum (combined survey)	Main				1890	0.400	(889-4019)
	Annual (all strata combined)					**1890**	**0.400**	**(889-4019)**
2009	Per survey pass	Main (1)	902	(828-989)	15	1361	0.406	(634-2925)
		Main (2)	1097	(1007-1199)	3	1640	0.399	(772-3483)
		Main (3)	1916	(1745-2150)	11	2870	0.433	(1273-6469)
		Main (4)	358	(323-398)	22	556	0.530	(209-1475)
		Main (5)	1102	(1002-1216)	33	1678	0.465	(705-3996)
		Main (6)	1403	(1283-1539)	20	2114	0.371	(1045-4276)
		Downstream (1)	5	(4-7)	NA	8	1.030	(1-40)
		Downstream (2)	0	(0-0)	NA	0	0.000	(0-0)
	Per stratum (combined passes)	Main	-	-	-	1703	0.185	(1188-2442)
		Downstream	-	-	-	4	1.030	(1-20)
	Annual (all strata combined)					**1707**	**0.185**	**(1191-2446)**
2014	Per survey pass	Main (1)	1721	(1550-1897)	NA	2568	0.414	(1177-5603)
		Main (2)	2354	(2132-2597)	17	3529	0.390	(1688-7379)
		Main (3)	1064	(958-1179)	48	1636	0.429	(731-3662)
		Main (4)	1209	(1057-1366)	38	1841	0.605	(616-5501)
		Main (5)	2083	(1902-2271)	26	3134	0.480	(1283-7658)
		Main (6)	741	(671-818)	49	1154	0.539	(429-3108)
		Main (7)	1832	(1644-2046)	22	2756	0.425	(1241-6121)

Year and strata		Stratum (pass)	Bootstrap abundance corrected for availability only		Saguenay counts	Abundance corrected for availability and perception & Saguenay counts		
			Median	CI		Value	CV	CI
	Per survey pass	Main (8)	1978	(1789-2190)	0	2952	0.566	(1050-8296)
		Downstream (1)	-	-	NA	0	0.000	-
		Downstream (2)	-	-	NA	0	0.000	-
	Per stratum (combined passes)	Main	-	-	-	2450	0.174	(1748-3434)
		Downstream	-	-	-	0	0.000	-
	Annual (all strata combined)					**2450**	**0.174**	**(1748-3434)**
2015	Per survey pass	Main (1)	3383	(3057-3760)	10	5717	0.443	(2493-13112)
		Main (2)	1089	(1009-1181)	NA	1836	0.355	(935-3604)
	Per stratum (combined passes)	Main	-	-	-	3782	0.346	(1957-7309)
	Annual (all strata combined)					**3782**	**0.346**	**(1957-7309)**
2016	Per survey pass	Main (1)	1980	(1779-2208)	NA	2955	0.465	(1241-7038)
		Main (2)	2868	(2615-3149)	NA	4279	0.454	(1833-9990)
		Downstream (1)	0	(0-0)	NA	0	0.000	(0-0)
	Per stratum (combined passes)	Main	-	-	-	3617	0.329	(1930-6778)
		Downstream	-	-	-	0	0.000	-
	Annual (all strata combined)					**3617**	**0.329**	**(1930-6778)**
2018	Per survey pass	Main (1)	2979	(2653-3358)	61	4507	0.274	(2662-7630)
		Main (2)	3504	(3136-3925)	22	5251	0.424	(2366-11651)
		Main (3)	2226	(2014-2466)	25	3346	0.389	(1603-6985)
		Main (4)	2136	(1907-2410)	92	3279	0.460	(1389-7736)
		Main (5)	3305	(2866-3701)	0	4932	0.438	(2170-11209)
		Downstream (1)	0	(0-0)	NA	0	0.000	(0-0)
		Downstream (2)	1827	(990-3436)	NA	2727	1.009	(528-14093)
		Downstream (3)	16	(11-22)	NA	24	98.889	(0-8961)
		Downstream (4)	84	(50-152)	NA	125	0.919	(27-578)
	Per stratum (combined passes)	Main	-	-	-	4263	0.182	(2990-6077)
		Downstream	-	-	-	719	1.255	(107-4834)
	Annual (all strata combined)					**4981**	**0.239**	**(3138-7907)**

Year and strata		Stratum (pass)	Bootstrap abundance corrected for availability only		Saguenay counts	Abundance corrected for availability and perception & Saguenay counts		
			Median	CI		Value	CV	CI
2019	Per survey pass	Main (1)	776	(724-831)	15	1525	0.332	(810-2874)
		Main (2)	1132	(1072-1202)	49	2252	0.340	(1178-4305)
		Main (3)	925	(864-983)	15	1814	0.282	(1055-3119)
		Main (4)	1077	(1009-1152)	85	2180	0.356	(1108-4289)
		Downstream (1)	0	(0-0)	NA	0	0.000	(0-0)
		Downstream (2)	15	(12-16)	NA	28	1.085	(5-159)
	Per stratum (combined passes)	Main	-	-	-	1943	0.168	(1401-2694)
		Downstream	-	-	-	14	1.085	(3-80)
	Annual (all strata combined)					**1957**	**0.167**	**(1414-2709)**
2020	Per survey pass	Main (1)	1802	(1652-1975)	40	2729	0.414	(1252-5948)
	Per stratum (combined surveys)	Main	-	-	-	2729	0.414	(1252-5948)
	Annual (all strata combined)					**2729**	**0.414**	**(1252-5948)**
2021	Per survey pass	Main (1)	1148	(1014-1302)	26	1740	0.408	(806-3755)
		Downstream (1)	353	(277-456)	NA	527	0.705	(152-1832)
	Per stratum (combined passes)	Main	-	-	-	1740	0.408	(806-3755)
		Downstream	-	-	-	527	0.705	(152-1832)
	Annual (all strata combined)					**2267**	**0.354**	**(1157-4442)**
2022	Per survey pass	Main (1)	666	(613-726)	163	1054	0.323	(569-1954)
		Downstream (1)	151	(108-215)	NA	203	1.039	(38-1083)
	Per stratum (combined passes)	Main	-	-	-	1054	0.323	(569-1954)
		Downstream	-	-	-	203	1.039	(38-1083)
	Annual (all strata combined)					**1257**	**0.318**	**(684-2311)**

Table 7. Visual survey estimates (with standard errors in parentheses) obtained while applying various corrections to surface indices calculated from raw group size. Abundance indices are either corrected for availability only using the fixed correction factor of 0.478 as in Kingsley and Gauthier (2002) or models of surface and dive durations from Lesage et al. (2023), or they are corrected for both availability based on the method of Lesage et al. (2023) and for perception biases using the approach developed in this study.

Year	Survey passes in Main stratum	Survey passes in Downstream stratum	Surface abundance		Abundance corrected for availability only, with fixed correction factor		Abundance corrected for availability bias only		Abundance corrected for availability and perception biases	
2001	1	0	887	(346)	1,855	(763)	2,029	(607)	3,042	(1,229)
2003	5	0	849	(120)	1,777	(273)	2,077	(292)	3,106	(587)
2005 (305m)	7	0	673	(74)	1,407	(171)	1,402	(147)	2,129	(310)
2005 (457m)	7	0	516	(77)	1,079	(171)	1,054	(154)	1,614	(280)
2007	1	1	816	(160)	1,707	(380)	1,736	(420)	2,619	(860)
2008	1	0	521	(153)	1,090	(351)	1,259	(370)	1,890	(755)
2009	6	2	469	(61)	981	(139)	1,132	(161)	1,707	(316)
2014	8	2	627	(31)	1,312	(92)	1,623	(232)	2,450	(425)
2015	2	0	939	(270)	1,963	(597)	2,236	(691)	3,782	(1,308)
2016	2	1	1,012	(263)	2,118	(584)	2,424	(637)	3,617	(1,189)
2018	5	4	1,306	(238)	2,732	(520)	3,312	(704)	4,981	(1,191)
2019	4	2	686	(111)	1,435	(252)	985	(156)	1,957	(327)
2020	1	0	766	(222)	1,603	(509)	1,802	(572)	2,729	(1,129)
2021	1	1	597	(175)	1,249	(389)	1,502	(424)	2,267	(802)
2022	1	1	354	(108)	741	(241)	818	(254)	1,257	(400)

FIGURES

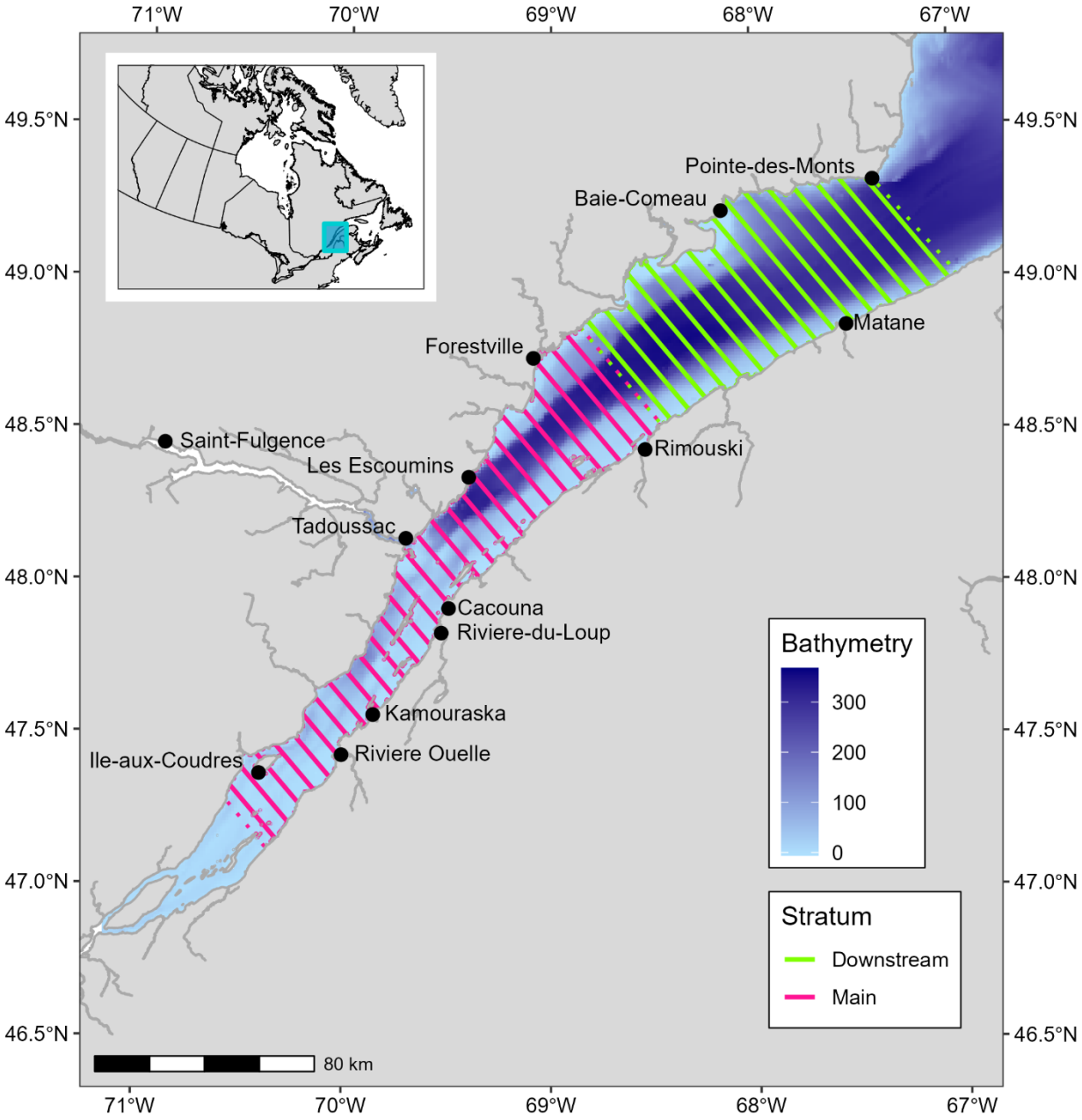

Figure 1. Extent of the study area and example of the systematic survey design with example of a random placement used for line transect visual surveys. The solid lines represent line transect flown every 4 nautical miles, and the dotted lines indicate the extremities of the Main and Downstream strata. The photographic surveys conducted in 2019 covered the Main portion of the estuary, using line transects with a spacing of 4 nautical miles as represented here.

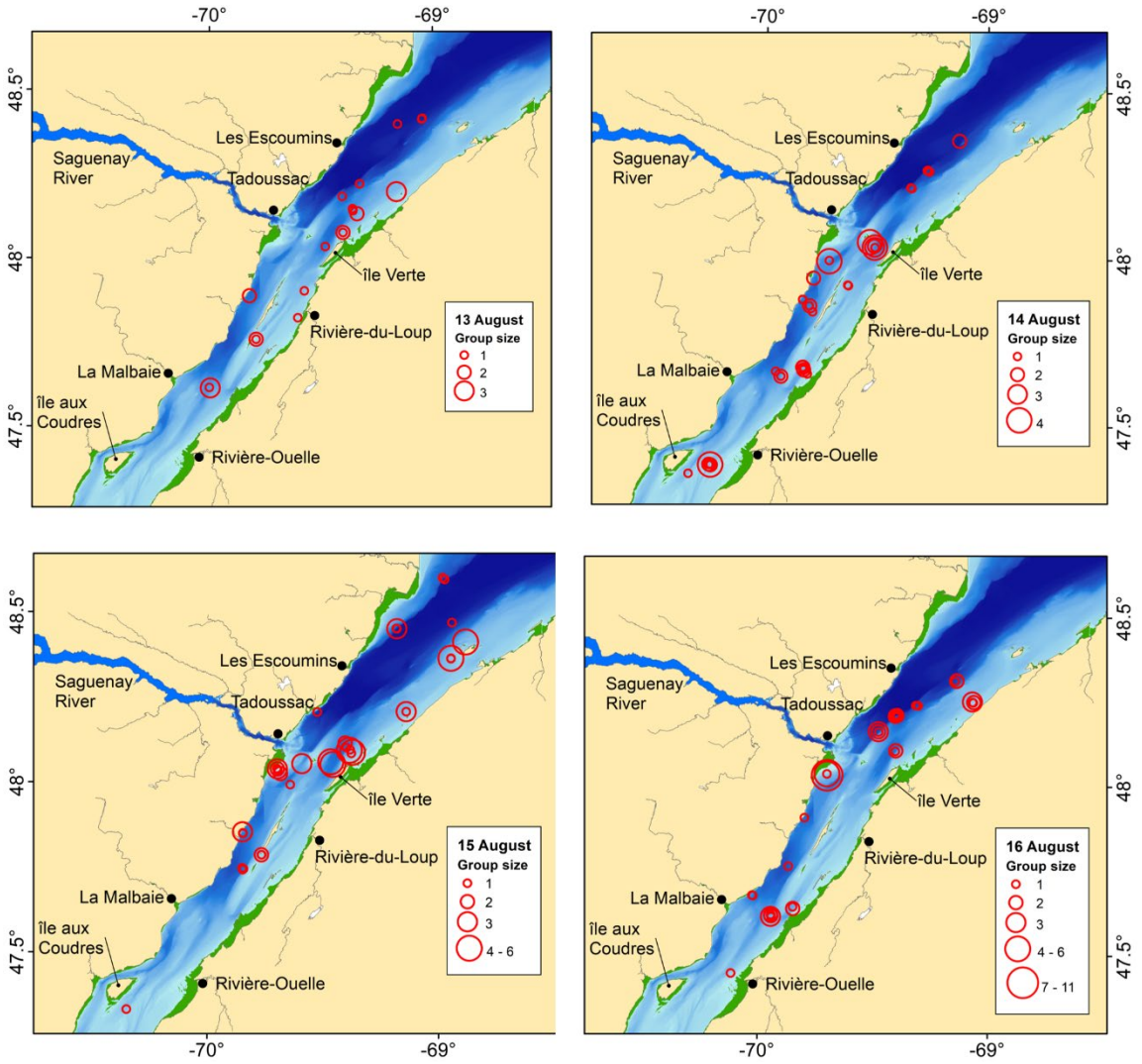

Figure 2. Distribution of sightings made during four photographic surveys of the St. Lawrence Estuary beluga summer range conducted from 13—16 August, 2019.

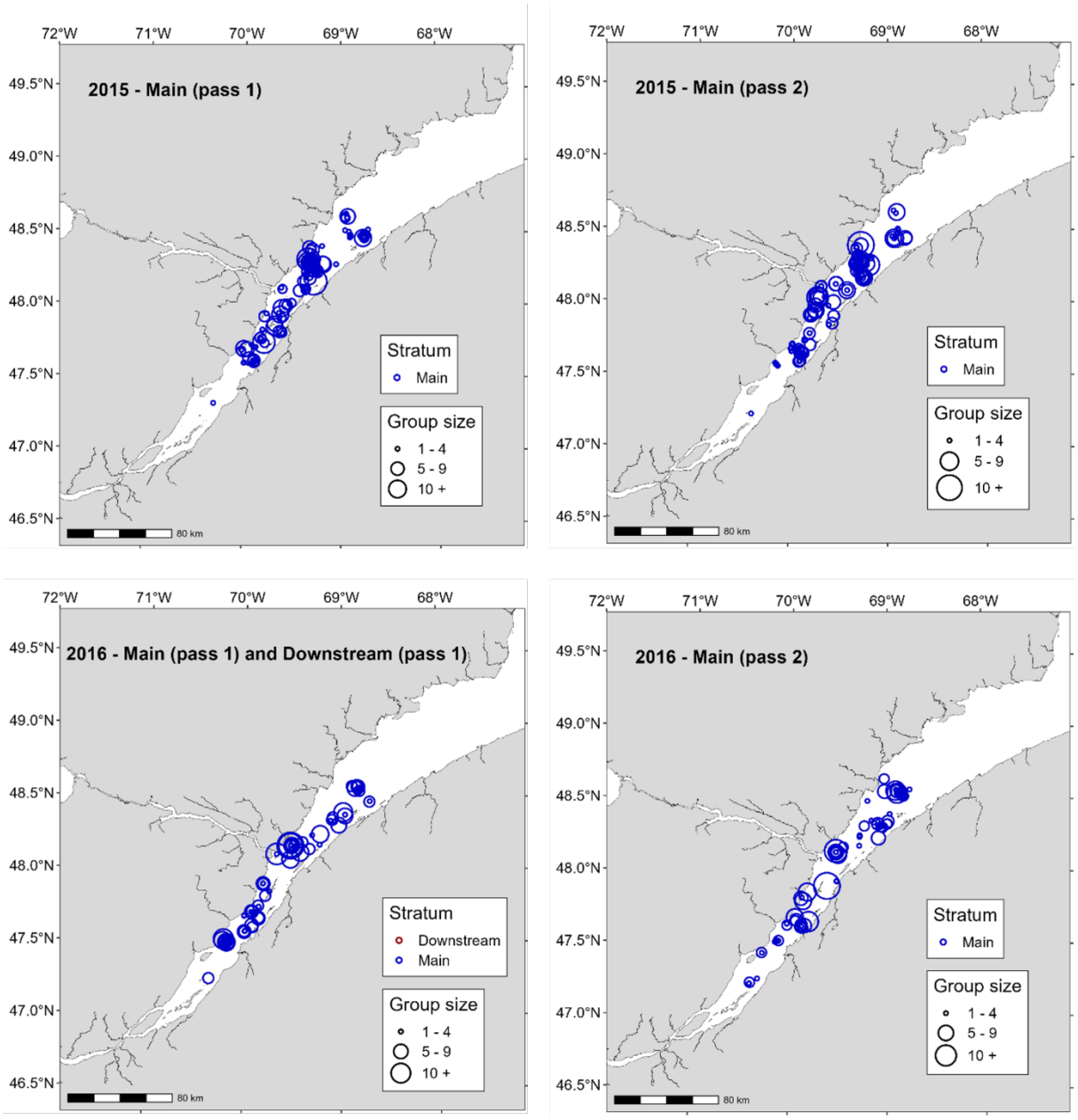

Figure 3. Locations and group sizes of beluga whales detected along transect lines during the two survey passes of 2015 (top) and 2016 (bottom). Figure continued on following pages.

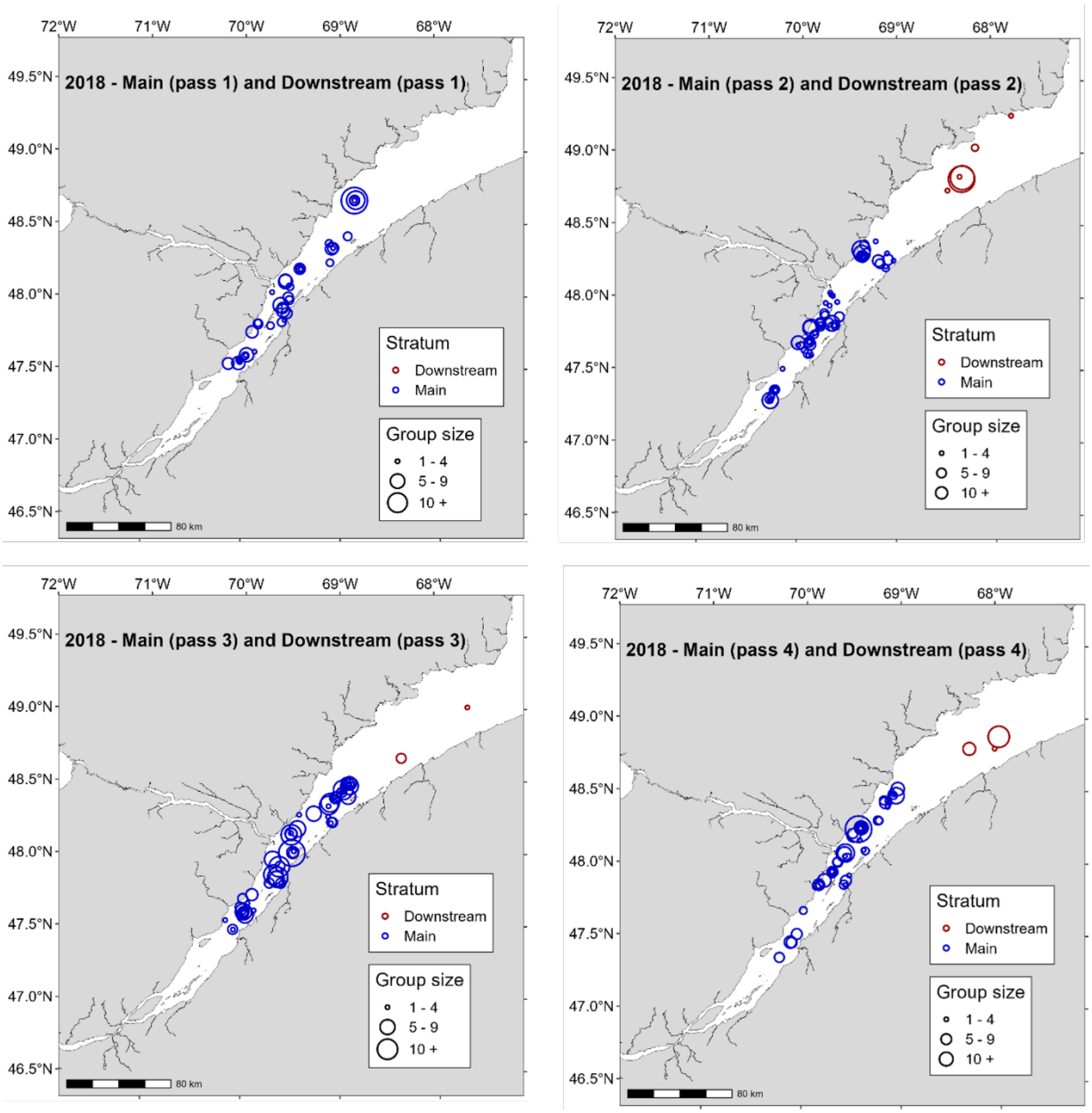

Figure 3. continued. Locations and group sizes of beluga whales detected along transect lines during the first four survey passes of 2018. Figure continued on following pages.

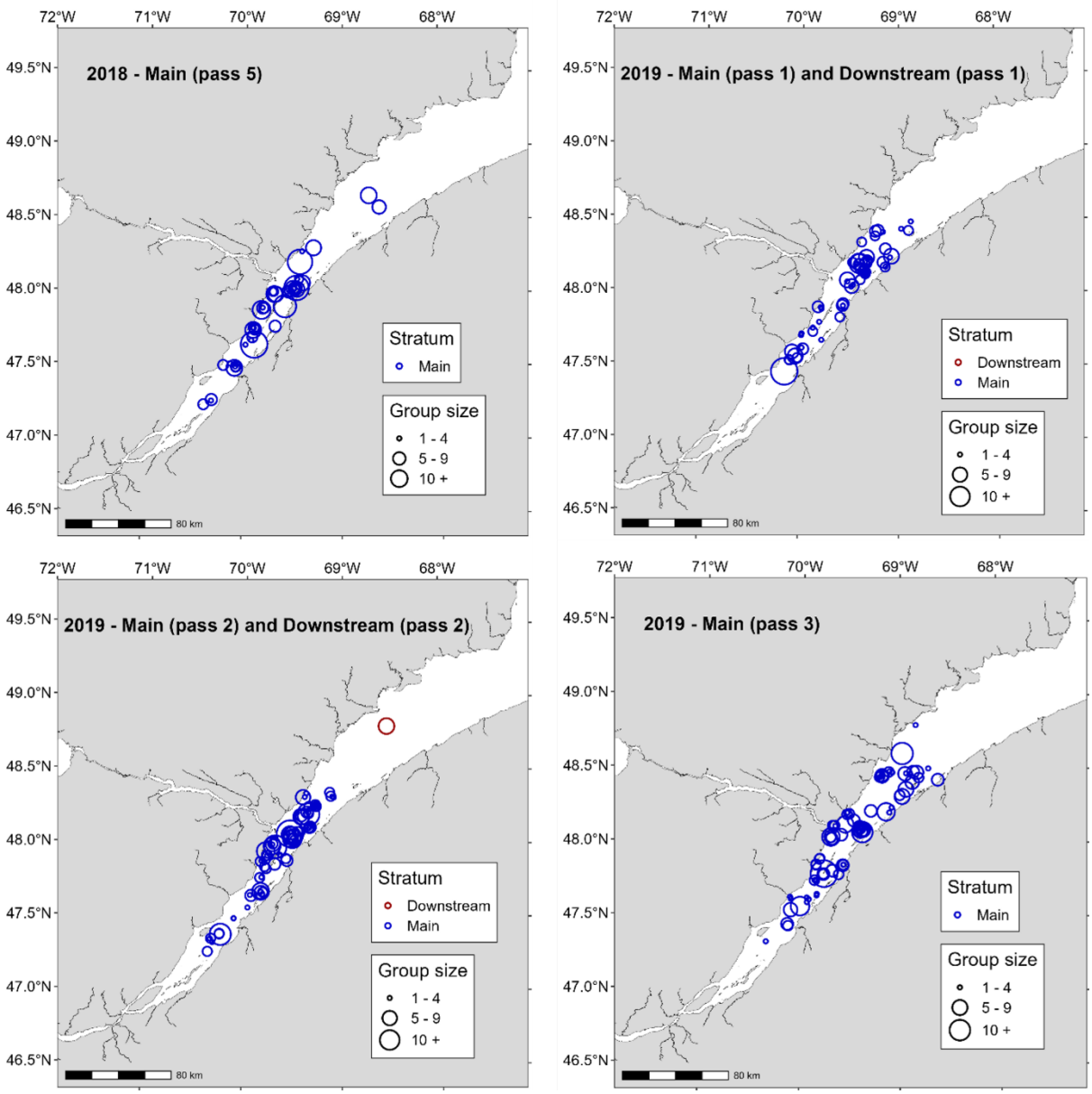

Figure 3. continued. Locations and group sizes of beluga whales detected along transect lines during the fifth survey pass of 2018 (top left) and the first three passes of 2019 (top right and bottom). Figure continued on following pages.

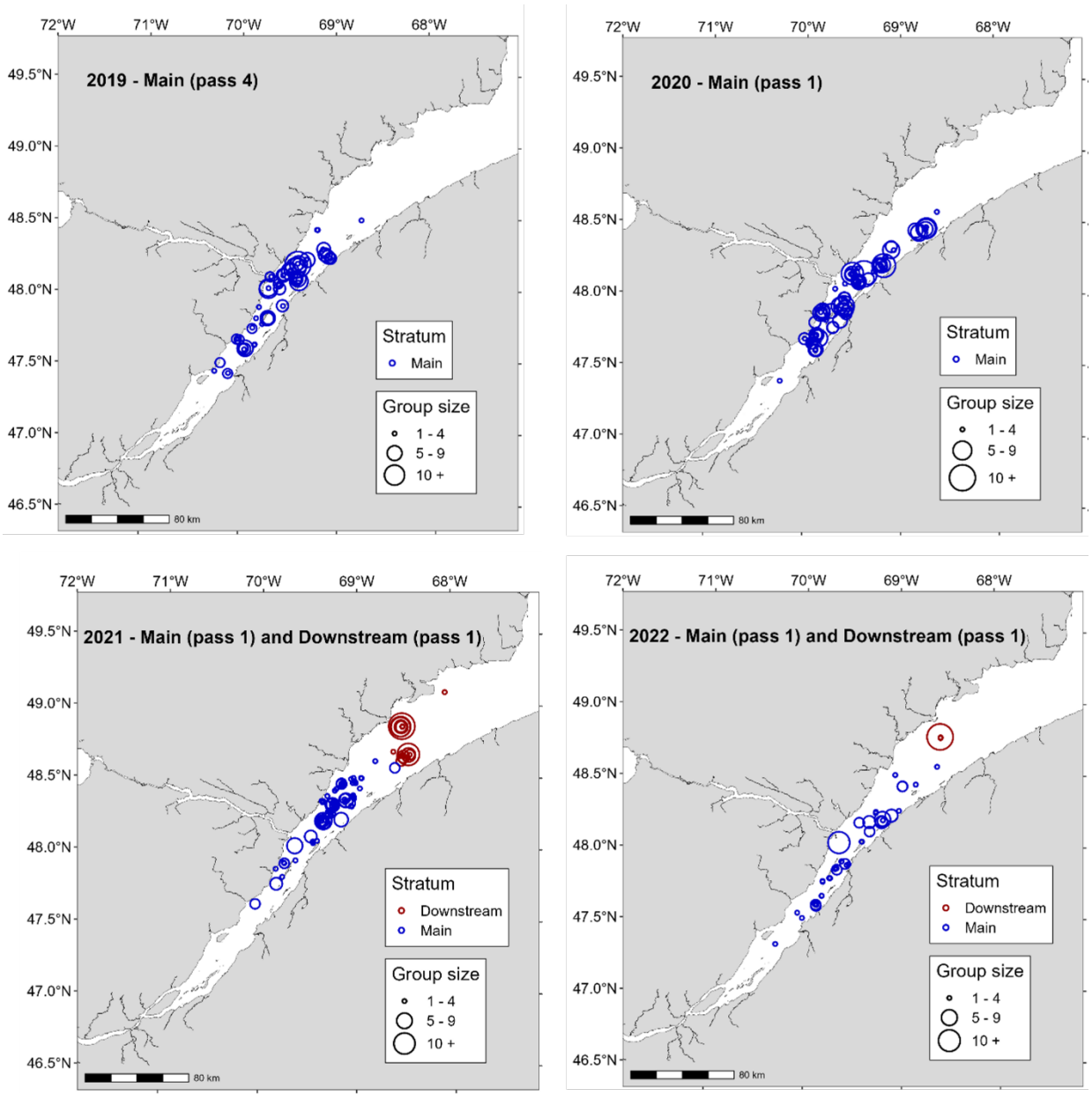

Figure 3. continued. Locations and group sizes of beluga whales detected along transect lines during the fourth survey pass of 2019 (top left), the 2020 survey (top right), the 2021 survey (bottom left) and the 2022 survey (bottom right).

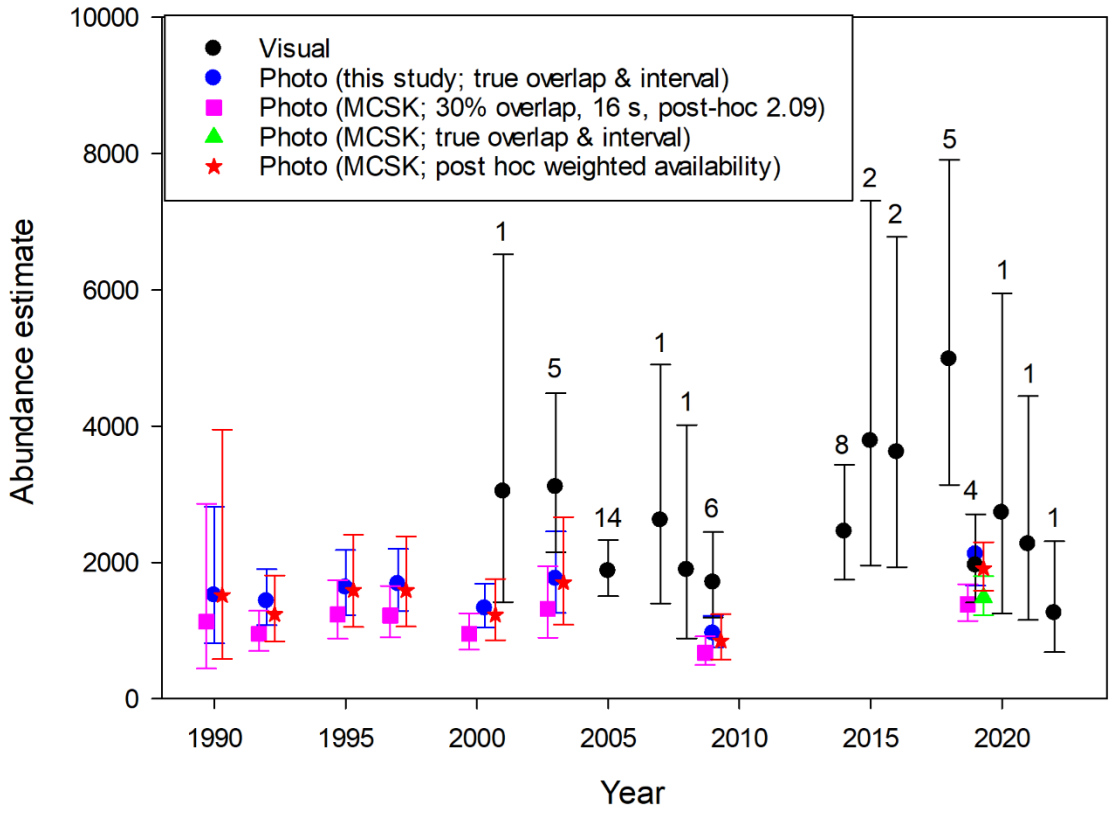

Figure 4. Fully corrected abundance estimates (and SE) from photographic (blue circles) and visual surveys (black circles) conducted between 1990 and 2022 in the St. Lawrence Estuary (this study). Abundance estimates obtained for the 2019 photographic surveys by applying various correction factor for availability bias a posteriori are also presented: using the weighted mean availability with a 4 m turbidity threshold from the 27 tagged beluga (0.367; SE = 0.019) while adjusting for photograph overlap and frame capture interval (red stars); and using the previously accepted correction factor for availability bias a posteriori (Kingsley and Gauthier 2002), adjusted (2.21—2.26; green triangle) and not adjusted (2.09; pink square) for differences in photograph overlap (29—39% vs 30%) and frame capture interval (3—6 s vs 16 s).

APPENDIX 1. OVERLAP AREA FOR THE 2019 PHOTOGRAPHIC SURVEYS

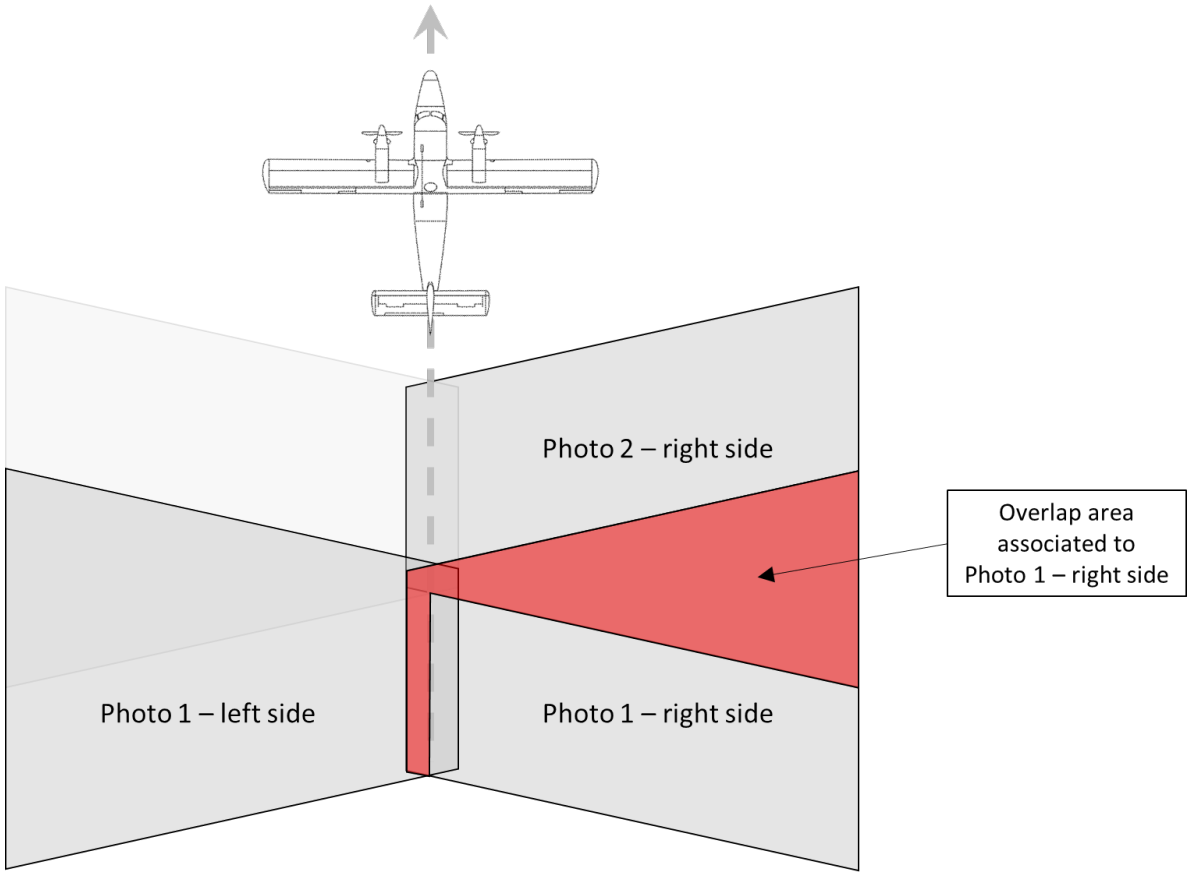

Figure A1.1. Representation of the area covered by subsequent images taken from the aircraft during the photographic survey, and their overlapping area.

APPENDIX 2. GLARE DETECTION ON PHOTOGRAPHS

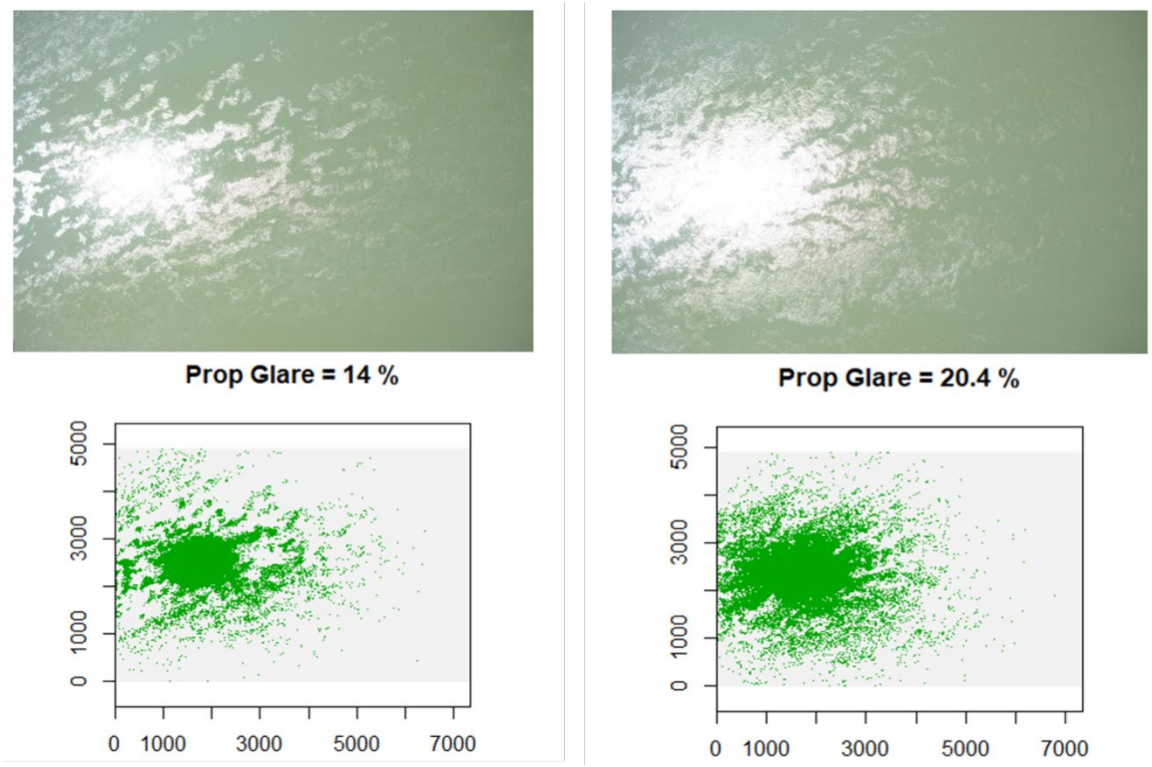

Figure A2.1. Illustration of the method for glare detection on photographs using a minimum value of 200 on each of the Red, Green and Blue layers of the RGB primary color spectrum to identify the proportion of a photo in which beluga detection is compromised due to sun reflection.

APPENDIX 3. DETAILED SURVEY DESIGN FOR PHOTOGRAPHIC SURVEYS

Table A3.1. Parameters for estimating availability bias and abundance for photographic surveys conducted from 1990 to 2019.

Year	Reference	Line spacing (nautical miles)	Interval between photos (s)	Photo overlap (%)	Altitude (m)
1990	Kingsley & Hammill 1991	variable	~18 [c]	20 [a,b]	Stratum 1: 1219 Stratum 2: 914 Stratum 3: 914
1992	Kingsley 1993	2	15—20 (18)	20 [a]	1219
1995	Kingsley 1996	2	14—17 (16)	33 [a]	1219
1997	Kingsley 1999	2	~16 [c]	30 [a]	1219
2000	Gosselin et al. 2001	2	~16 [c]	29	1223
2003	Gosselin et al. 2007	2	~16 [c]	31	1219
2009	Gosselin et al. 2014	2	~19	17	1219
2019	St-Pierre et al. In press	4	6 s pass 1; 3 s passes 2—4	29% pass 1; 37—39% passes 2—4; 36% overall	334—337

[a] Targeted overlap; not achieved overlap
[b] Overlap said to be 'minimal' but estimated from photos using a posteriori landmarks or water fronts and debris at ~20%
[c] Estimated from overlap and flight altitude

APPENDIX 4. COVERAGE ACHIEVED DURING PHOTOGRAPHIC SURVEYS, 13–16 AUGUST, 2019

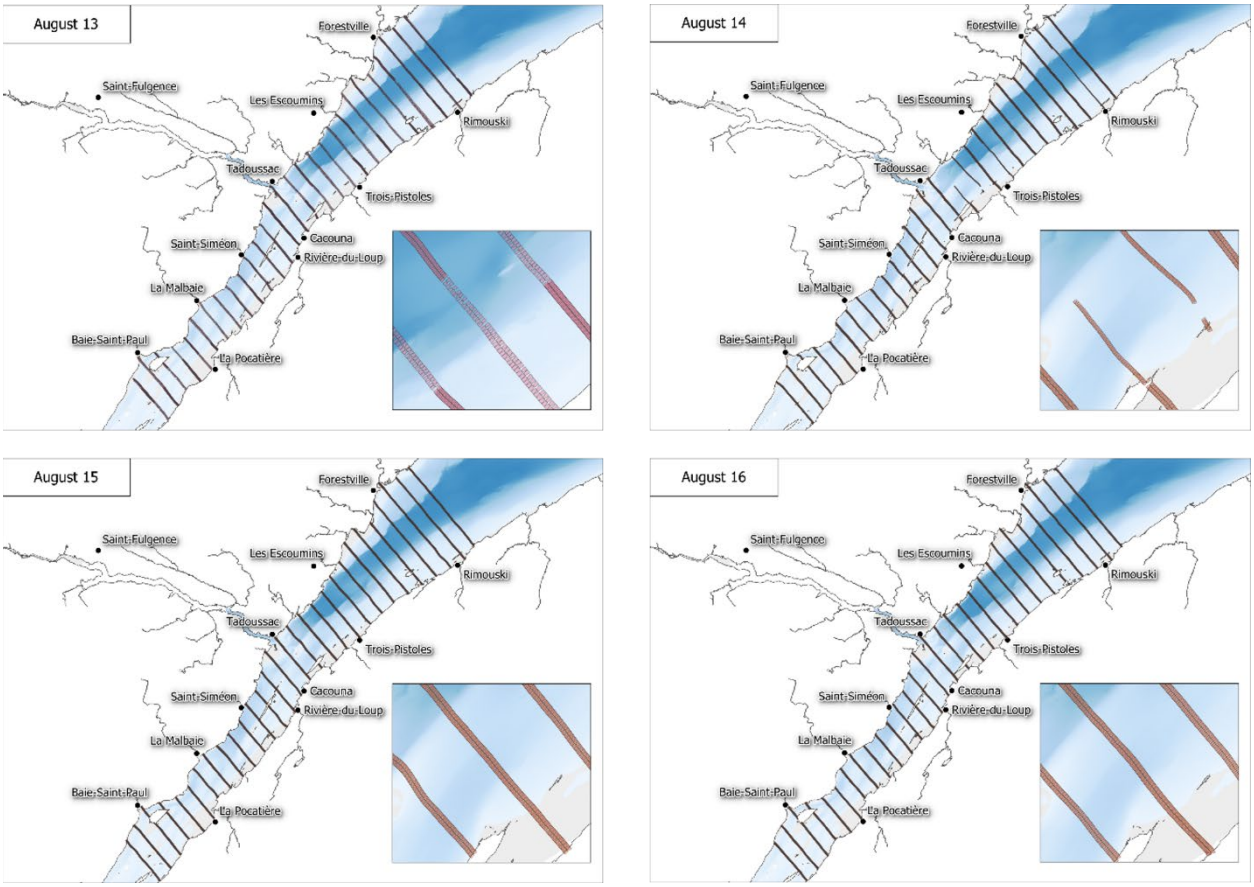

Figure A4.1. Illustration of the photographs acquired along the transect lines flown during the surveys of 2019.

APPENDIX 5. BELUGA COUNTS ON PHOTOGRAPHS TAKEN DURING STRIP-TRANSECT AERIAL SURVEYS, 13–16 AUGUST, 2019

Table A5.1. Percent glare, overlap and number of beluga counted on 6,700 digital images on 13 August, 2019 after removing duplicates on overlap of adjacent photographs along transects.

Line number	N frames	Count	Overlap %	Glare %
1	500	-	40.1	0.0
2	421	-	29.9	0.1
3	520	-	37.1	0.1
4	296	-	27.5	0.0
5	247	-	18.3	0.1
6	252	2	18.0	0.2
7	273	1	27.0	0.3
8	219	-	22.3	0.3
9	234	3	28.7	0.2
10	125	4	4.5	0.6
11	158	8	8.4	1.0
12	221	3	27.8	0.9
13	203	1	28.9	1.2
14	289	-	32.2	3.4
15	363	1	51.2	2.7
16	239	2	30.3	1.1
17	214	4	34.6	1.5
18	194	3	25.4	3.3
19	194	-	38.7	5.1
20	146	-	23.5	11.5
21	133	4	8.6	5.4
22	113	-	5.0	2.8
23	151	-	25.0	11.1
24	168	-	25.5	10.9
25	204	-	35.6	18.9
26	147	-	22.2	14.3
27	247	-	31.1	16.6
28	229	-	36.5	6.8

Table A5.2. Percent glare, overlap and number of beluga counted on 8,835 digital images on 14 August, 2019 after removing duplicates on overlap of adjacent photographs along transects.

Line number	N of frames	Count	Overlap %	Glare %
1	640	-	41.6	0.1
2	374	-	37.3	0.2
3	616	-	41.9	0.1
4	482	-	39.6	0.2
5	437	-	42.6	0.2
6	451	-	41.2	0.2
7	406	2	42.3	0.3
8	369	-	40.9	0.3
9	236	5	39.2	0.5
10	325	3	40.7	0.3
11	128	-	44.2	0.3
12	126	-	37.3	0.2
13	319	15	43.8	0.6
14	287	-	35.1	0.9
15	311	8	39.5	0.0
16	288	2	39.0	0.1
17	280	7	40.7	1.0
18	231	-	37.1	0.7
19	238	13	37.8	2.8
20	205	5	36.6	1.8
21	262	-	36.0	1.9
22	217	-	34.6	4.2
23	232	-	47.1	9.2
24	228	-	36.9	10.1
25	276	21	39.3	13.0
26	239	1	35.1	9.0
27	322	-	37.3	9.7
28	310	-	34.8	6.2

Table A5.3. Percent glare, overlap and number of beluga counted on 10,062 digital images on 15 August, 2019 after removing duplicates on overlap of adjacent photographs along transects.

Line number	N of frames	Count	Overlap %	Glare %
0	625	-	41.2	0.3
2	557	-	32.5	0.2
3	661	-	40.4	0.2
4	522	6	33.7	0.2
5	449	1	40.2	0.9
6	462	6	38.3	0.2
7	433	5	42.2	0.5
8	380	-	37.3	0.1
9	346	7	36.8	0.3
10	346	-	40.4	0.3
11	310	-	38.7	0.3
12	338	15	43.1	0.2
13	284	10	37.7	0.5
14	311	3	39.4	1.0
15	325	10	39.1	5.1
16	312	-	41.1	4.1
17	268	-	39.2	8.9
18	270	9	40.3	5.0
19	230	3	38.9	5.6
20	254	-	41.6	2.9
21	231	-	41.5	5.7
22	261	-	43.0	3.1
23	213	-	36.3	4.6
24	234	-	37.2	5.9
25	253	-	39.3	10.2
26	247	-	38.1	5.2
27	302	1	39.6	6.2
28	336	-	42.6	4.0
29	302	-	38.1	6.5

Table A5.4. Percent glare, overlap and number of beluga counted on 9,846 digital images on 16 August, 2019 after removing duplicates on overlap of adjacent photographs along transects.

Line number	N of frames	Count	Overlap %	Glare %
1	541	-	34.6	0.0
2	619	-	37.5	0.1
3	605	-	35.6	0.6
4	541	-	39.0	0.0
5	406	-	34.3	0.9
6	478	-	37.2	2.1
7	416	-	35.7	0.0
8	379	12	38.5	0.1
9	315	-	35.4	0.1
10	372	6	43.8	0.0
11	297	16	33.2	2.3
12	351	9	41.9	0.1
13	275	-	34.8	0.4
14	325	-	39.4	0.1
15	311	16	34.6	27.0
16	300	-	34.8	3.9
17	264	1	37.4	1.3
18	262	-	36.9	15.7
19	222	1	40.3	3.4
20	240	3	37.0	0.2
21	227	13	39.3	0.3
22	254	-	42.3	19.9
23	213	-	39.4	1.0
24	225	1	33.3	0.3
25	247	-	39.8	15.0
26	240	-	40.1	31.6
27	310	-	38.0	32.1
28	325	-	41.8	46.8
29	286	-	41.4	85.8

APPENDIX 6. DISTRIBUTION OF BELUGA DETECTED IN SURVEYS FROM 2001 TO 2014

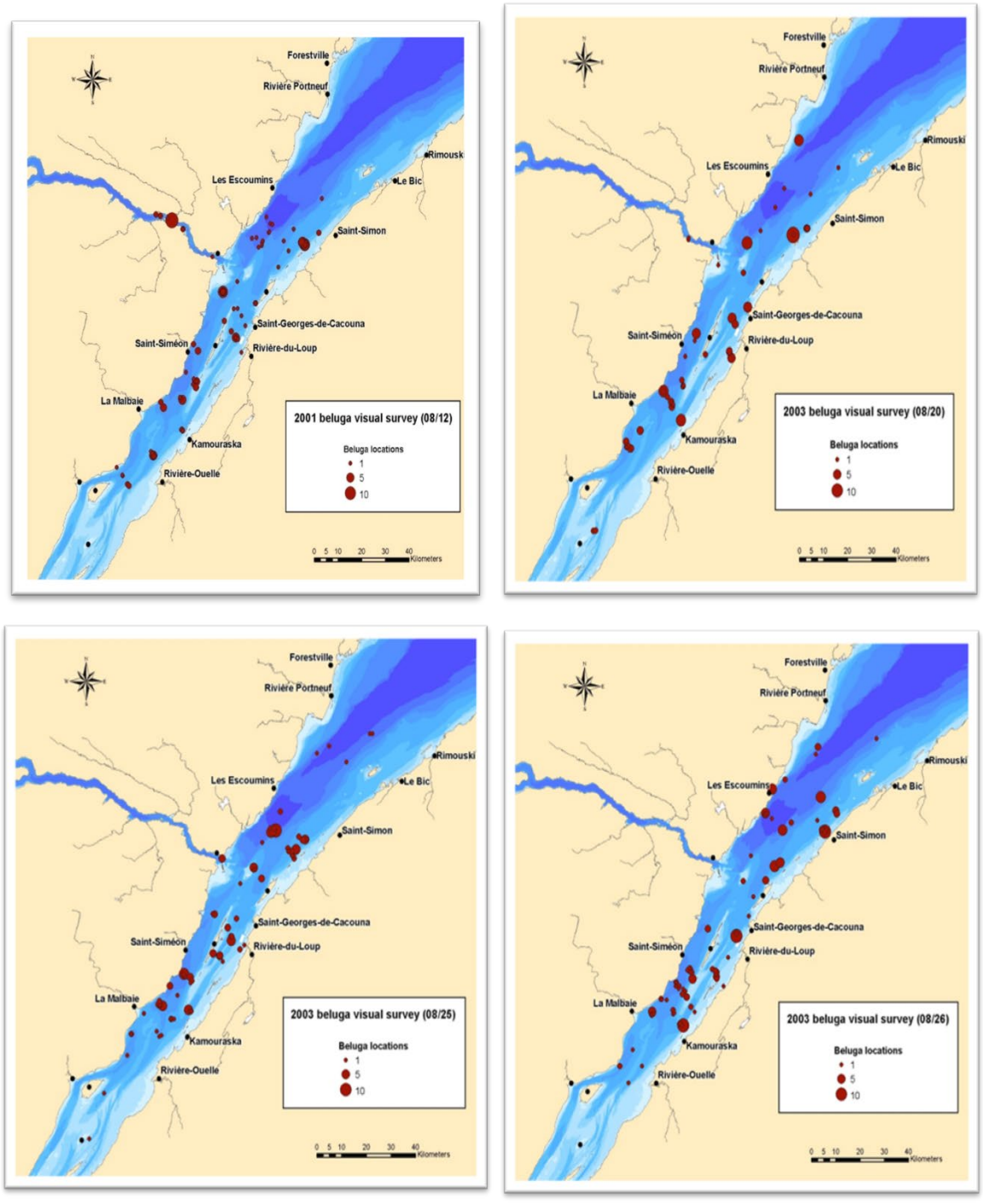

Figure A6.1. Locations and group sizes of beluga whales detected along transect lines flown August 12 (top left), 20 August (top right), 25 August (bottom left) and 26 August 2003 (bottom right). From Gosselin et al 2014.

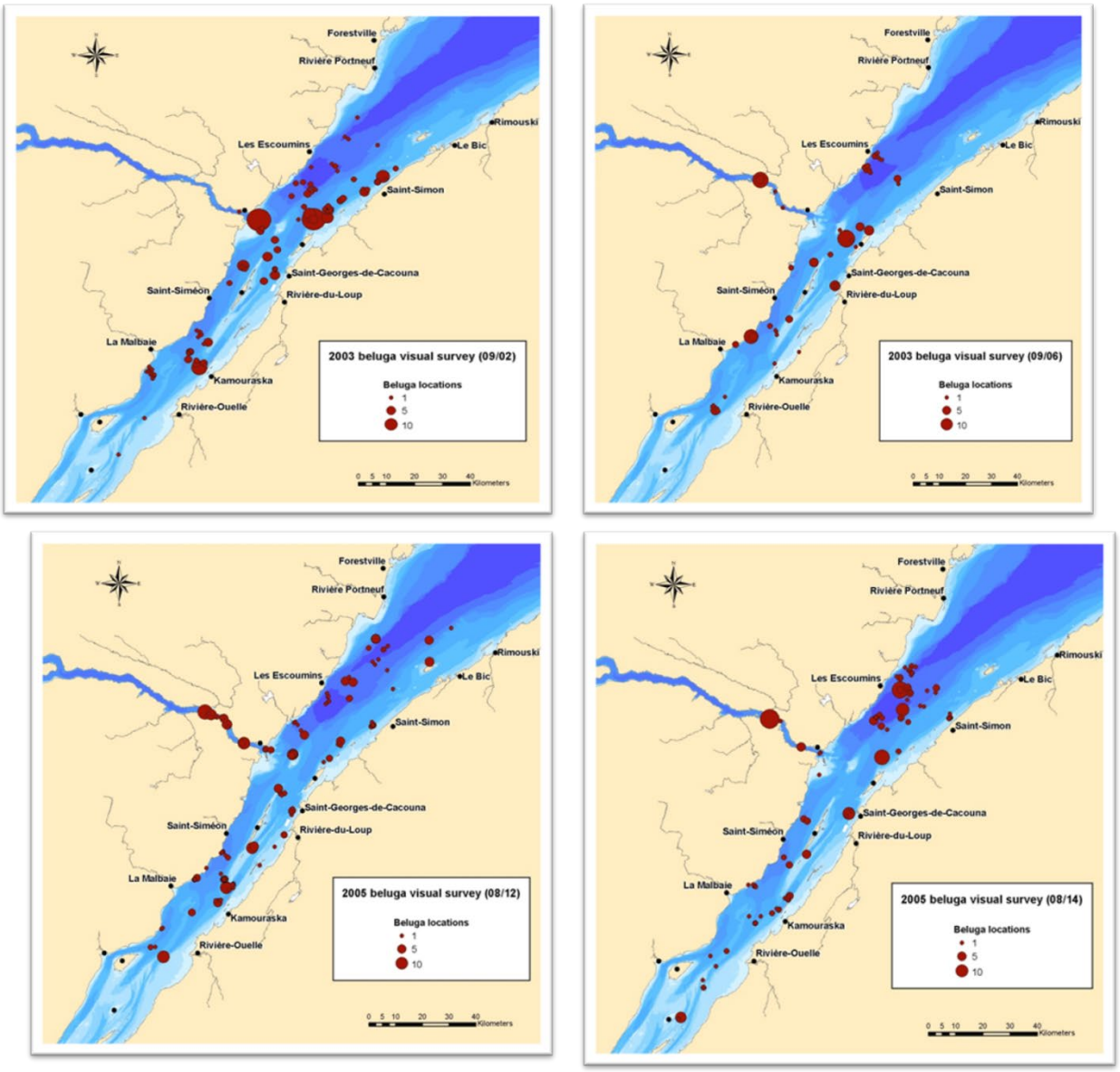

Figure A6.2. Locations and group sizes of beluga whales detected along transect lines flown 2 September 2003 (top left), 4 September 2003 (top right), 12 August 2005 (bottom left) and 14 August 2005 (bottom right). From Gosselin et al 2014.

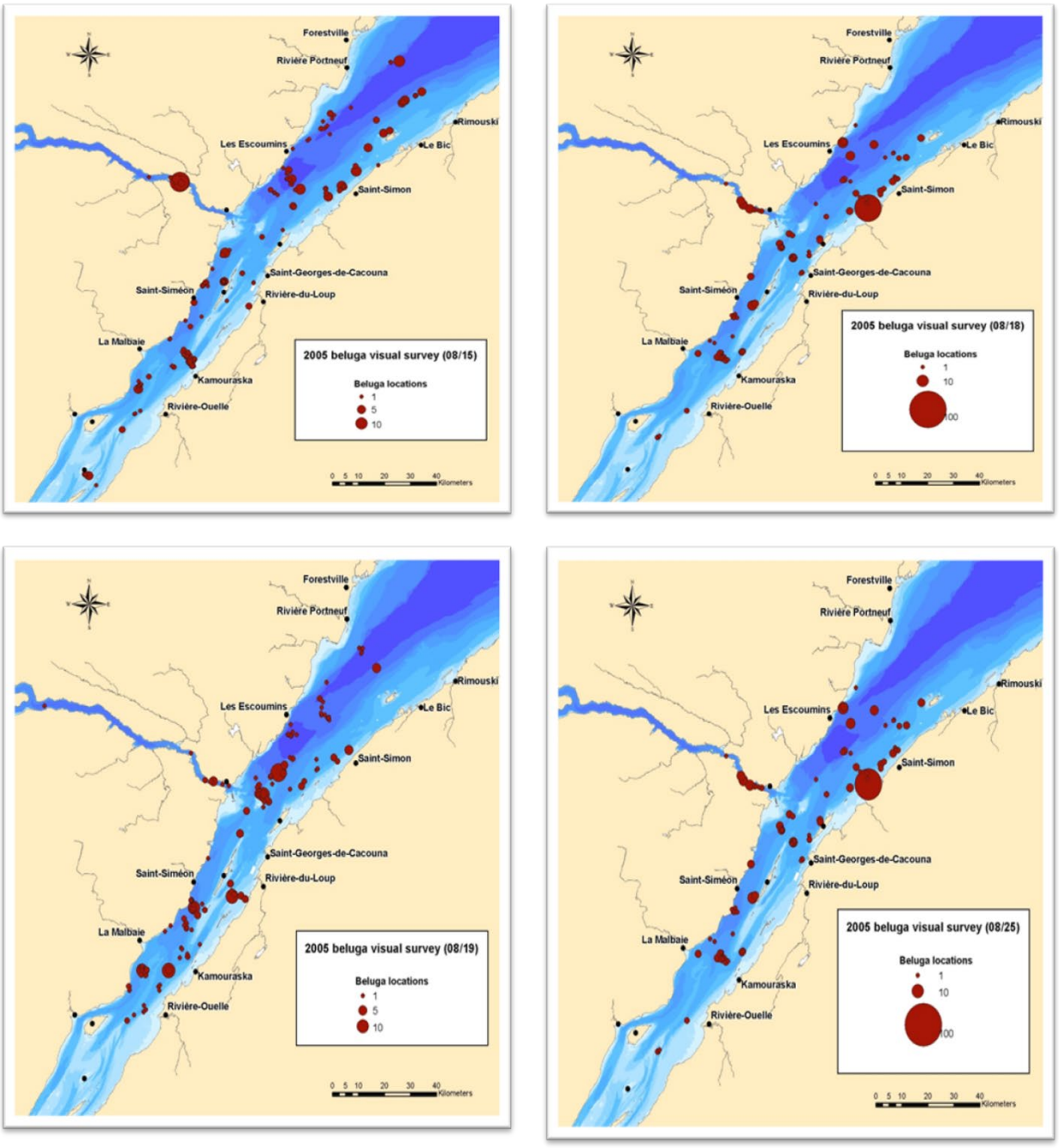

Figure A6.3. Locations and group sizes of beluga whales detected along transect lines flown 15 August 2005 (top left), 18 August 2005 (top right), 19 August 2005 (bottom left) and 25 August 2005 (bottom right). From Gosselin et al 2014.

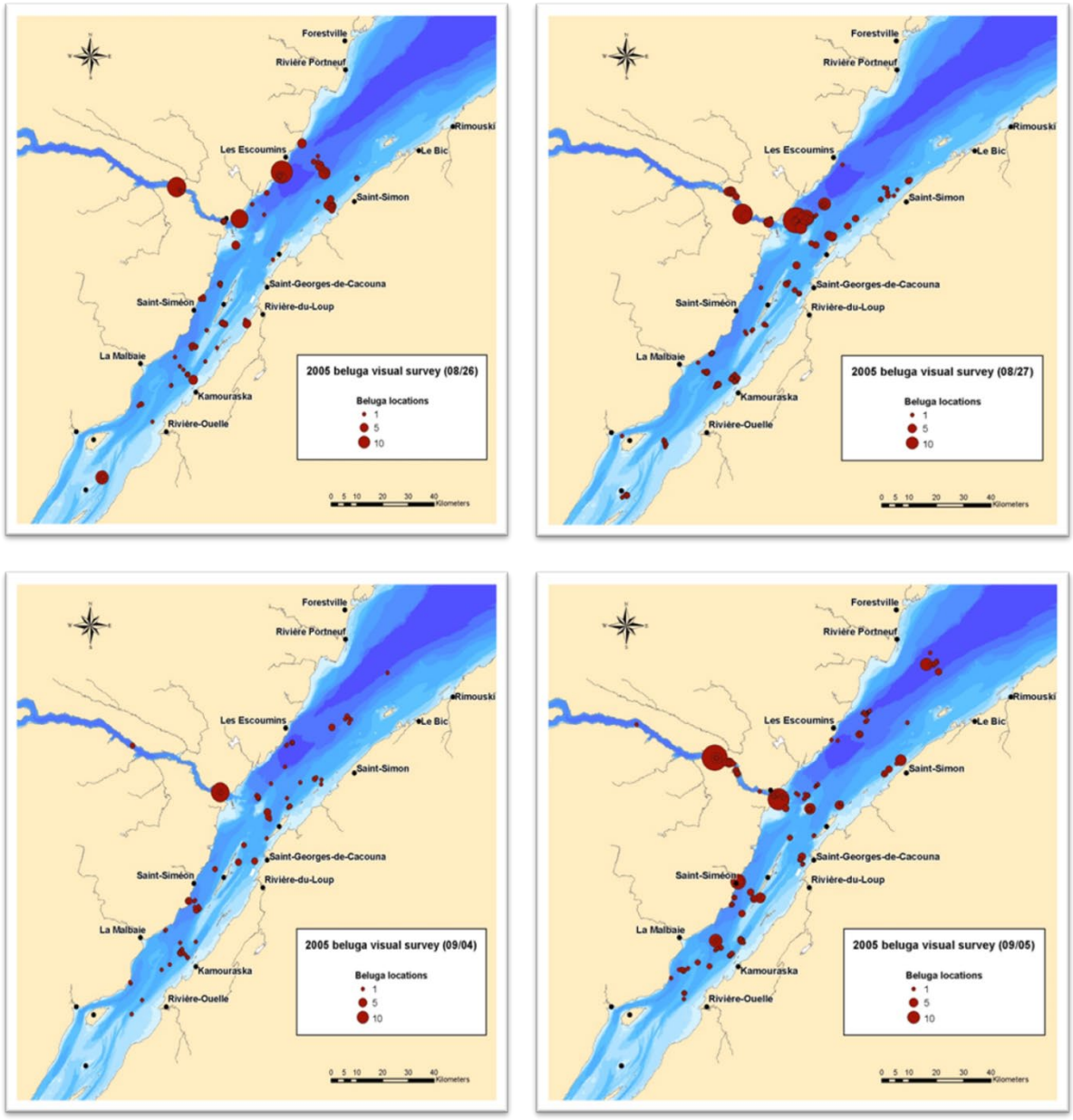

Figure A6.4. Locations and group sizes of beluga whales detected along transect lines flown 26 August 2005 (top left), 27 August 2005 (top right), 4 September 2005 (bottom left) and 5 September 2005 (bottom right). From Gosselin et al 2014.

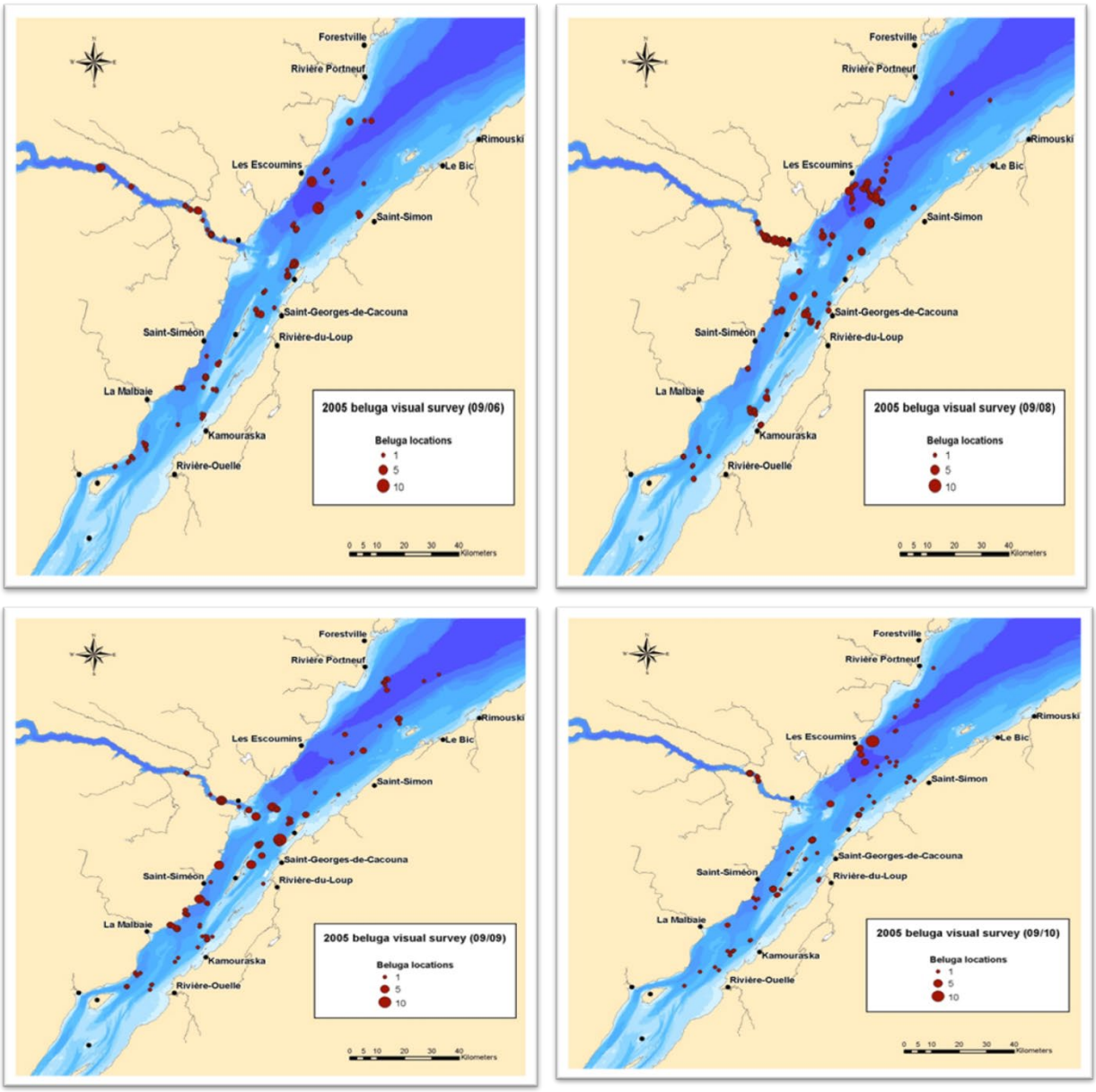

Figure A6.5. Locations and group sizes of beluga whales detected along transect lines flown 6 September (top left), 8 September 2005 (top right), 9 September 2005 (bottom left) and 10 September 2005 (bottom right). From Gosselin et al 2014.

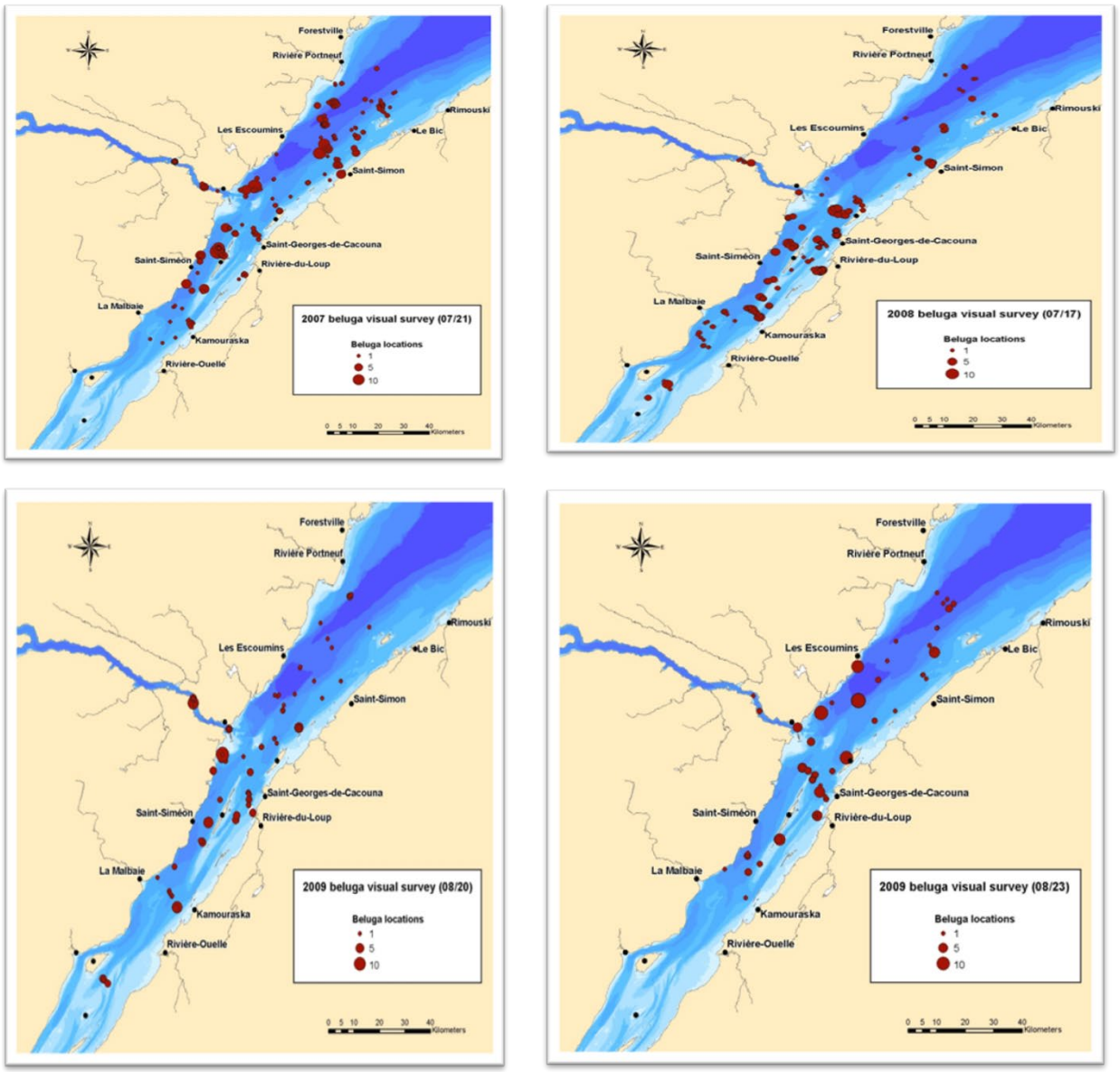

Figure A6.6. Locations and group sizes of beluga whales detected along transect lines flown 21 July 2007 (top left), 17 July 2008 (top right), 20 August 2009 (bottom left) and 23 August 2009 (bottom right). From Gosselin et al 2014.

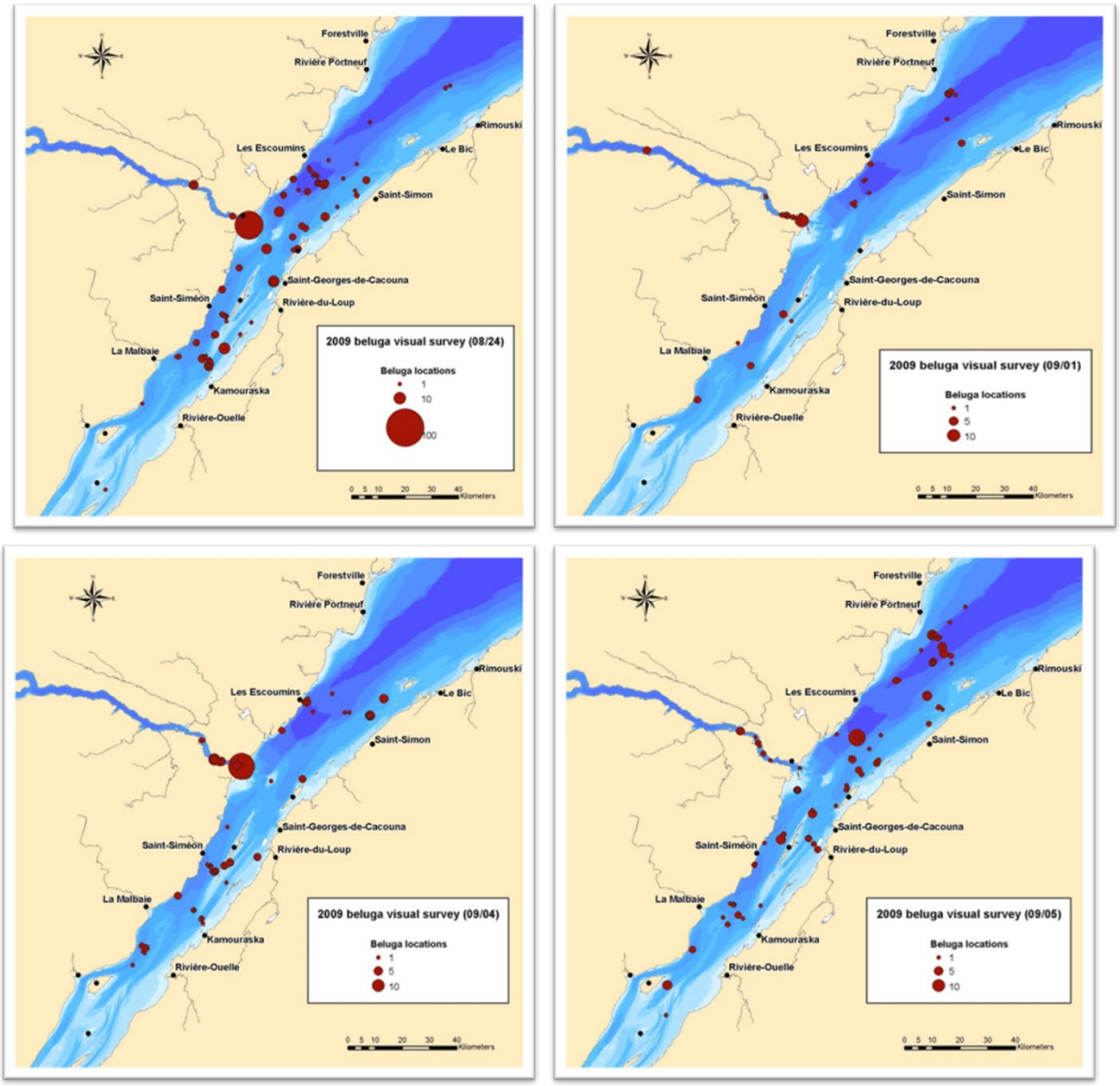

Figure A6.7. Locations and group sizes of beluga whales detected along transect lines flown 24 August 2009 (top left), 1 September 2009 (top right), 4 September 2009 (bottom left) and 5 September 2009 (bottom right). From Gosselin et al 2014.

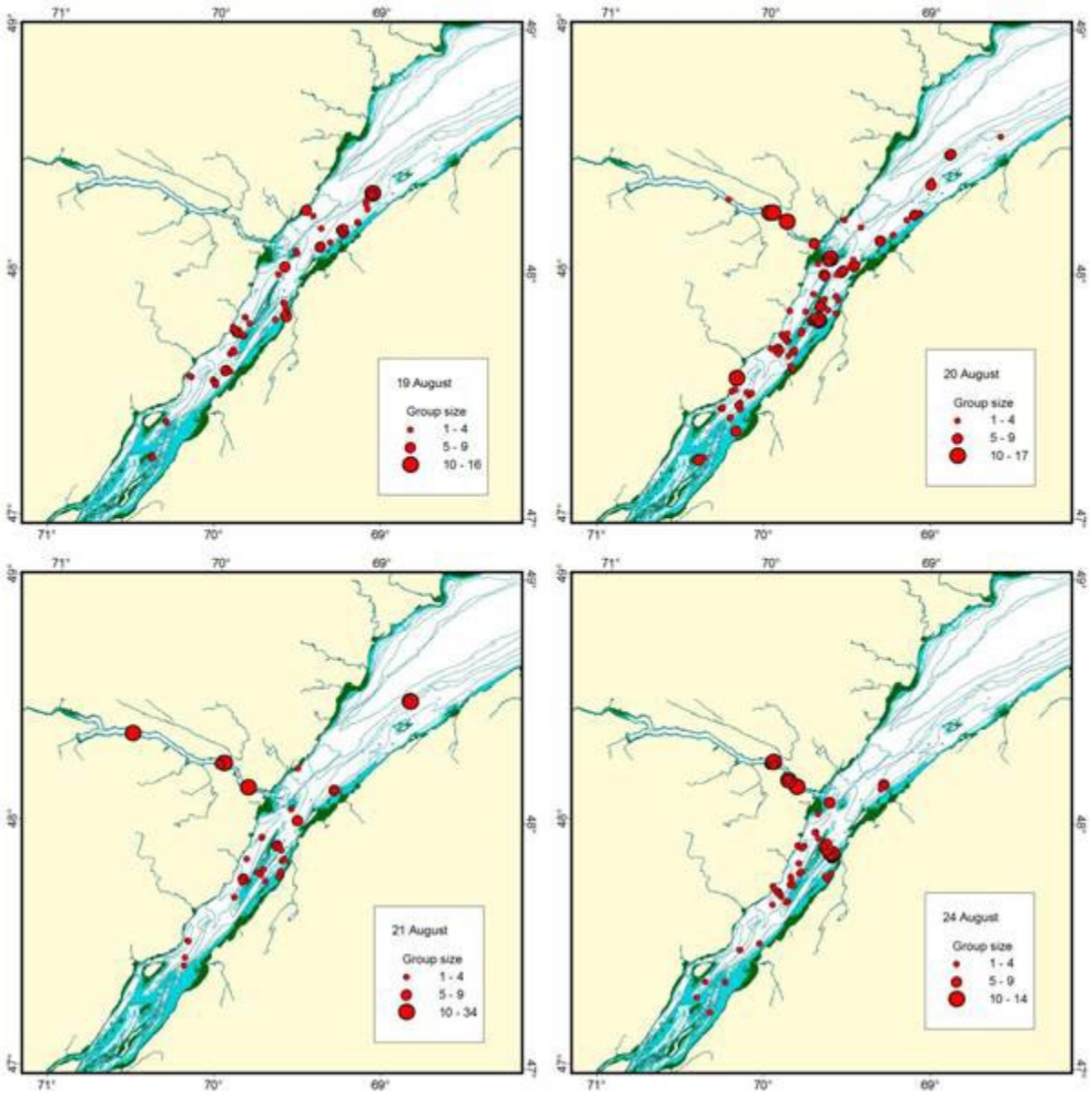

Figure A6.8. Locations and group sizes of beluga detected along transect lines flown in the St Lawrence Estuary and the Saguenay River from 19 August to 10 September 2014. The Saguenay River was not surveyed on the 19 August. From Gosselin et al 2017.

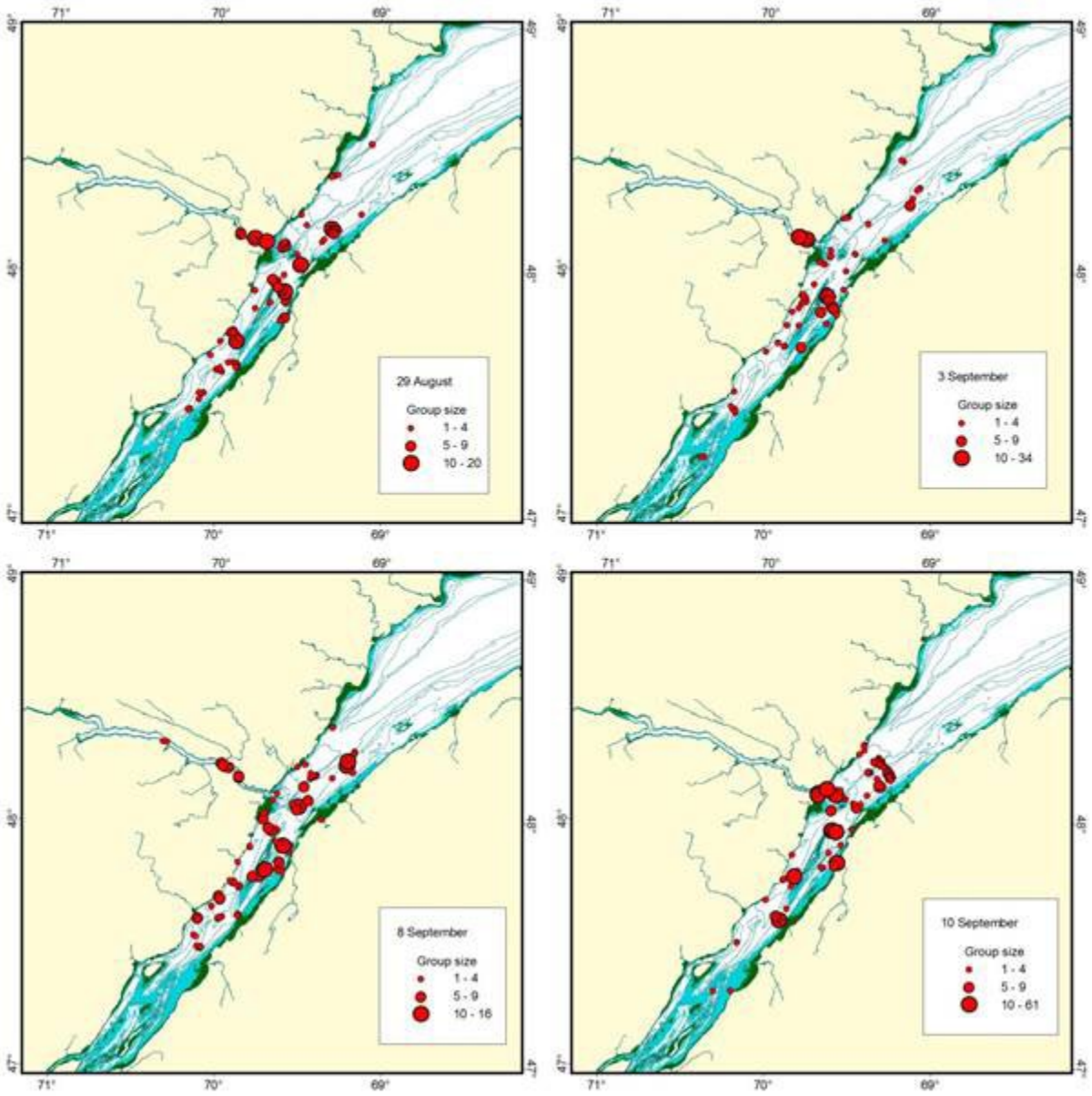

Figure A6.9. Locations and group sizes of beluga detected along transect lines flown in the St Lawrence Estuary and the Saguenay River from 19 August to 10 September 2014. From Gosselin et al 2017.

APPENDIX 7. DETECTION CURVES FROM THE VISUAL SURVEYS

Refer to Table 3 for further information regarding the right truncation distances, key functions, and covariates applied for each curve.

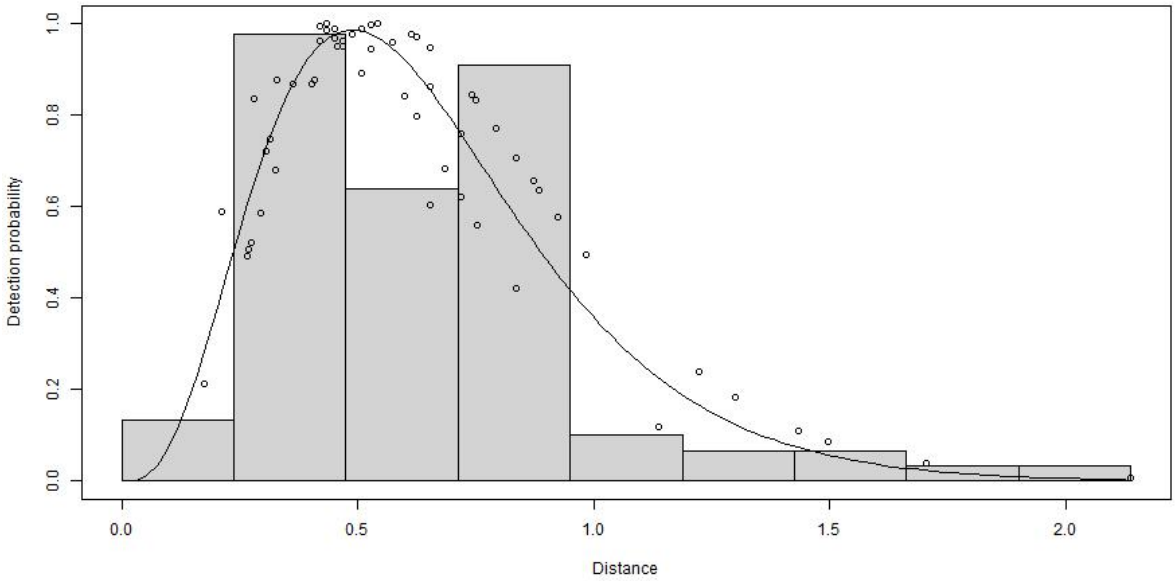

Figure A7.1. Detection curve for the 2001 survey. This analysis used a right truncation distance at the furthest distance observed, and Gamma key function (without adjustment term) with Beaufort as covariate. The number of sightings used in the detection curve was 88, and the effective strip half-width (ESHW) was 705 m. Distances on the X-axis are in kilometer.

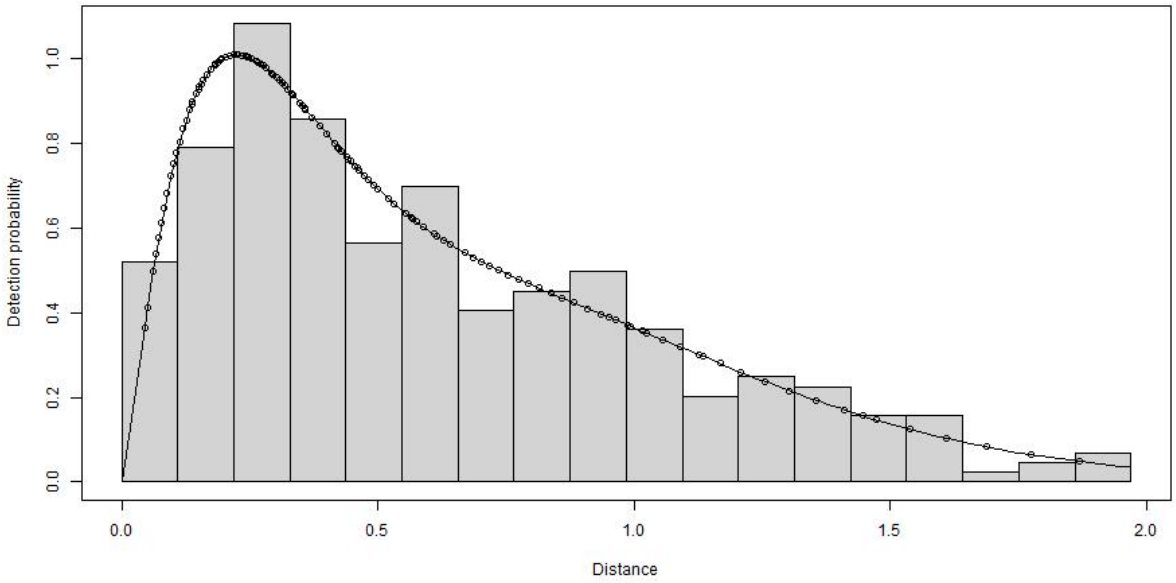

Figure A7.2. Detection curve for the 2003 survey. This analysis used a right truncation distance at 1970 m, and Gamma key function (with polynomial adjustment term) without covariates. The number of sightings used in the detection curve was 326, and the effective strip half-width (ESHW) was 805 m. Distances on the X-axis are in kilometer.

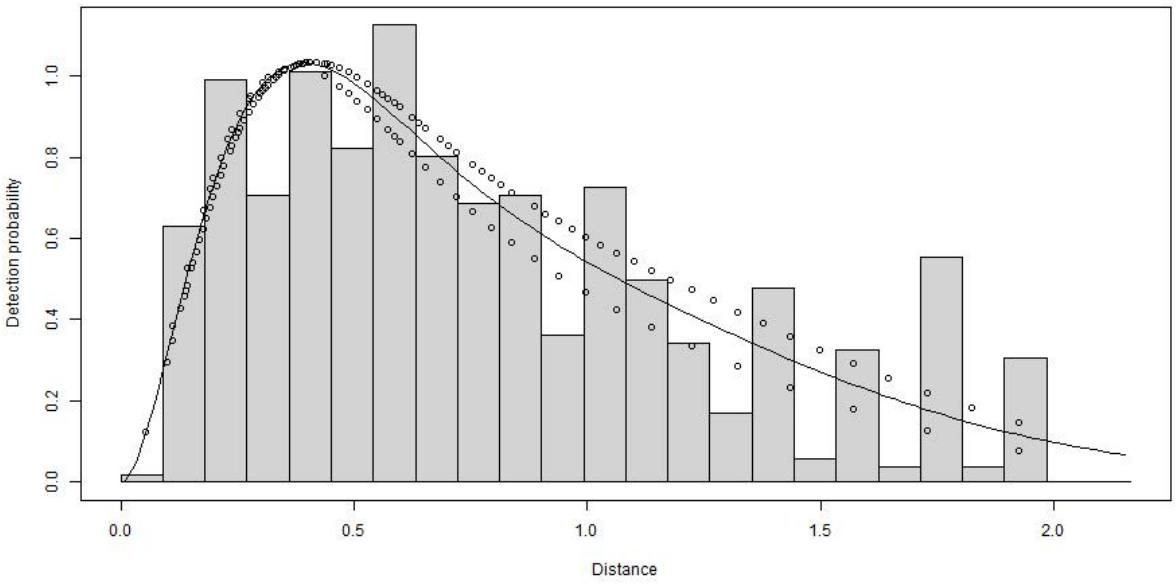

Figure A7.3. Detection curve for the 2005 survey flown at 305 m of altitude. This analysis used a right truncation distance at 2,165 m, and Gamma key function (with polynomial adjustment term) with observer identity as covariate. The number of sightings used in the detection curve was 597, and the effective strip half-width (ESHW) was 1,027 m. Distances on the X-axis are in kilometer.

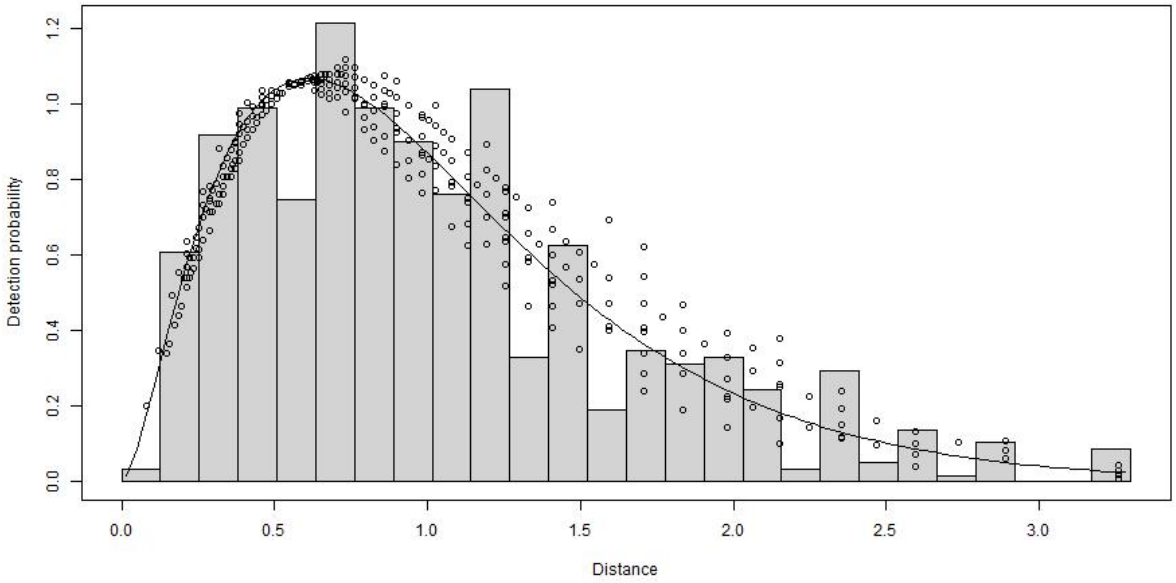

Figure A7.4. Detection curve for the 2005 survey flown at 457 m of altitude. This analysis used a right truncation distance at 3300 m, and Gamma key function (with polynomial adjustment term) with Beaufort and observer identity as covariates. The number of sightings used in the detection curve was 653, and the effective strip half-width (ESHW) was 1433 m. Distances on the X-axis are in kilometer.

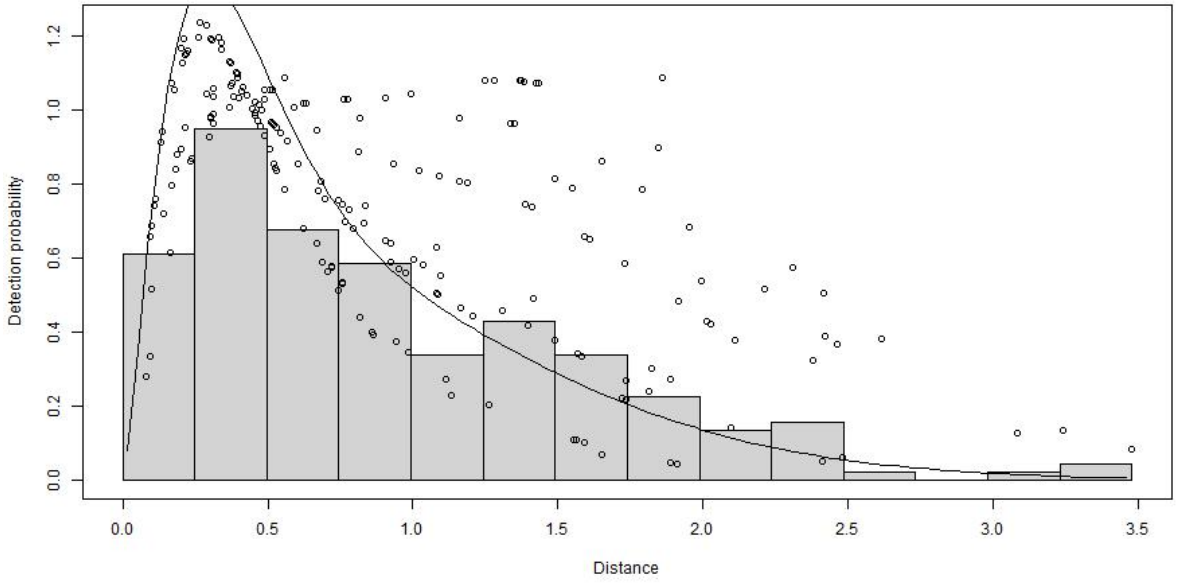

Figure A7.5. Detection curve for the 2007 survey. This analysis used a right truncation distance at the furthest distance observed, and Gamma key function (with polynomial adjustment term) with observer identity and water colour as covariates. The number of sightings used in the detection curve was 201, and the effective strip half-width (ESHW) was 1,127 m. Distances on the X-axis are in kilometer.

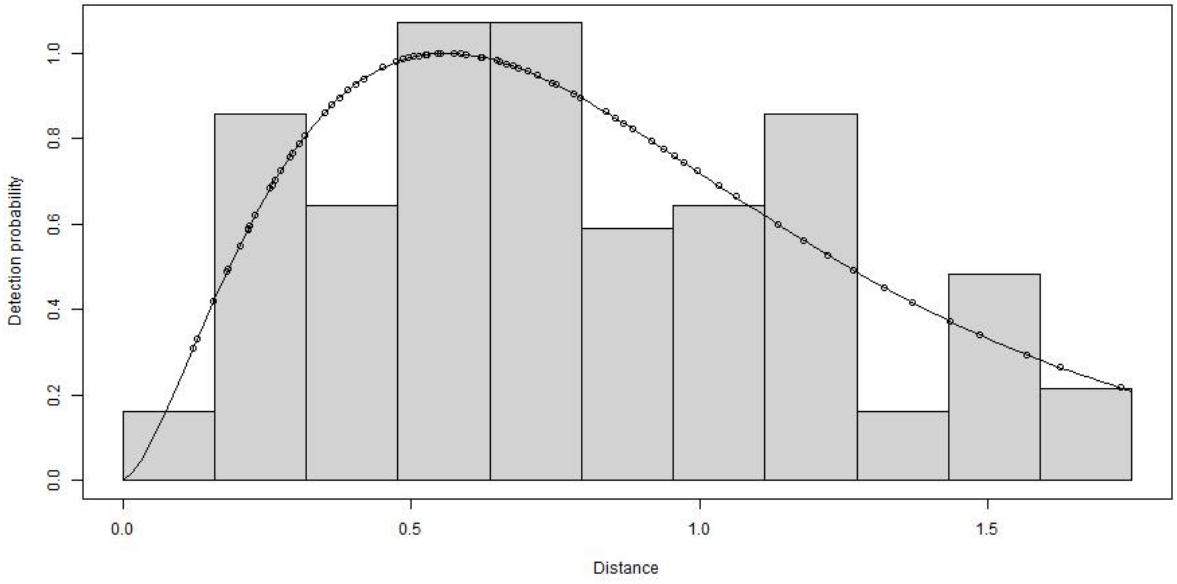

Figure A7.6. Detection curve for the 2008 survey. This analysis used a right truncation distance at 1,750 m, and Gamma key function (without adjustment term) without covariates. The number of sightings used in the detection curve was 126, and the effective strip half-width (ESHW) was 1,074 m. Distances on the X-axis are in kilometer.

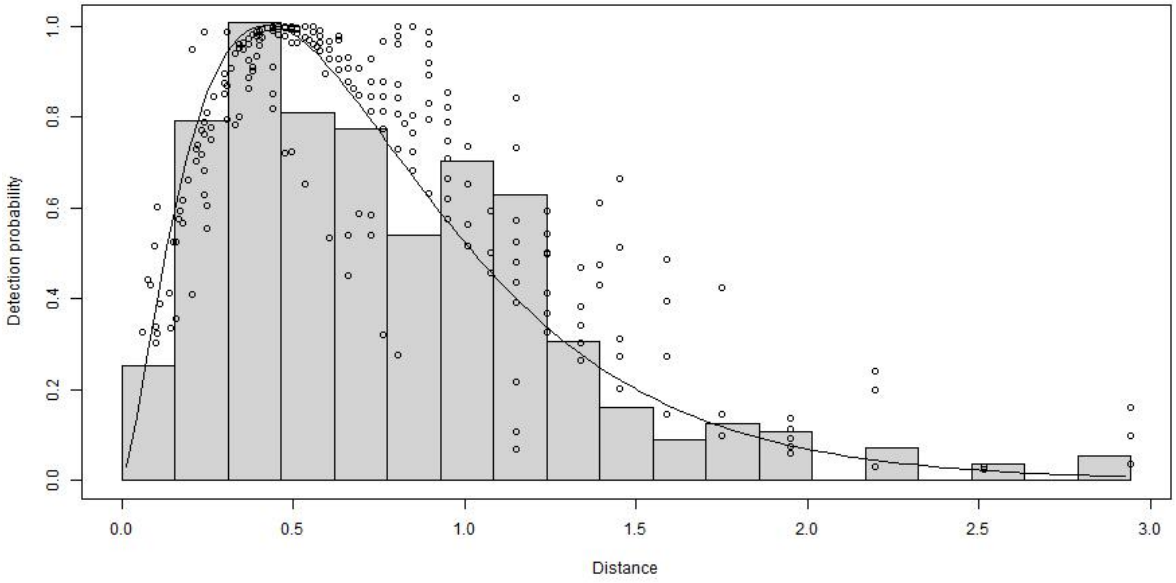

Figure A7.7. Detection curve for the 2009 survey. This analysis used a right truncation distance at the furthest distance observed, and Gamma key function (with polynomial adjustment term) with glare intensity and uncorrected cluster size as covariates. The number of sightings used in the detection curve was 359, and the effective strip half-width (ESHW) was 1,001 m. Distances on the X-axis are in kilometer.

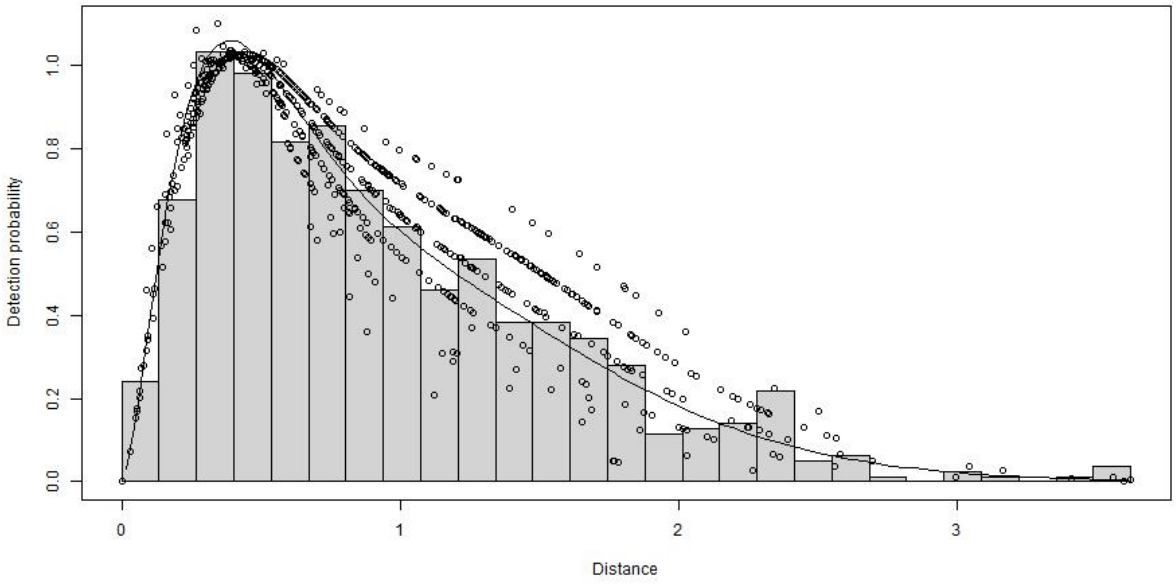

Figure A7.8. Detection curve for the 2014 survey. This analysis used a right truncation distance of 2580, and Gamma key function (with polynomial adjustment term) with observer identity and glare intensity as covariates. The number of sightings used in the detection curve was 709, and the effective strip half-width (ESHW) was 1,221 m. Distances on the X-axis are in kilometer.

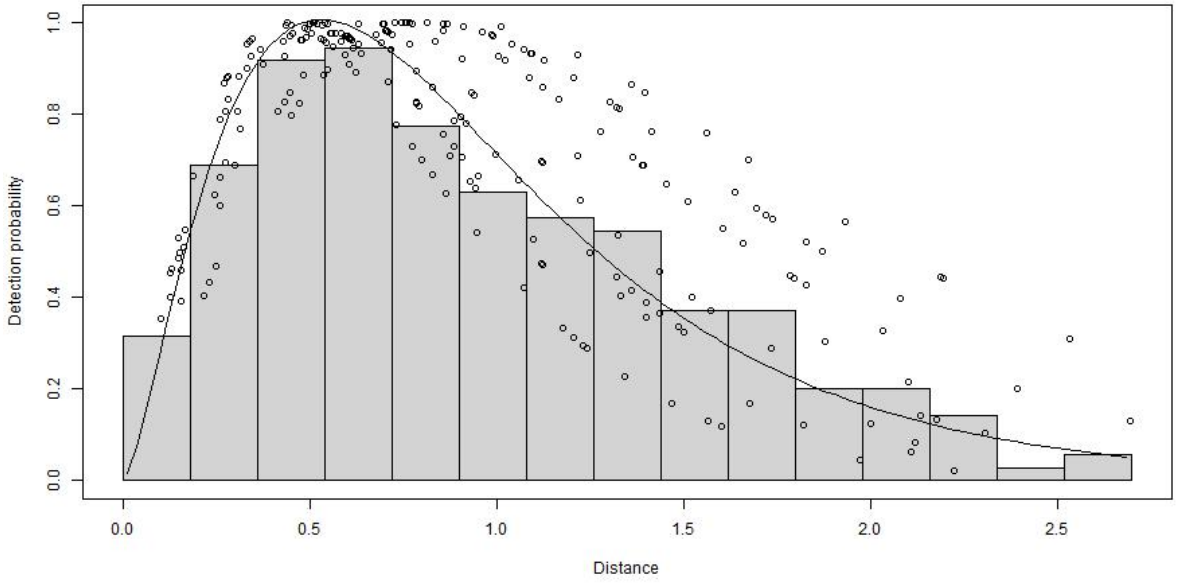

Figure A7.9. Detection curve for the 2015 survey. This analysis used a right truncation distance of 2700, and Gamma key function (without adjustment term) with observer identity and Beaufort as covariates. The number of sightings used in the detection curve was 236, and the effective strip half-width (ESHW) was 1,217 m. Distances on the X-axis are in kilometer.

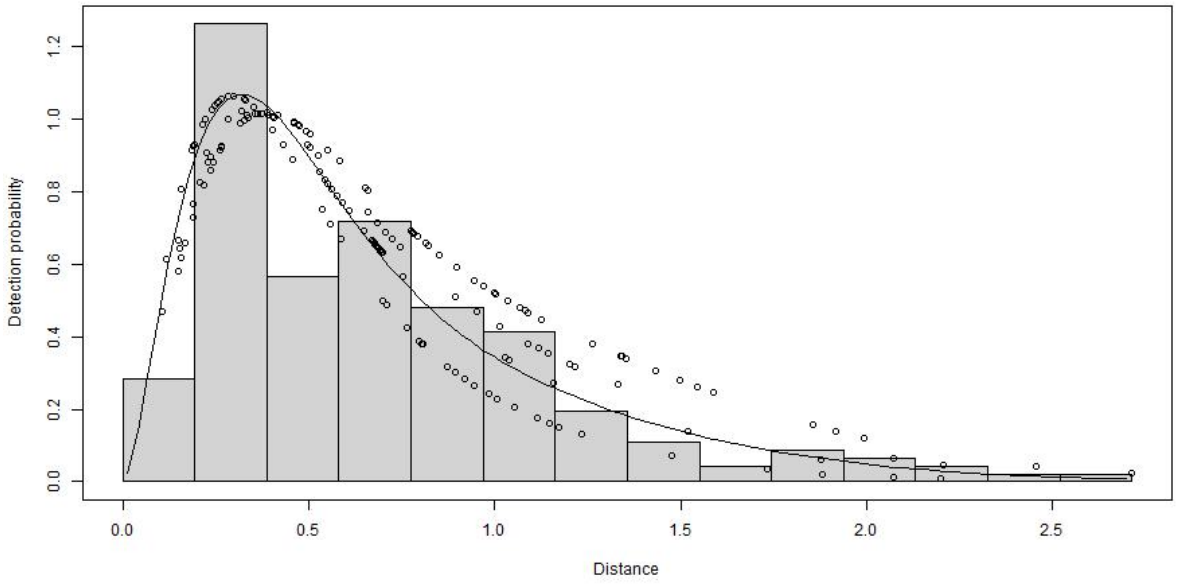

Figure A7.10. Detection curve for the 2016 survey. This analysis used a right truncation distance at the furthest distance observed, and Gamma key function (with polynomial adjustment term) with observer identity as covariate. The number of sightings used in the detection curve was 198, and the effective strip half-width (ESHW) was 834 m. Distances on the X-axis are in kilometer.

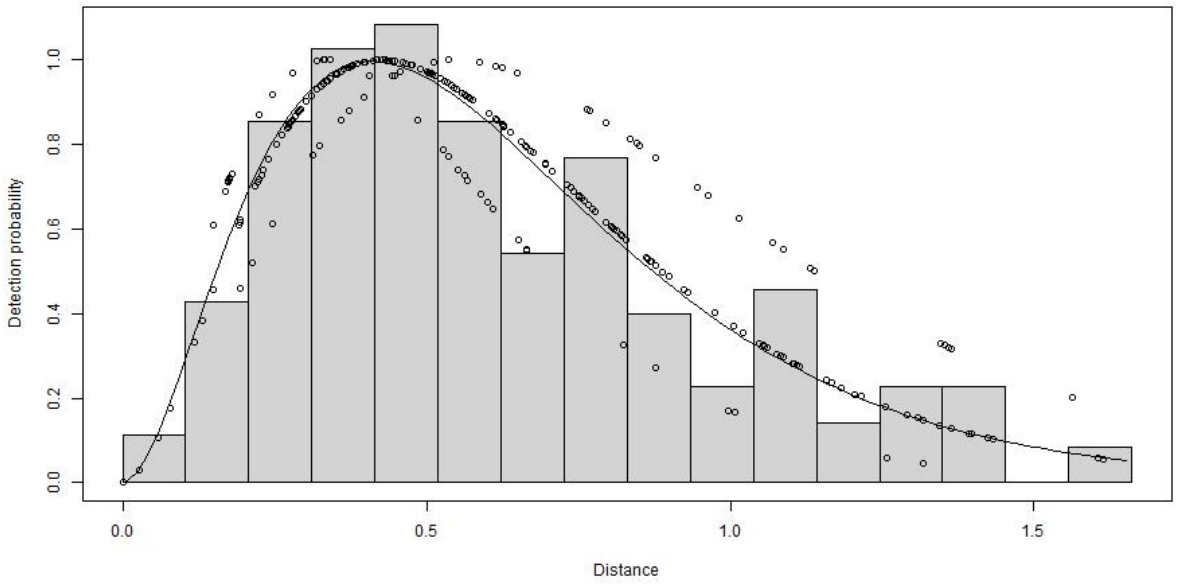

Figure A7.11. Detection curve for the 2018 survey. This analysis used a right truncation distance of 1661, and Gamma key function (without adjustment term) with glare intensity as covariate. The number of sightings used in the detection curve was 261, and the effective strip half-width (ESHW) was 773 m. Distances on the X-axis are in kilometer.

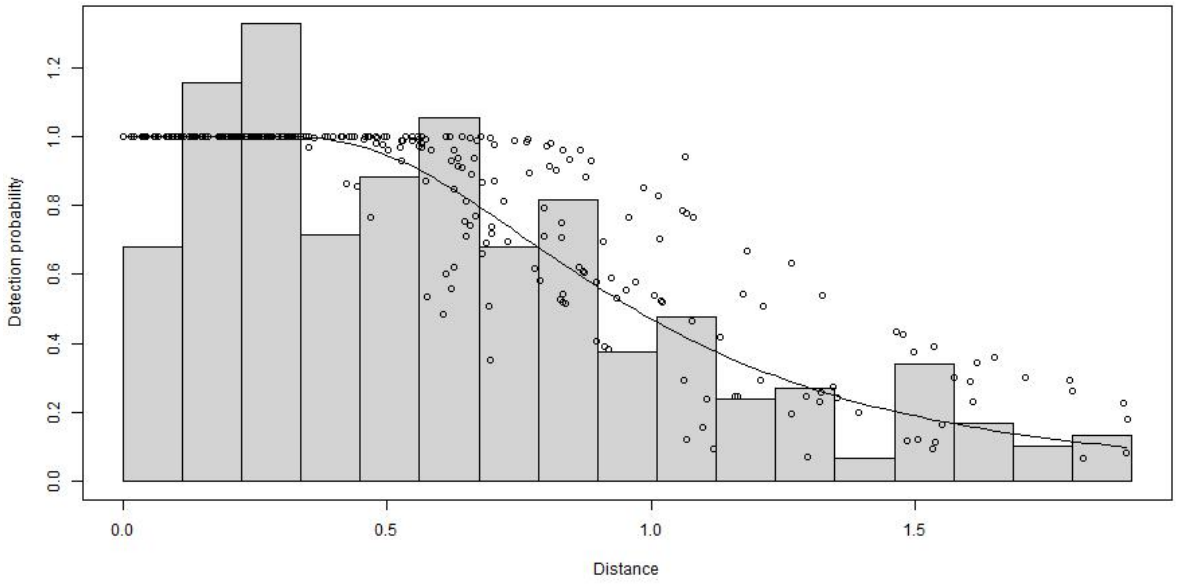

Figure A7.12. Detection curve for the 2019 survey. This analysis used a right truncation distance of 1910, and hazard-rate key function (without adjustment term) with observer identity and cloud cover as covariates. The number of sightings used in the detection curve was 279, and the effective strip half-width (ESHW) was 1,066 m. Distances on the X-axis are in kilometer.

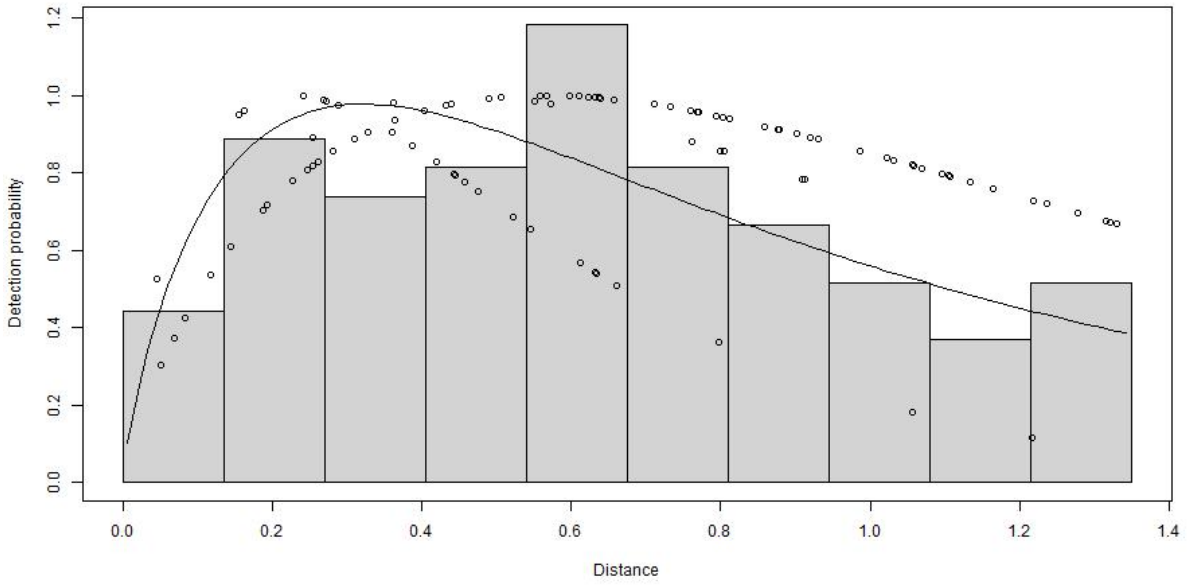

Figure A7.13. Detection curve for the 2020 survey. This analysis used a right truncation distance of 1350, and Gamma key function (without adjustment term) with Beaufort as covariate. The number of sightings used in the detection curve was 94, and the effective strip half-width (ESHW) was 951 m. Distances on the X-axis are in kilometer.

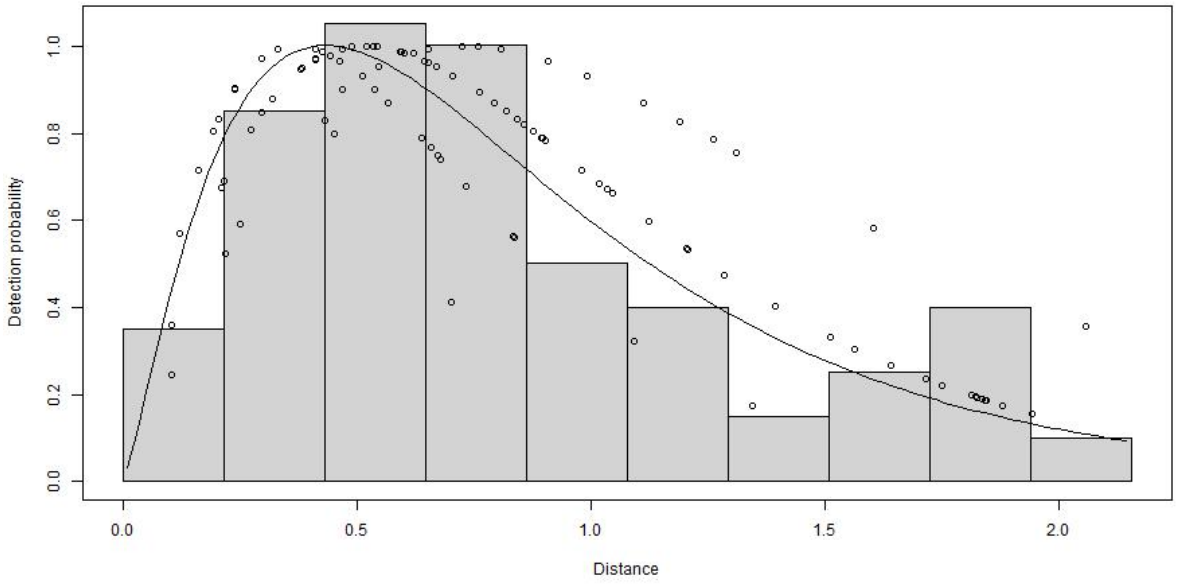

Figure A7.14. Detection curve for the 2021 survey. This analysis used a right truncation distance of 2155, and Gamma key function (without adjustment term) with Beaufort as covariate. The number of sightings used in the detection curve was 101, and the effective strip half-width (ESHW) was 1,090 m. Distances on the X-axis are in kilometer.

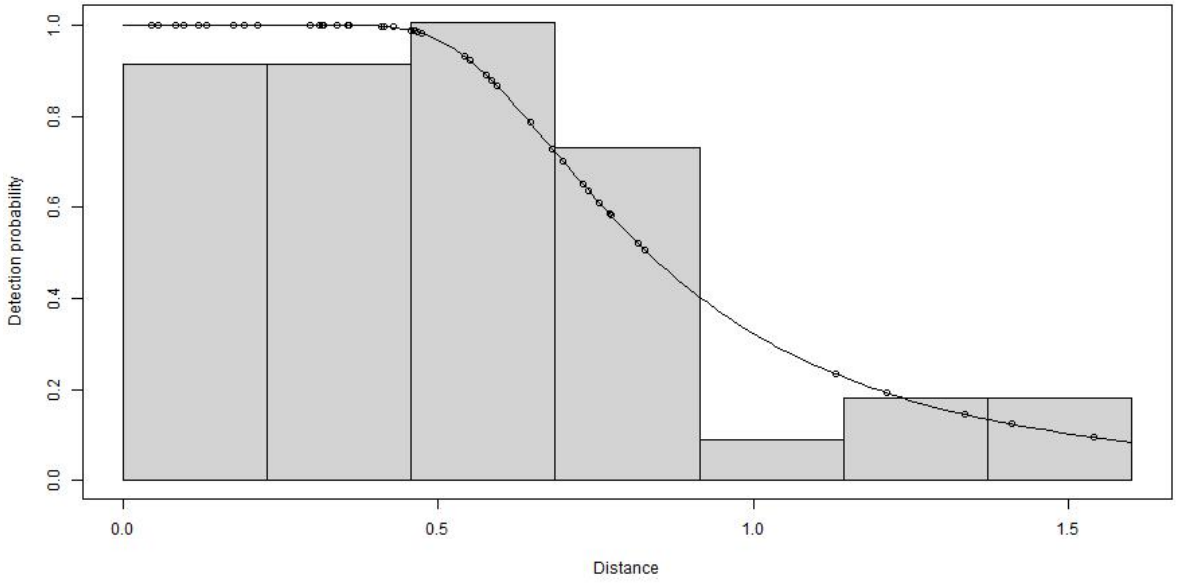

Figure A7.15. Detection curve for the 2022 survey. This analysis used a right truncation distance of 1600, and hazard-rate key function (without adjustment term) with observer identity and cloud cover as covariates. The number of sightings used in the detection curve was 44, and the effective strip half-width (ESHW) was 920 m. Distances on the X-axis are in kilometer.

APPENDIX 8. DISTRIBUTION OF OBSERVED GROUP SIZE (RECORDED BY THE PRIMARY OBSERVERS) PER SURVEY YEAR

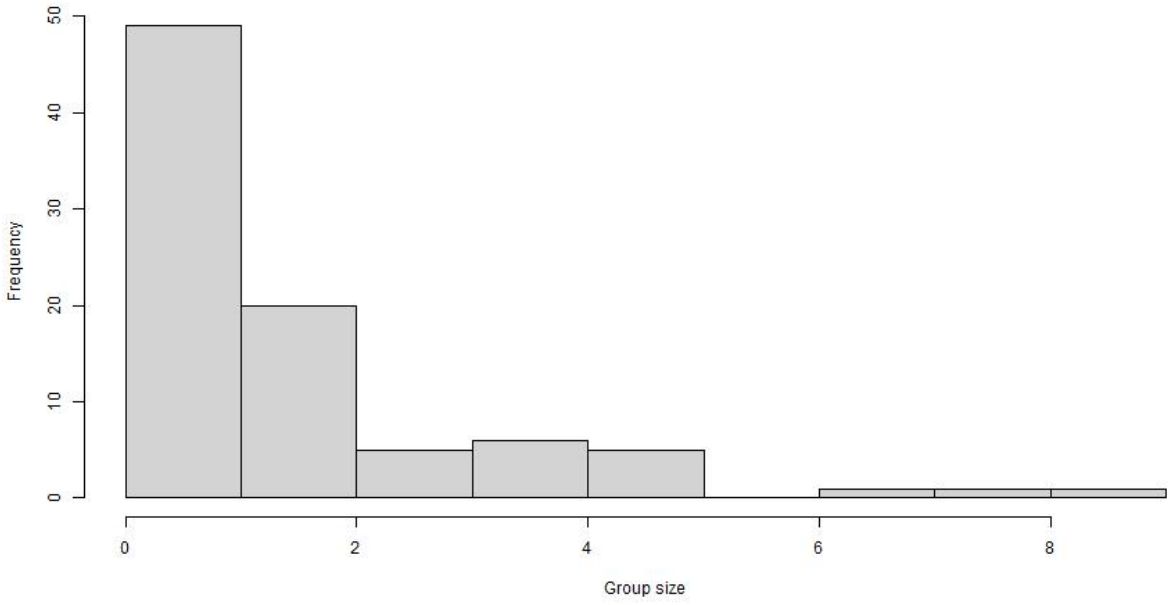

Figure A8.1. Distribution of observed group size (not corrected for availability bias) in 2001.

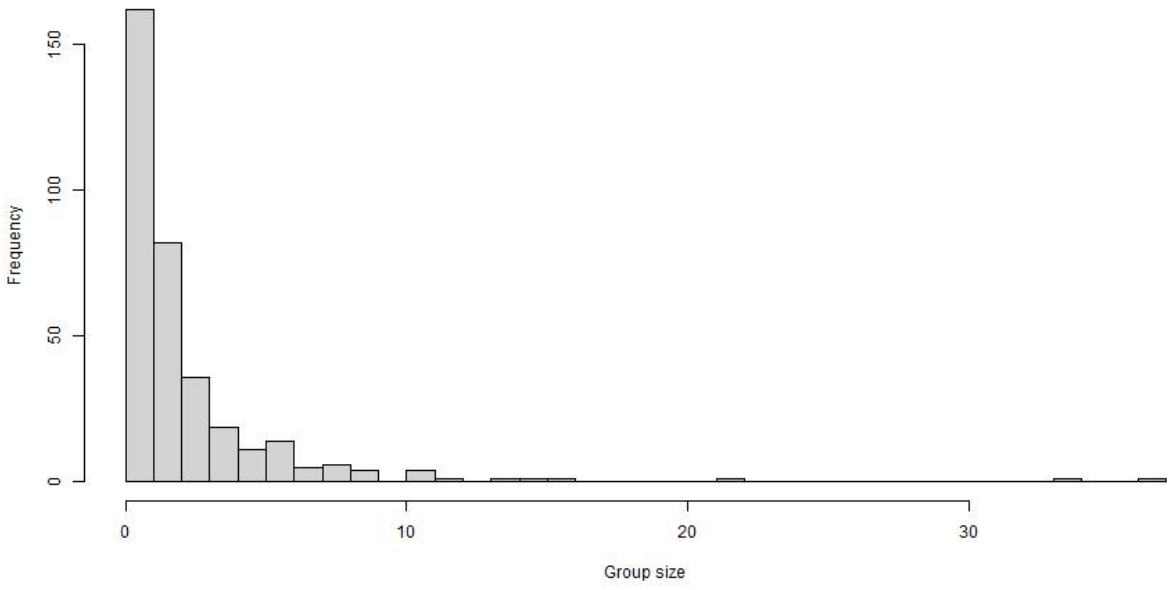

Figure A8.2. Distribution of observed group size (not corrected for availability bias) in 2003.

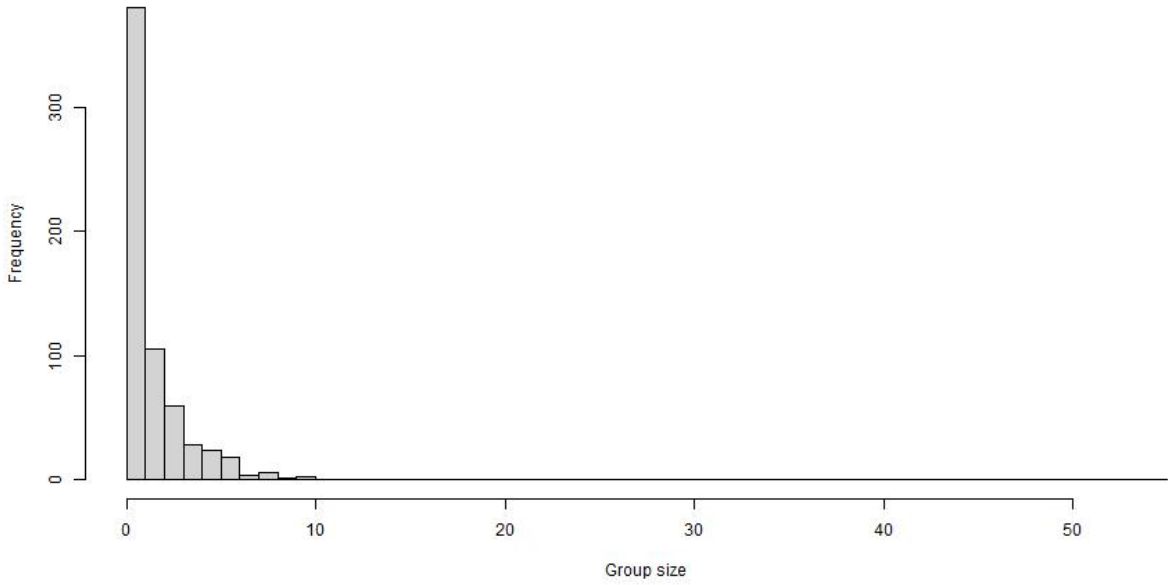

Figure A8.3. Distribution of observed group size (not corrected for availability bias) in 2005, during surveys flown at 305 m of altitude.

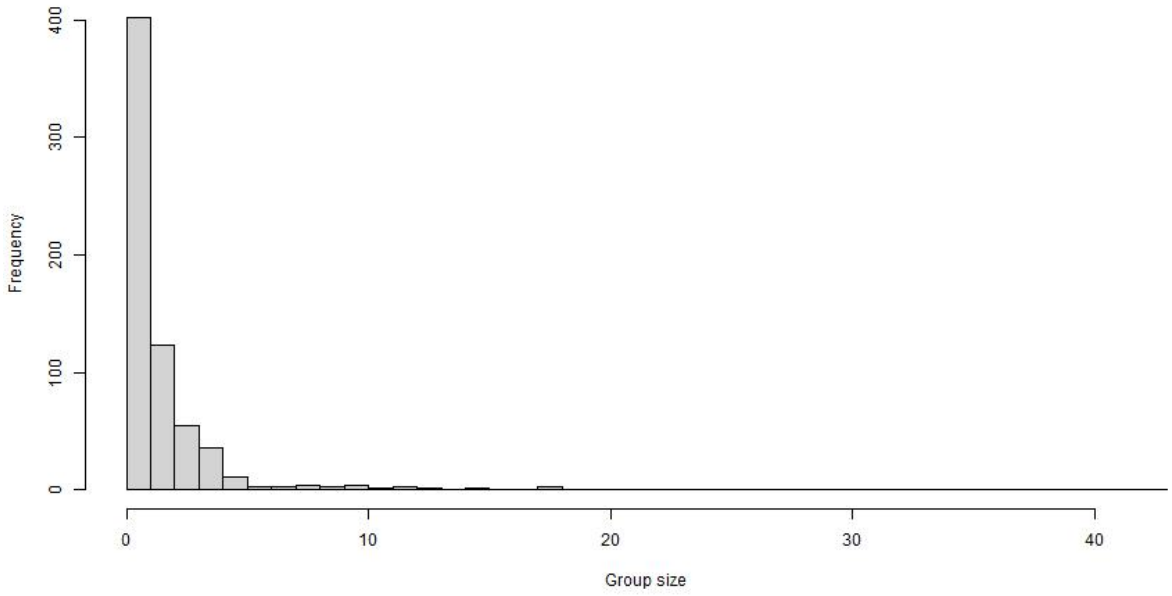

Figure A8.4. Distribution of observed group size (not corrected for availability bias) in 2005, during surveys flown at 457 m of altitude.

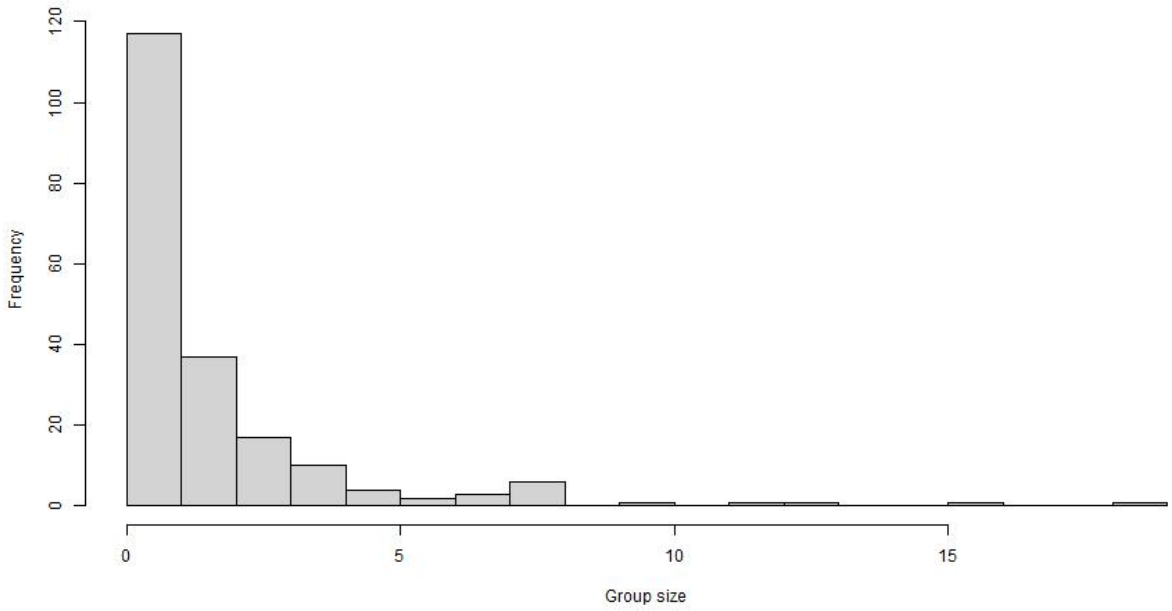

Figure A8.5. Distribution of observed group size (not corrected for availability bias) in 2007.

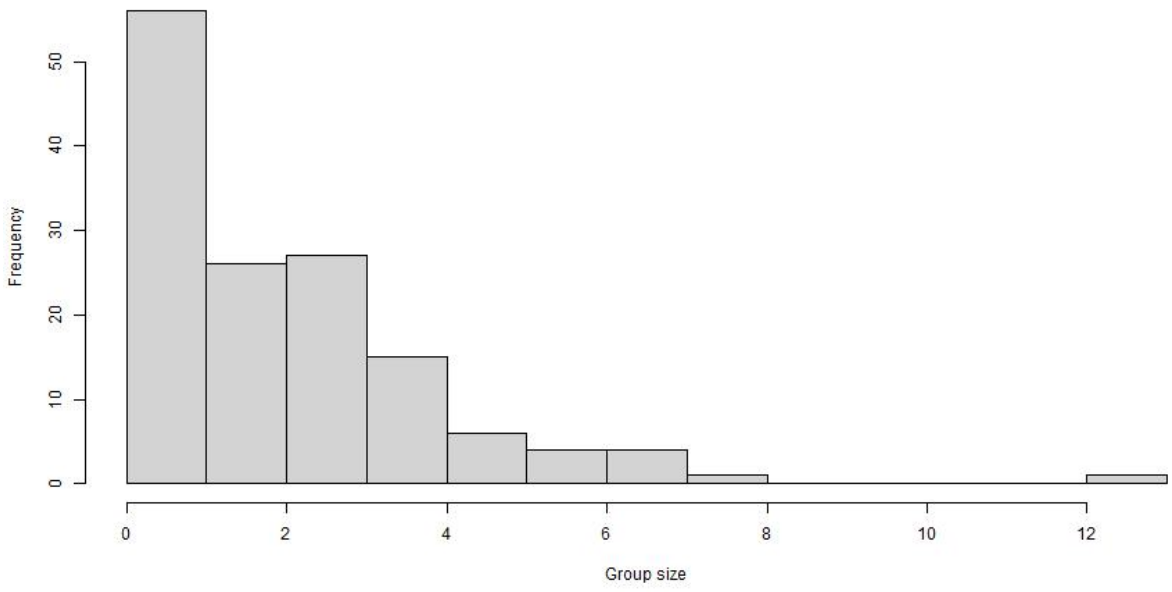

Figure A8.6. Distribution of observed group size (not corrected for availability bias) in 2008.

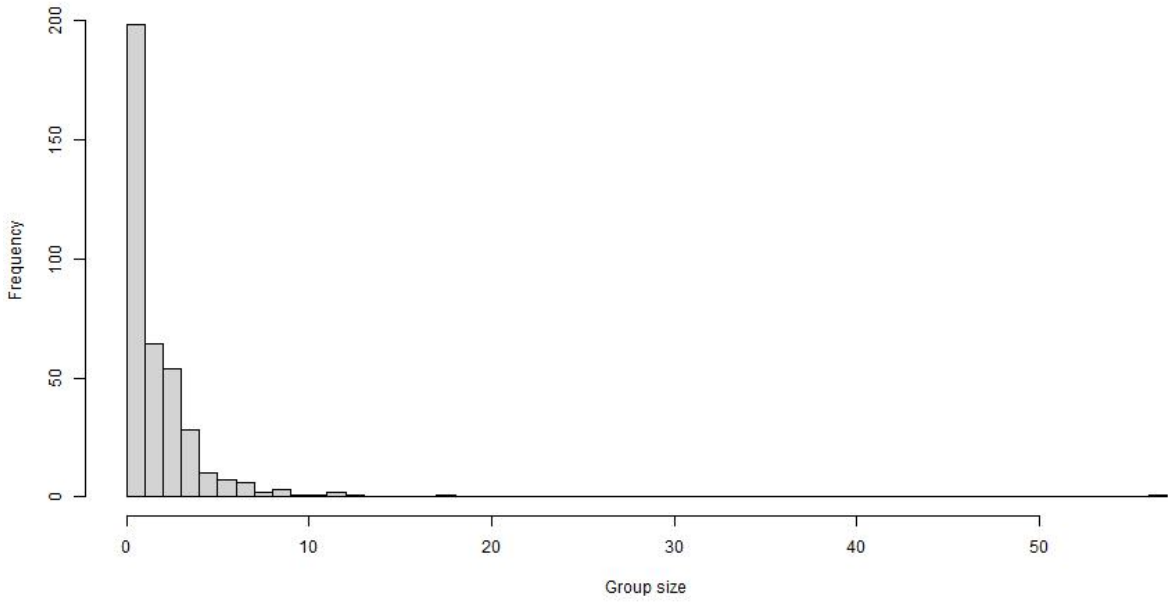

Figure A8.7. Distribution of observed group size (not corrected for availability bias) in 2009.

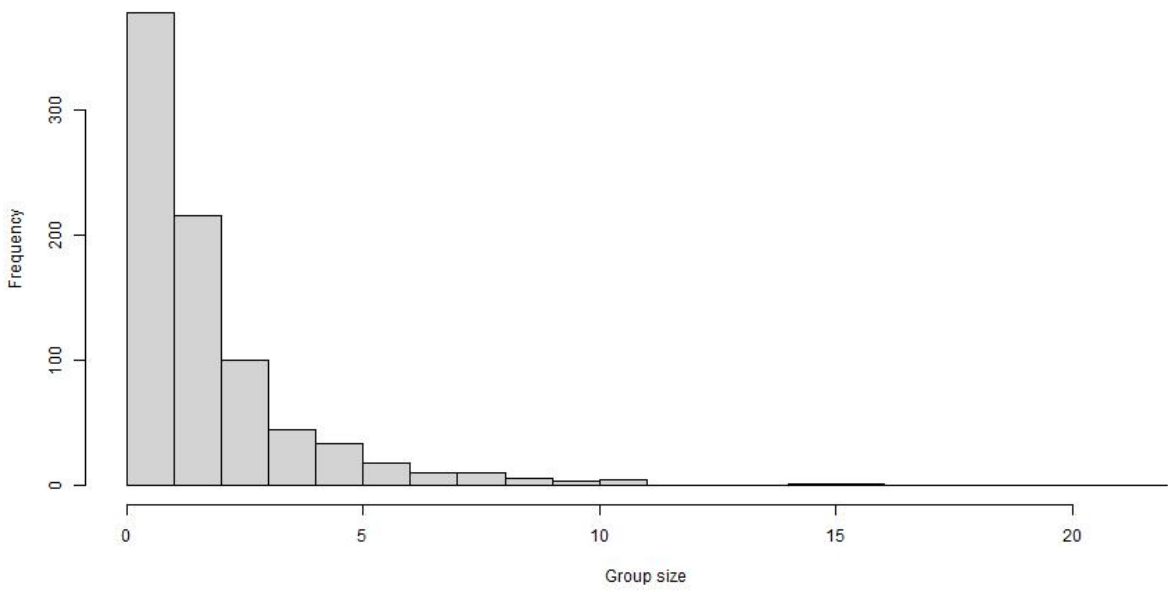

Figure A8.8. Distribution of observed group size (not corrected for availability bias) in 2014.

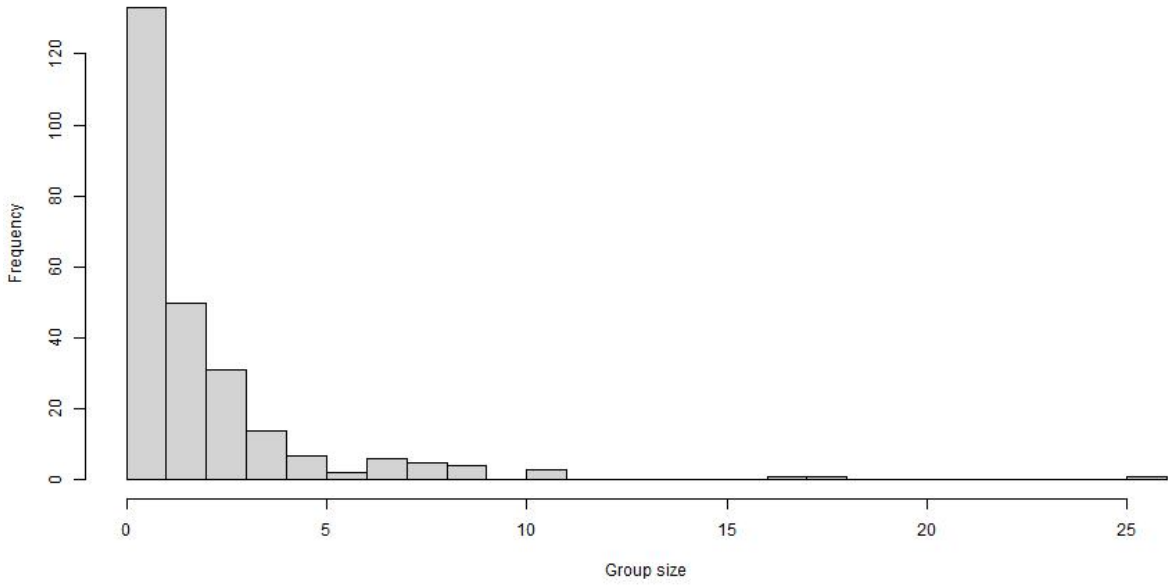

Figure A8.9. Distribution of observed group size (not corrected for availability bias) in 2015.

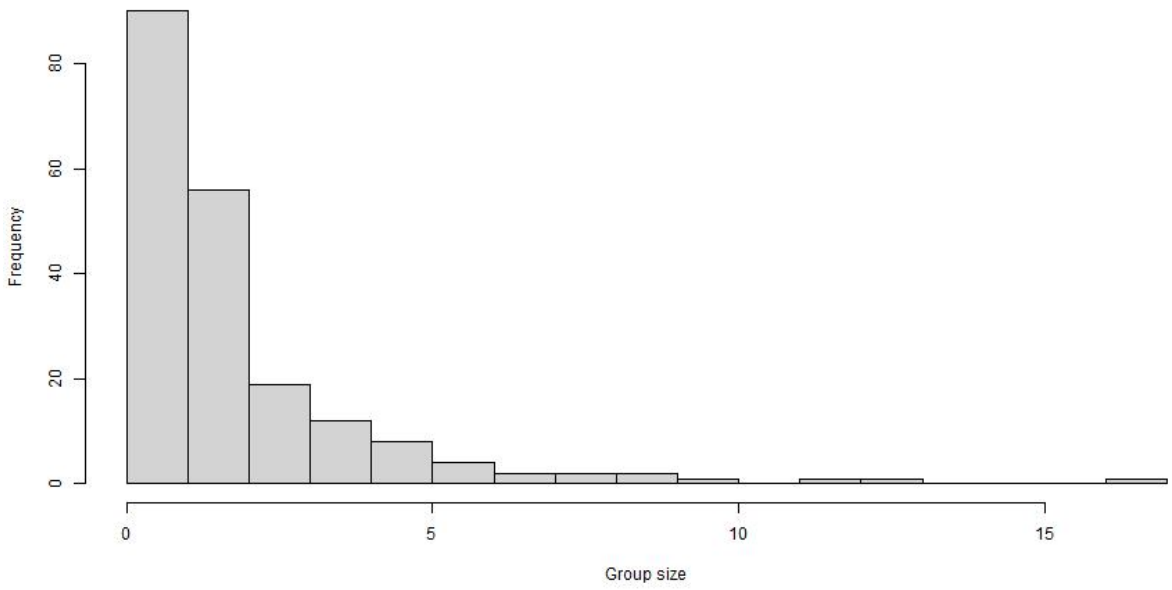

Figure A8.10. Distribution of observed group size (not corrected for availability bias) in 2016.

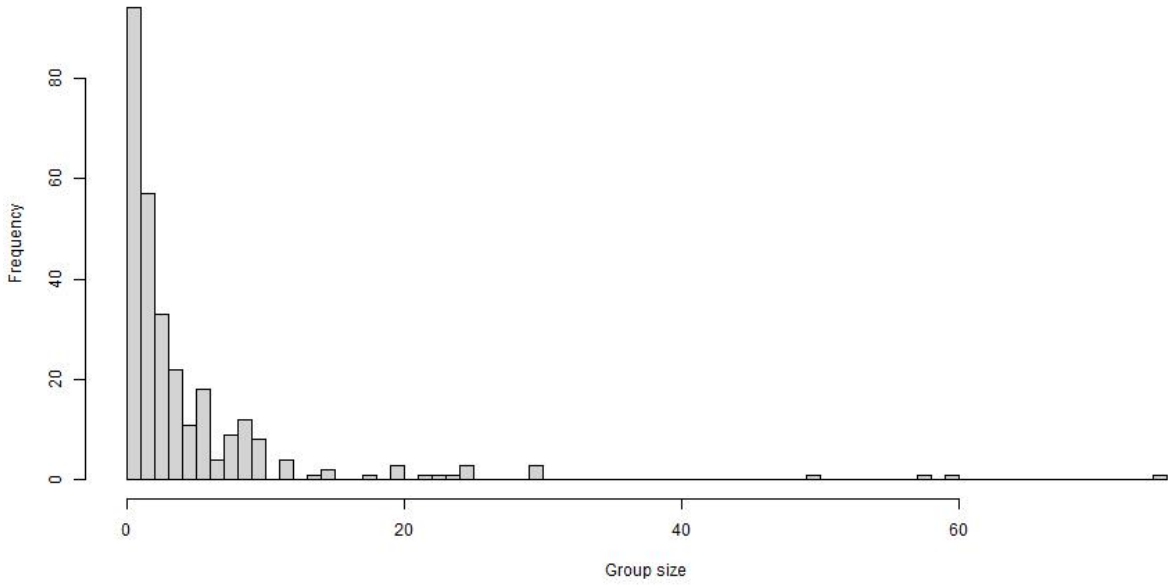

Figure A8.11. Distribution of observed group size (not corrected for availability bias) in 2018.

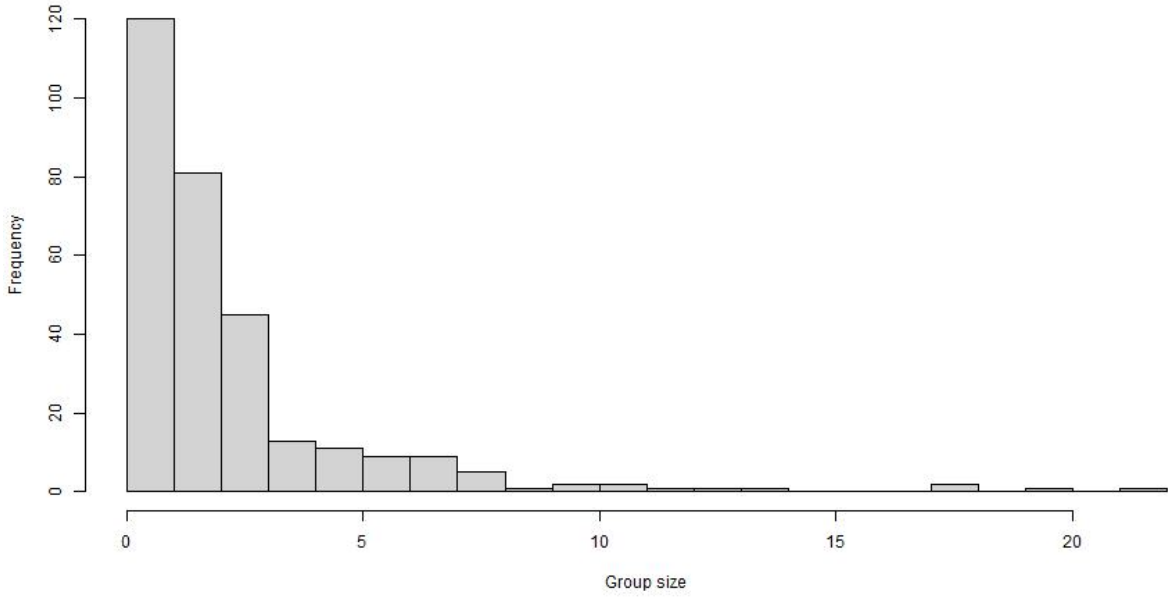

Figure A8.12. Distribution of observed group size (not corrected for availability bias) in 2019.

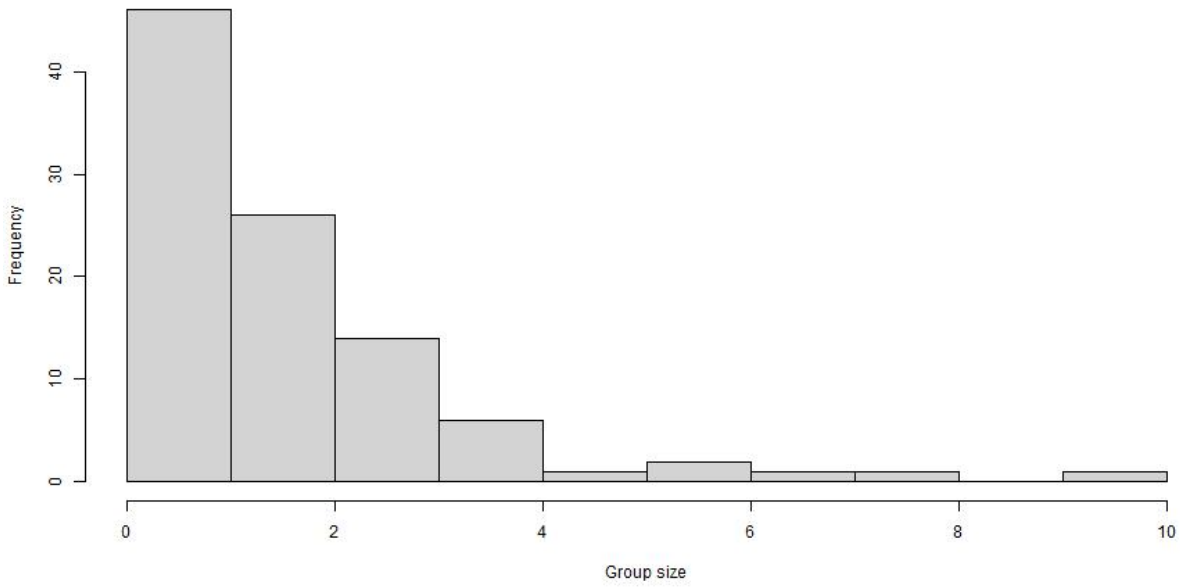

Figure A8.13. Distribution of observed group size (not corrected for availability bias) in 2020.

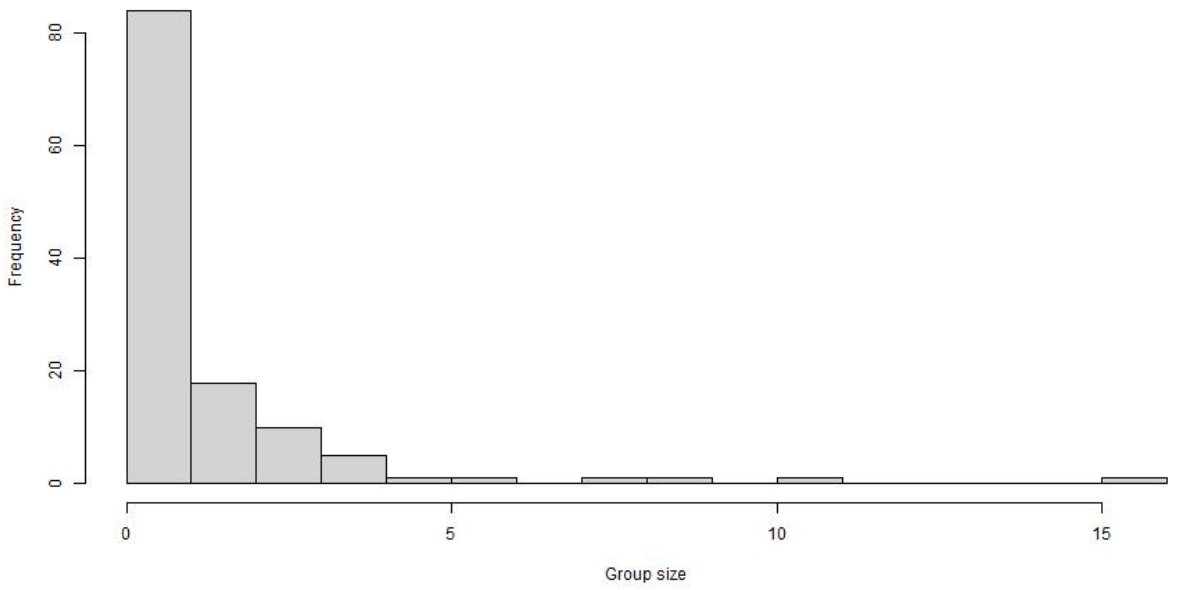

Figure A8.14. Distribution of observed group size (not corrected for availability bias) in 2021.

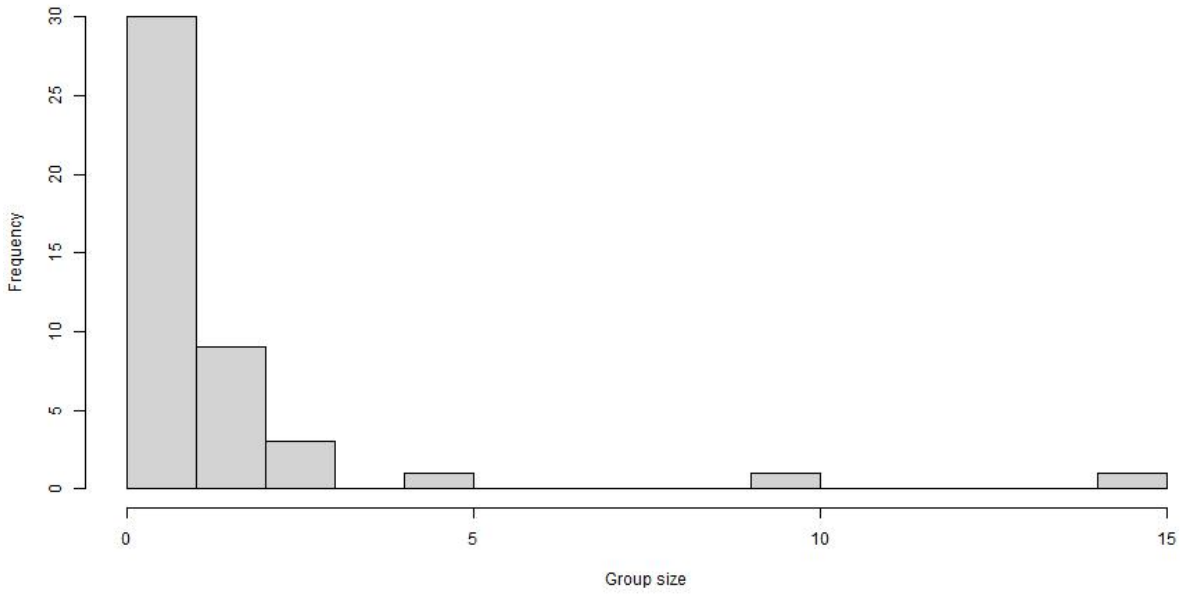

Figure A8.15. Distribution of observed group size (not corrected for availability bias) in 2022.